ABSTRACT

AN EXPERIMENTAL INVESTIGATION OF A NON-ISOTHERMAL TURBULENT WALL JET

by Jack Duane Wilson

The characteristics of the flow field produced by a given ventilation inlet is of primary importance in the design of a ventilation system. This investigation was conducted to determine the characteristics of the temperature and velocity fields resulting from a slotted inlet in a wall, adjacent to the ceiling. The velocity field, produced by such an inlet arrangement, is described as a wall jet. A simulated wintertime ventilation application was investigated. Thus the temperature of the incoming ventilation air was lower than that of the ambient room air.

The experimental arrangement consisted of a four feet wide by twelve feet long "section" of a ceiling, with a 48 inch long by .49 inch high slotted inlet at one end and adjacent to the ceiling. A means was provided to control both the temperature and the velocity of the incoming ventilation air. Mean velocities were determined using a constant temperature hot film anemometer and mean temperatures were measured with thermocouples.

The independent variables of the investigation were the inlet air temperature and the inlet air velocity. Five inlet velocities were selected as representative of those

encountered in ventilation practices. They were: 1200, 1000, 800, 600 and 400 ft/min. For each velocity the isothermal case plus three temperature differences, between the incoming ventilation air and the room air, were investigated. The temperature differences were approximately 50°F, 40°F and 20°F. Velocity and temperature profiles were determined at eight different longitudinal distances from the inlet.

Assuming that similarity of the temperature profiles applied, analysis indicated that the decay of the maximum temperature difference is a power function of the longitudinal distance from the inlet (e.g. $\triangle \bar{T}_m = C_2 x^b$). The same analysis indicated that the growth of the thermal boundary layer, as represented by a characteristic length δ_t , is a linear function of the longitudinal distance from the inlet.

Using theory already available the mean velocity results were analyzed. The mean velocity profiles generally appeared to be congruent when plotted in dimensionless form. The decay of maximum velocity was fairly well represented by a relationship of the form $\bar{U}_m=C_1x^a$. The average value of a from all tests was -.53.

The mean temperature profiles were plotted in dimensionless form. Generally, similarity of temperature profiles was indicated except for the 400 ft/min inlet velocity cases. An exponential relationship due to Reichardt (1941) was found to represent reasonably well the data in the outer portion of the dimensionless temperature profiles.

For all cases the growth of the thermal boundary layer

was a linear function of x. The rate of growth of the thermal boundary layer was found to be inversely proportional to the inlet Reynolds number.

The experimental results indicated that the decay of the maximum temperature difference was reasonably well represented by the previously mentioned power law relationship. The average value of the exponent b for all tests was -.63. This was considerably higher than the velocity decay exponent. indicating a faster rate of decay for temperature than for velocity. The rate of decay of the maximum temperature difference appeared to be inversely proportional to the inlet Reynolds number, indicating less thermal mixing of the cold air with the warm air, at the higher inlet Reynolds numbers.

Buoyancy forces appeared to be negligible at the higher inlet Reynolds numbers. However, at the 600 ft/min and 400 ft/min inlet velocities, there was an indication that buoyancy forces were influencing the flow field.

An expression was found for determining the temperature at any position in the thermal boundary layer. calculations made using this expression indicated it was reasonably accurate.

Approved Merle F Comay
Major Professor

AN EXPERIMENTAL INVESTIGATION OF A NON-ISOTHERMAL TURBULENT WALL JET

 $\mathbf{B}\mathbf{y}$

Jack Duane Wilson

A THESIS

Submitted to
Michigan State University
in partial fulfillment of the requirements
for the degree of

DOCTOR OF PHILOSOPHY

Department of Agricultural Engineering

651554

ACKNOWLEDGMENTS

The author wishes to express his sincere appreciation to Dr. M.L. Esmay (Agricultural Engineering), whose continued interest and encouragement made this investigation a rewarding one.

The assistance of Dr. S. Persson (Agricultural Engineering) throughout the investigation, is greatly appreciated by the author.

Thankful acknowledgment is extended to the other members of the guidance committee: Dr. J.V. Beck (Mechanical Engineering), Dr. N.A. Hills (Mathematics) and Dr. B.A. Stout (Agricultural Engineering).

To the author's wife, Joanne, whose unfailing love and devotion sustained the author throughout the challenges and frustrations of the graduate program, this manuscript is dedicated.

TABLE OF CONTENTS

														Page
ACKNOWLE	DGMENTS								•	•	•	•	•	ii
LIST OF	TABLES			• •					•	•	•	•	•	v
LIST OF I	FIGURES	• • •		• •					•	•	•	•	•	vii
LIST OF	APPENDIC	ES .		• •	• •	• •			•	•	•	•	•	x
LIST OF	SYMBOLS	• • •		• •	• •	• •	• •		•	•	•	•	•	xi
Chapter														
1. II	NTRODUCI	CION .				• •			•	•	•	•	•	1
2. L	ITERAT UF	RE REV	IEW	• •			• •		•	•	•	•	•	4
2	.1 Horiz Free		ly Pi	rojec	cted	Non-	-isoi	ther	na]	•	•	•	•	4
2.	.2 Gener in th	ral Ob ne Pre								et •	8	•	•	7
2.	.3 Wall	Jets	• •	• •	• •	• •			•	•	•	•	•	9
	2.3a	Defin	itior	n of	a w	all .	jet	• •	•	•	•	•	•	9
	2.3b	Wall	jet s	simi]	lari	ty.	• •	• •	•	•	•	•	•	9
	2.3c	Maxim growt		eloci	ity	leca;	y and	l wa:		-		•	•	13
	2.3d	Veloc: layer	-	list:	ribu	tion	in t	the :	inn	er •	•	•	•	16
	2.3e	Tempe	ratui	re pi	rofi	les :	in th	ne wa	a ll	. j	et		•	18
2.	.4 Wall	Jet S	neari	ing S	Stre	ss .			•	•	•	•	•	20
2.	.5 Eddy	Diffu	sivit	ty Fo	or M	omen	tum		•	•	•	•	•	21
2.	.6 Turbu	lent 1	rand	iti N	Numb	er .						•		22

Cha	ptei	r																				Page
	3.	ANAL	YTICA	TC	ons	IDI	ERA	TI	ON	S	•	•	•	•	•	•	•	•	•	•	•	25
			Dimer Equat					•		•	f	tr •	ne •	Go •	•	err •	ir •	ıg •	•	•	•	26
			3.1a		lys ati				he.	• b	ou •	nd •	la:	• •	18	•	er •	•	•	•	•	26
			3.1b	Ord mom														tì	ne •		•	29
			Maxim and I																•	•	•	33
	4.	EXPE	RIMEN	TAL	PR	OCI	EDU	IRE	A	ND	E	QU	JIE	ME	en i	2	•	•	•	•	•	40
		4.1	Equip	men	it.	•	•	•	•	•	•	•	•	•	•	•	•	•	•	•	•	40
			4.1a	Mea	n v	elo	oci	ty	, p	ro	fi	.16	8	•	•	•	•	•	•	•	•	45
			4.1b	Mea	n t	em	per	at	ur	·e	pr	of	[1]	Les	3	•	•	•	•	•	•	47
		4.2	Scope	of	Te	st	3	•	•	•	•	•	•	•	•	•	•	•	•	•	•	49
		4.3	Exper	ime	nta	1 1	Pro	oce	dų	re		•	•	•	•	•	•	•	•	•	•	49
	5.	EXPE	RIMEN	ITAL	RE	ເຣບາ	LTS	3	•	•	•	•	•	•	•	•	•	•	•	•	•	53
		5.1	Mean	Vel	.oci	ty	Re	ອຣນ	ılt	s	•	•	•	•	•	•	•	•	•	•	•	53
			Simil			•													8	•	•	68
			Therm		•						_											86
			Resul				·												•			
		_	ments		• •	•	•	•	•	•	•	•	•	•	•	•	•	•	•	•	•	91
	6.	APPL	ICATI	ON		•	•	•	•	•	•	•	•	•	•	•	•	•	•	•	•	103
	7.	CONC	LUSIC)NS		•	•	•	•	•	•	•	•	•	•	•	•	•	•	•	•	105
	8.	RECO	MMENI	ATI	ONS	F	OR	FU	TU	RE	W	OF	RΚ	•	•	•	•	•	•	•	•	107
APP	ENDI	cx .	• • •	•		•	•	•	•	•	•	•	•	•	•	•	•	•	•	•	•	109
REF	EREN	ICES		•		•	•	•		•		•	•	•	•	•	•		•	•		139

LIST OF TABLES

Table		Page
2.1	Summary of results, for decay of maximum velocity and growth of a wall jet, of various investigators	17
4.1	Velocity and temperature conditions for all tests	52
5.1	Experimentally determined constants for velocity decay	67
5.2	Experimentally determined constants for thermal boundary layer growth	88
5•3	Experimentally determined constants for temperature decay	100
A.1	Measured mean velocity data for test no. 1, \bar{U}_1 =1368 ft/min, isothermal case	115
A.2	Measured mean velocity data for test no. 2, \overline{U}_1 =1235 ft/min, $\triangle \overline{T}_1$ =20.7°F	116
A. 3	Measured mean velocity data for test no. 3. $\bar{U}_1=1224$ ft/min, $\Delta \bar{T}_1=41.8$ · · · · · · · · · · · · · · · · · · ·	117
A.4	Measured mean velocity data for test no. 4, \bar{U}_1 =1230 ft/min, $\triangle \bar{T}_1$ =52.3°F	118
A. 5	Measured mean velocity data for test no. 5, \bar{U}_1 =1020 ft/min, isothermal case	119
A. 6	Measured mean velocity data for test no. 6, $\bar{U}_1=981$ ft/min, $\triangle \bar{T}_1=21.3$ °F	120
A.7	Measured mean velocity data for test no. 7. $\overline{U}_1=996$ ft/min, $\triangle \overline{T}_1=40^{\circ} F$	121
A. 8	Measured mean velocity data for test no. 8, $\overline{U}_1=1015$ ft/min, $\triangle \overline{T}_1=54.8$ °F	122
A. 9	Measured mean velocity data for test no. 9, \bar{U}_1 =820 ft/min, isothermal case	123

Table		Page
A.10	Measured mean velocity data for test no. 10, \bar{U}_1 =769 ft/min, $\triangle \bar{T}_1$ =21.8°F	124
A.11	Measured mean velocity data for test no. 11, \bar{U}_1 =771 ft/min, $\triangle \bar{T}_1$ =41.4°F	125
A.1 2	Measured mean velocity data for test no. 12, \bar{U}_1 =760 ft/min, $\triangle \bar{T}_1$ =55.1°F	126
A.13	Measured mean velocity data for test no. 13, \bar{U}_1 =604 ft/min, isothermal case	127
A.14	Measured mean velocity data for test no. 14, \bar{U}_1 =570 ft/min, $\triangle \bar{T}_1$ =21.9°F	128
A.1 5	Measured mean velocity data for test no. 15, \bar{U}_1 =550 ft/min, $\triangle \bar{T}_1$ =38.5°F	129
A. 16	Measured mean velocity data for test no. 16, \overline{U}_1 =620 ft/min, $\triangle \overline{T}_1$ =50.1°F	130
A.17	Measured mean velocity data for test no. 17, \vec{U}_1 =450 ft/min, isothermal case	131
A.18	Measured mean velocity data for test no. 18, \bar{U}_1 =410 ft/min, $\triangle \bar{T}_1$ =18.2°F	132
A. 19	Measured mean velocity data for test no. 19, \bar{U}_1 =443 ft/min, $\triangle \bar{T}_1$ =40.8°F	133
A. 20	Temperature difference at the ceiling and maximum temperature difference, for all tests	134

LIST OF FIGURES

Figure		Page
2.1	A schematic view of the wall jet configuration	10
3.1	A schematic view of the thermal boundary layer of the wall jet	37
4.1	Overall view of the experimental equipment	41
4.2	Ceiling with adjacent slotted inlet, thermocouples indicated by lighter areas in the center	41
4.3	A schematic view of the nozzle-plenum assembly	42
4.4	Venturi and manometer used in measuring the air-flow rates	44
4.5	Temperature control units, fan and mixing box	44
4.6	Temperature and velocity instrumentation	46
4.7	Traversing mechanism with velocity probe and temperature sensing unit	46
4.8	Closeup view of velocity probe and thermo-couple stack	48
5.1	Mean velocity profile for station 3, test 17, \overline{U}_1 =450 ft/min, isothermal case	54
5.2	Mean velocity profile for station 3, test 2, \bar{U}_1 =1235 ft/min, $\triangle \bar{T}_1$ =20.7°F	54
5•3	Dimensionless velocity profile for test no. 1, \bar{U}_1 =1368 ft/min, isothermal case	56
5.4	Dimensionless velocity profile for test no. 4, \overline{U}_1 =1230 ft/min, $\triangle \overline{T}_1$ =52.3°F	59
5•5	Dimensionless velocity profile for test no. 13, $\overline{U}_{1}=604$ ft/min, isothermal case	61

Figure		Page
5.6	Dimensionless velocity profile for test no. 16, \bar{U}_1 =620 ft/min, $\triangle \bar{T}_1$ =50.1°F	62
5.7	Velocity decay results for test no. 8, \overline{U}_1 =1015 ft/min, $\triangle \overline{T}_1$ =54.8°F	65
5.8	Velocity decay results for test no. 1, \overline{U}_1 =1368 ft/min, isothermal case	65
5•9	Velocity decay results for test no. 9, \bar{U}_{1} =820 ft/min, isothermal case	66
5.10	Velocity decay results for test no. 17, \overline{U}_1 =450 ft/min, isothermal case	66
5.11	Plot of inlet Reynolds number versus the velocity decay exponent	69
5.12	Plot of inlet Grashoff number versus the velocity decay exponent	69
5.13	Dimensionless temperature profile for test no. 2, \overline{U}_1 =1235 ft/min, $\triangle \overline{T}_1$ =20.7°F	71
5.14	Dimensionless temperature profile for test no. 3, \overline{U}_1 =1224 ft/min, $\triangle \overline{T}_1$ =41.8°F	72
5.15	Dimensionless temperature profile for test no. 4, \bar{U}_1 =1230 ft/min, $\triangle \bar{T}_1$ =52.3°F	73
5.16	Dimensionless temperature profile for test no. 6, \bar{U}_1 =981 ft/min, $\triangle \bar{T}_1$ =21.2°F	75
5.17	Dimensionless temperature profile for test no. 7. $U_1=996$ ft/min, $\triangle T_1=40^{\circ}F$	76
5.18	Dimensionless temperature_profile for test no. 8, \overline{U}_1 =1015 ft/min, $\triangle \overline{T}_1$ =54.8°F	77
5.19	Dimensionless temperature profile for test no. 10, \bar{U}_1 =769 ft/min, $\triangle \bar{T}_1$ =21.8°F	79
5.20	Dimensionless temperature profile for test no. 11, $\bar{U}_1 = 771$ ft/min, $\triangle \bar{T}_1 = 41.4$ °F	80
5.21	Dimensionless temperature profile for test no. 12, \bar{U}_1 =760 ft/min, $\triangle \bar{T}_1$ =55.1 F	81
5.22	Dimensionless temperature profile for test no. 14, \bar{U}_1 =570 ft/min, $\triangle \bar{T}_1$ =21.9°F	82

Figure			Page
5.23	Dimensionless temperature profile for test no. 15, \bar{U}_1 =550 ft/min, $\triangle T_1$ =38.5°F	•	83
5.24	Dimensionless temperature profile for test no. 16, \bar{U}_1 =620 ft/min, $\triangle \bar{T}_1$ =50.1°F	•	84
5 .2 5	Inlet Reynolds number versus the virtual origin	•	90
5.26	Inlet Reynolds number versus Co, the coefficient representing the slope of the thermal boundary layer	•	90
5.27	Maximum temperature difference decay results for test no. 2, \bar{U}_1 =1235 ft/min, $\triangle \bar{T}_1$ =20.7°F	•	93
5 .2 8	Maximum temperature difference decay results for test no. 3, \bar{U}_1 =1224 ft/min, $\triangle \bar{T}_1$ =41.8 F	•	93
5.29	Maximum temperature difference decay results for test no. 4, $\overline{U}_1=1230$ ft/min, $\triangle \overline{T}_1=52.3$ F	•	94
5.30	Maximum temperature difference decay results for test no. 6, $\overline{\text{U}}_{1}\text{=}981$ ft/min, $\triangle\overline{\text{T}}_{1}\text{=}21.3^{\circ}\text{F}$.	•	94
5.31	Maximum temperature difference decay results for test no. 7, \bar{U}_1 =996 ft/min, $\triangle T_1$ =40°F	•	95
5.32	Maximum temperature difference decay results for test no. 8, \bar{U}_1 =1015 ft/min, $\triangle T_1$ =54.8°F	•	95
5•33	Maximum temperature difference decay results for test no. 10, \bar{U}_1 =769 ft/min, $\triangle \bar{T}_1$ =21.8°F	•	96
5.34	Maximum temperature difference decay results for test no. 11, \bar{U}_1 =771 ft/min, $\triangle \bar{T}_1$ =41.4°F	•	96
5.35	Maximum temperature difference decay results for test no. 12, \bar{U}_1 =760 ft/min, $\triangle \bar{T}_1$ =55.1 F	•	97
5.36	Maximum temperature difference decay results for test no. 14, \bar{U}_1 =570 ft/min, $\triangle \bar{T}_1$ =21.9 F	•	97
5.37	Maximum temperature difference decay results for test no. 15, \bar{U}_1 =550 ft/min, $\triangle \bar{T}_1$ =38.5°F	•	98
5.38	Maximum temperature difference decay results for test no. 16, \bar{U}_1 =620 ft/min, $\triangle \bar{T}_1$ =50.1 F	•	98
5•39	Plot of inlet Reynolds number versus the temperature decay exponent	•	101

LIST OF APPENDICES

A ppendix		Page
A.1	Correcting for Error in Velocity Measurements Due to Fluid Property Changes	109
A.2	Heat Transfer Through the Ceiling	111
A. 3	Calculating Temperature Using Empirical Expression	113
A.4	Measured Mean Velocity Data	115

LIST OF SYMBOLS

- a = exponent of maximum velocity decay defined by eqn.
 (3.43)
- \propto = thermal diffusivity = $k/\rho c_p$, ft^2/sec
- b = exponent of maximum temperature difference decay defined by equation (3.41)
- β = coefficient of expansion of gas, $1/R^{\circ}$
- c = a constant which represents the slope (e.g. rate of growth) of the thermal boundary layer, defined by equation (3.33)
- C_5 = a constant defined by equation (3.41)
- C_7 = a constant defined by equation (3.43)
- δ_t = distance from the wall (e.g. ceiling) in the y-direction to where $\triangle T = \triangle T_m/2$
- $\delta_m = \underset{\overline{U}=\overline{U}_m/2}{\text{distance from the wall in the y-direction to where}}$
- $c_{D} = \text{specific heat, BTU/lb}_{m} F^{O}$
- e_h = turbulent eddy diffusivity for heat, defined by equation (3.10), ft²/sec
- $\varepsilon_{\rm m}$ = turbulent eddy diffusivity for momentum, defined by equation (3.3), ft²/sec
- η = a dimensionless variable defined by equation (3.18)
- $f(\eta)$ = dimensionless function defined by equation (3.15)
- $g_1(\eta)$ = dimensionless function defined by equation (3.16)
- $g_2(\eta) = dimensionless function defined by equation (3.17)$
- g = acceleration due to gravity, ft/sec²
- Gr = Grashoff number = $g\beta\theta h^3/\gamma^2$, dimensionless
- $Gr_1 = Grashoff number evaluated at inlet = <math>g\beta \triangle \bar{T}_1 L^3/\gamma^2$
- h = a characteristic length
- k = thermal conductivity, BTU/hr-ft-F°
- L = slot height
- μ = absolute viscosity, lb_m/ft -sec

- γ = kinematic viscosity, ft²/sec
- Pr = Prandtl number = $c_p \mu/k$, dimensionless
- Pr_{t} = turbulent Prandtl number = $\epsilon_{m}/\epsilon_{H}$, dimensionless
- p = hydrostatic pressure, lb_f/ft^2
- Re = Reynolds number = ρ Vh/ μ , dimensionless
- Re, = Reynolds number evaluated at the inlet = $\rho \bar{U}_1 L/\mu$
- ρ = mass density, $lb_{f} sec^{2}/ft^{4}$
- T = mean temperature
- $\Delta \bar{T}$ = mean temperature difference
- t = fluctuating component of temperature
- θ = a characteristic temperature difference
- u = fluctuating component of the instantaneous velocity
 in the x-direction
- = mean component of the instantaneous velocity in the x-direction
- v = fluctuating component of the instantaneous velocity in the y-direction
- \overline{V} = mean component of the instantaneous velocity in the y-direction
- x = longitudinal distance from the inlet, perpendicular to the gravitational acceleration
- y = transverse distance from the ceiling, parallel to the gravitational acceleration
- x_o = distance to virtual origin (see Figure 3.1)
- $x' = x + x_0$

Subscripts

- i = refers to the inlet
- c = refers to a characteristic value
- m = refers to the maximum value

Superscripts

' (primes) = refers to dimensionless quantities

1. INTRODUCTION

The concept of controlled environment housing of livestock was first introduced in the United States ten to fifteen
years ago. Its advantages include a means of providing
environmental conditions the year around which are favorable
to optimum livestock production and a situation which lends
itself to better management practices. Because of these
advantages, this type of housing has gained wide acceptance
with livestock producers.

The success of controlled environment housing depends largely on the fulfillment of three requirements. First it is necessary to maintain temperature at an optimum level within the structure. The removal of moisture and the keeping of undesirable gases at a tolerable level are the last two requirements. The structure's ventilation system is primarily responsible for meeting these requirements.

Most ventilation systems currently available do a satisfactory job of controlling the temperature, moisture level and gas levels within the structure. These same ventilation systems however, leave something to be desired when it comes to the problem of ventilation air distribution, that is, ventilating as evenly as possible all areas of the structure. The reasons for this can be viewed as twofold. One is that economic considerations provide a limitation on the sophisti-

cation of the system. Secondly there is a lack of basic research results on room air distribution as influenced by the ventilation system.

An obvious place to begin research on ventilation systems is with the inlet.

One type of ventilation inlet system used in controlled environment structures utilizes a continuous slot in the ceiling adjacent to the wall. A hinged baffle is used to deflect the air across the ceiling for wintertime ventilation or directly downward adjacent to the wall for summertime ventilation. The wintertime application provides maximum mixing of the cold air with the warm air near the ceiling, before it comes into contact with the occupants. Both summer and winter inlet systems provide a jet of air defined in the literature as a wall jet.

Tuve (1953) noted that when the ceiling or wall coincides with one edge of a ventilation inlet a greater throw of the air stream resulted than for the same inlet discharging into an open space (e.g. a free jet). Borque and Newman (1960) discovered the explanation for this phenomenon to be a result of the Coanda effect.

Glauert (1956) was the first to examine theoretically the similarity problem (e.g. congruency of dimensionless velocity profiles) of the laminar and turbulent, radial and plane wall jet. He realized that a wall jet is characterized by two regions, one close to the wall which resembles boundary layer flow over a flat plate, and an outer region

which closely resembles free jet flow. He succeeded in establishing that similarity does indeed exist for both the laminar and turbulent wall jet.

Myers, Schauer and Eustis (1963_b) investigated heat transfer to plane turbulent wall jets. Their analytical development and experimental results showed that similarity of temperature profiles existed for the wall region of the jet. Buoyancy effects were neglected since the outlet velocities used were quite high. They also noted a greater spread of the temperature profile than the velocity profile.

This investigation was concerned with a chilled wall jet as might be encountered in wintertime ventilation. The effect of the initial temperature difference between the incoming and ambient air and the slot inlet velocity on the mean temperature and velocity profiles, was investigated.

2. LITERATURE REVIEW

2.1 Horizontally Projected Non-isothermal Free Jets

A number of researchers have investigated heated and chilled free jets at velocities encountered in ventilation.

Nottage, Slaby and Gojsza (1952) observed a significant effect of buoyancy forces on the trajectory of a chilled round free jet. In their investigation the temperature of the incoming air was 40°F below that of the room air and the outlet velocity was 8.33 ft/sec. The following empirical relation was found to correlate their data.

$$Z_{a}=K(x/d_{o})^{2}$$
 (2.1)

where:

 Z_a =displacement of the jet axis below the horizontal

K =an empirical constant (.02 for their tests)

x =distance from the outlet

d_=outlet diameter

Koestal (1955) worked on the problem of horizontally projected heated and chilled jets. By means of a theoretical approach he arrived at the following equation expressing displacement of the centerline of the jet axis in terms of the independent variables.

$$\pm (y/d_0) = (\triangle T_0 \beta g d_0 / U_0^2) [(a/b + 1)6K] (x/d_0)^2$$
 (2.2)

y =distance from the horizontal

T_=temperature difference at the outlet

 β =coefficient of expansion of air

g =acceleration due to gravity

U_=outlet velocity

a/b=a function of the turbulent Prandtl number

K =an empirical constant

The dimensionless group $\triangle T_0 \beta g d_0 / U_0^2$ is actually equal to the Grashoff number divided by the square of the Reynolds number. This relationship is shown below.

$$\triangle T_o \beta g d_o / U_o^2 = (\triangle T_o \beta g d_o^3 / \gamma^2) (\gamma^2 / U_o^2 d_o^2) = Gr_o / Re_o^2 \quad (2.3)$$

The o in the subscript means that both of these dimensionless groups are evaluated at the outlet for this particular case. The Grashoff number is the free convection dimensionless modulus and can be considered as the ratio of buoyancy forces to viscous forces. The Reynolds number is considered a measure of the ratio of the inertia forces to the viscous forces. Thus the ratio $\text{Gr}_0/\text{Re}_0^2$ might be thought of as a ratio of buoyancy forces to inertia forces. Koestal's derived equation applies only if the slope of the trajectory of the jet centerline is not greater than approximately 15 degrees. This seriously limits the applicability of his expression.

Baturin (1959) investigated non-isothermal plane jets and arrived at the following equation relating jet centerline displacement with the independent variables.

$$(y/L)A_r\sqrt{T_u/T_o}=(0.226/a^2)(a(x/L) + 0.025)^{5/2}$$
 (2.4)

 T_{n} =absolute temperature of the medium

T_=absolute temperature of the air stream

L =outlet height

a =turbulence coefficient (0.09 to .20 for a two-dimensional jet)

$$A_r = gL(T_u - T_o)/U_o^2T_u$$

Abramovich (1938) investigated both warm and cold air free jets. His analytical approach assumed the buoyancy force was balanced by the vertical acceleration of the mass flow of the air + the change due to the mass change of entrainment. He arrived at the following equation which expresses the relationship between the displacement of the jet axis from the horizontal and the independent variables of outlet temperature and outlet velocity.

$$Y=0.026KX^3$$
 (2.5)

where:

 $Y = 2(y/d_0)$

 $X = 2(x/d_0)$

 $K = (gd_o/2U_o^2)(T_o/T_h)$

 T_h =temperature of the air in the space

Abramovich found this equation to predict very closely his experimental results for the outlet velocity range from 5.89 to 20.3 ft/sec. and temperature differences at the outlet from 142 to $454^{\circ}F$.

In summarizing, Koestal arrived at results which indicate one of the independent variables to be a dimensionless group analogous to the hydrodynamic Froude number. Baturin's equation includes an experimentally determined coefficient which is dependent on turbulence conditions. Koestal's equation includes a number which is a function of the turbulent Prandtl number. This may be questionable since numerous researchers have found the turbulent Prandtl number for a free jet to be nearly independent of test conditions and equal to approximately 0.71.

All of these researchers agree that at the lower velocities encountered in ventilation practices, buoyancy forces do have an effect on the trajectory of the free jet centerline.

2.2 General Observations on Ventilation Jets in the Presence of Solid Boundaries

It is not always possible to delineate the difference between a true wall jet and a jet at some distance from, parallel to and bounded by a solid surface (semi-bounded jet). Indeed in some cases of a semi-bounded jet the resulting flow condition might be accurately described as a wall jet. With this in mind the following section of literature review is presented.

Nottage (1951) found that when the axis of a circular jet is close to a wall, floor or ceiling and parallel with it, the spread of the jet in the transverse direction is reduced.

Kerka as reported by Tuve (1953) in a series of tests on circular jets with and without adjacent walls found a greater throw for the jet with an adjacent wall. He also found the angle of divergence in a transverse direction to the wall was less than one-half that of a free jet. Parker and White (1965) also observed that when the jet inlet is in the proximity of a wall or a ceiling an increase in throw is obtained.

Parker and White (1965), Becker (1950) and Farquharson (1952) concluded that jets in the proximity of solid bounaries will be drawn to and remain close to that surface. It was not until Borque and Newman (1960) did their definitive study on the reattachment of a two-dimensional jet that any real physical explanation could be offered for the above mentioned phenomenon. The reattachment problem, which comes under the general area of the Coanda effect, was explained thusly by Borque and Newman. After the fluid leaves the slot the highly unstable shear layers on both sides of the jet quickly become turbulent and entrainment takes place. fluid which is entrained near the wall is slightly accelerated. thus causing a corresponding decrease in static pressure along the wall. The pressure at the wall now being less than that of the surroundings, the jet curves towards the wall further reducing the pressure there. Thus eventually, the wall being long enough, the flow attaches to it. They explain that the establishment of this flow phenomenon is favored by approximately two-dimensional conditions. They also observed, that

for given upstream conditions, the mass flow from the slot is greater than that of a free jet if the flow is subsonic. Although their investigation was aimed towards aerodynamic applications, their findings indicate the reason for the behavior of a ventilation air jet near a solid boundary.

2.3 Wall Jets

2.3a Definition of a wall jet

Schwarz and Cosart (1960) describe a wall jet as a jet of fluid which impinges onto a wall at an angle from 0 to 90 degrees. Kruka and Eskinazi (1964) describe a plane wall jet as a flow of fluid emanating from a narrow slot and flowing over a rigid wall. Glauert (1956) writes, for a wall jet as for a free jet, the corresponding condition is that the radial velocity component falls to zero at the outer edge of the jet. Figure 2.1 shows a typical wall jet configuration. The name wall jet seems to have been ascribed by Glauert (1956), although the terms partially open jet, surface jet, and submerged jet have been used by Forthmann (1934), Zerbe and Selma (1946) and Poreth and Cermak (1959) respectively.

2.3b Wall jet similarity

In boundary layer flows as represented by Prandtl's approximations to the momentum equations, it is common to solve the equation or equations by finding a similarity parameter $f(\eta)$ in the velocity field. In this case η is the transverse distance made dimensionless with a x-dependent

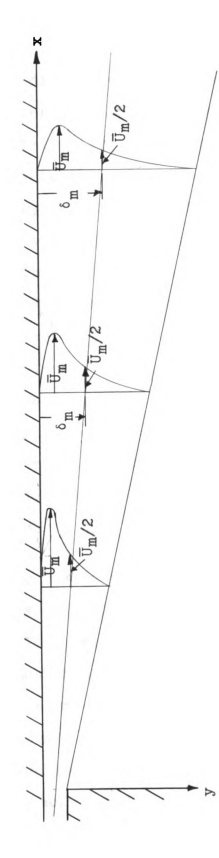


Figure 2.1-- A schematic view of the wall jet configuration

characteristic dimension. This allows transformation of the partial differential equation to a total differential equation which is comparatively easy to solve. In the physical sense similarity means that the velocity profiles at different longitudinal distances from the outlet can be made congruent by the proper choice of a velocity scale factor and a width scale factor (pg. 130, Schlichting (1959)).

The earliest known work on the turbulent wall jet was done by Forthmann (1934) who observed the similarity nature of the wall jet.

Glauert (1956) was the first to attack the similarity problem of the wall jet. The form of the equation for the boundary layer approximation to the equation of motion for a steady, plane, turbulent, incompressible flow with constant properties is given by Glauert as:

$$\vec{U}\frac{\partial \vec{U}}{\partial X} + \vec{V}\frac{\partial \vec{U}}{\partial y} = \frac{\partial}{\partial y} \varepsilon_{\text{II}} \frac{\partial \vec{U}}{\partial y} \tag{2.6}$$

Here the barred quantities refer to mean values while ϵ_m is the eddy diffusivity for momentum as defined in Eckert and Drake, 1959, p. 219. Some assumption had to be made about the behavior of ϵ_m . Glauert assumed initially in his analysis that ϵ_m behaved according to the hypothesis of Prandtl (1942). This assumes that it has a constant value across the boundary layer and is proportional to the product of the maximum mean velocity and a characteristic width of the boundary layer. However, experiments by Bakke (1957) indicated considerable deviation from such an assumption, near the wall the velocity

gradient being much higher than that predicted by Prandtl's hypothesis. Glauert then assumed that the behavior of the eddy diffusivity for momentum near the wall is governed by the empirical equation due to Blasius (1913), based on a study of turbulent pipe flow. This equation is:

$$\tau_{0}=0.0225/0\bar{U}^{2}(\frac{Y}{\bar{U}y})^{1/4}$$
 (2.7)

where:

 τ_0 =the wall shear stress ρ =the fluid density

γ = the kinematic viscosity

Using the concept according to Boussinesq (1877) the equation becomes:

$$\tau_0 = \epsilon_{\underline{\underline{w}}} \frac{\partial \overline{\underline{U}}}{\partial y} = 0.0225 \overline{\underline{U}}^2 (\frac{Y}{\overline{\underline{U}}y})^{\frac{1}{4}}$$
 (2.8)

This equation implies that $\overline{U}\alpha y^{1/7}$. Glauert observed further that Blasius's equation may be expected to hold near the wall in any turbulent boundary layer flow, outside the viscous sublayer. These assumptions suggest that the wall jet may be divided into an inner layer which acts much like boundary layer flow over a flat plate and an outer layer which behaves much like a free jet. This theory has been shown to be valid by Myers, Schauer and Eustis (1963_b), Schwarz and Cosart (1960) and Kruka and Eskinazi (1964). Glauert realized that because of the two layer nature of the wall jet, complete similarity is not attainable. However, confident predictions can be made about the nature of the maximum velocity decay

and the rate of growth of the wall jet. Glauert hypothesized that the following relationships were valid.

$$\bar{\mathbf{U}}_{\mathbf{m}} \propto \mathbf{C}_{\mathbf{1}} \mathbf{X}^{\mathbf{a}}$$
 (2.9)

$$\delta \propto C_2 X^{b} \tag{2.10}$$

where:

 δ =a characteristic dimension of the wall jet These hypotheses were made according to the conditions of Goldstein (1939) for the existence of similarity conditions in boundary layer flow.

2.3c Maximum velocity decay and wall jet growth

Myers et al (1963_a) investigated a wall jet in a still They used integral methods applied to the incompressible boundary layer equations to obtain a prediction for the decay of the maximum velocity and the growth of the boundary layer. They built on Glauerts analysis, notably assuming that Blasius's relation held in the inner layer while in the outer layer the hypothesis by Prandtl applies. Their theoretical analysis showed no Reynolds number effect on the velocity decay while their data seemed to indicate a slight Reynolds number effect with the higher Reynolds numbers exhibiting a slower velocity decay. The effect of Reynolds number on the wall jet growth was predicted to be small by their analysis and no effect could be observed in their data. The boundary layer thickness (e.g. δ) was shown to grow as $x^{.95\pm.05}$. Their δ was defined to be the point where $\overline{U}/\overline{U}_{m}=\frac{1}{2}$. The following equation was found to fit their experimental data which was

taken in the outlet Reynolds number range from 7100 to 56,000, corresponding to outlet velocities from 28 to 222 ft/sec.

$$\bar{\mathbf{U}}_{m}/\bar{\mathbf{U}}_{0}=3.45(x/L)^{-0.49}$$
 (2.11)

where:

 $\overline{\mathbf{U}}_{\mathbf{m}}$ =the maximum velocity at any given longitudinal position

U_o=the outlet velocity

x = the distance from the outlet

L =the slot height

Data were taken in the dimensionless slot width (e.g. x/L) range from 24 to 180. Their mean velocity profiles exhibited similarity for the test conditions given above.

Schwarz and Cosart (1960) used the similarity approach in determining a relationship for decay of the maximum velocity and growth of the wall jet, in a still medium. Their analysis involved selection of appropriate transformation functions and a transformation variable. This enabled transformation of the partial differential equation of motion into an ordinary differential equation. Analysis of this transformed equation indicated the same relationships for maximum velocity decay and wall jet growth as were given by Glauert (1956). Their experimental data were taken in the outlet Reynolds number range from 13,000 to 40,000, corresponding to outlet velocities of 27 to 83 ft/sec. Data were taken in the dimensionless slot number (e.g. x/L) range from 18 to 66. The equation which fit their data for the decay of maximum

velocity is:

$$\bar{U}_{m}/\bar{U}_{0}=5.395(x/L + 11.2)^{-.555}$$
 (2.12)

where the variables are the same as those used above in the equation of Myers et al. Schwarz and Cosart found no systematic dependence on Reynolds number of the wall jet growth, with the following equation representing their experimental data:

$$\delta/L=0.0678(x/L + 11.2)$$
 (2.13)

where:

 $\delta=$ the transverse distance to where $\overline{U}/\overline{U}_m=\frac{1}{2}$ They also found that when $\overline{U}/\overline{U}_m$ was plotted versus y/ δ the data were correlated well over the entire wall jet (e.g. the resultant profiles were congruent). Thus their similarity assumption was verified.

Schwarz and Cosart attempted to fit the outer part of their universal velocity profile with functional curves. The two functional relationships used were:

$$\overline{U}/\overline{U}_{m} = \exp \left[-A(\eta - \eta_{m})^{2}\right]$$
 (2.14)

and

$$\overline{U}/\overline{U}_{m}=\operatorname{sech}^{2}\eta$$

where:

$$\eta = y/\delta$$

$$\eta_{m} = (y/\delta)_{\overline{U} = \overline{U}_{m}}$$

Neither curve represented the data particularly well.

Seban and Back (1961) investigated a wall jet injected

into a turbulent boundary layer (e.g. into a free stream flow). The ratios of free stream to slot outlet velocity were between .2 and .11. The slot outlet velocities used were from 56 to 211 ft/sec. Measurements were taken for 2.4\leq x/L\leq 62.4. Their measured mean velocity profiles indicated similarity for x/L greater than 37. Their results generally conformed to Glauert's theory for a wall jet in a still medium. However, the values of the exponent for their velocity decay results were slightly lower than those found by Schwarz and Cosart (1960) and Myers et al (1963_a), for wall jets in a still medium.

Kruka and Eskinazi (1964) used the similarity approach in investigating the wall jet in a moving stream. Their analysis predicted a power law relationship for the decay of maximum velocity. This power law relationship had the same form as the one given by Glauert (1956). The value of the exponent was shown by their experimental results to be dependent on the ratio of the slot outlet velocity to free stream velocity.

Table 2.1 provides a summary of the results of the various investigators concerning wall jet growth and the maximum velocity decay.

2.3d Velocity distribution in the inner layer

Glauert (1956) assumed that the equation due to Blasius (1913) governed the behavior of the eddy diffusivity for momentum in the inner layer of the wall jet. This equation implies the following relationship:

Table 2.1 Summary of results for the decay of maximum velocity and growth of a wall jet, of various investigators

Type of wall jet	Ū _m	δ
Plane wall jet in a still medium (Myers et al)	x -•50	x
Plane wall jet in a still medium (Schwarz and Cosart)	x555	x
Plane wall jet in a still medium (Glauert)	x-•533	x
Plane wall jet injected into a turbulent boundary layer (Kruka and Eskinazi) $\beta=.1$	x-• ⁴⁵	x
Plane wall jet injected into a turbulent boundary layer (Seban and Back) $\beta=.055$	x510	x

 $[\]beta \frac{\text{Slot outlet velocity}}{\text{Free stream velocity}}$

$$U \propto y^{(1/n)} \tag{2.16}$$

n=7.0

The observations of Forthmann (1934) also indicated this to be the case. However, Schwarz and Cosart (1960) and Myers et al (1963_b) found a value of n=14 to describe their data in the inner layer. In his investigation of a wall jet in a moving stream Patel (1962) found n=11 in the inner layer. Kruka and Eskinazi (1964), in their study of a wall jet in a moving stream, found n to be dependent on the ratio of slot outlet velocity to free stream velocity and in all cases to be substantially higher than 7. Schwarz and Cosart believed that the intermittant nature of the outer layer of the wall jet was the probable reason for the difference between the velocity distribution in the boundary layer of free stream flow over a flat plate and that for the inner layer of the wall jet.

2.3e Temperature profiles in the wall jet

Only one source of literature was found which dealt with the non-isothermal wall jet in a still medium. Myers, Schauer and Eustis (1963_b) investigated the heat transfer to a wall jet for the case of a step temperature distribution. In their analysis they assumed that the temperature profile for the inner portion of the wall jet was given by:

$$\overline{T} = \overline{T}_{W} \left[1 - (y/\delta_{t})^{1/7} \right]$$
 (2.17)

 $\overline{\mathbf{T}}$ =the temperature difference above ambient $\overline{\mathbf{T}}_{\mathbf{w}}$ =the temperature at the wall above ambient

 $\delta_{\rm t}=$ the thermal boundary layer thickness. Their experimental data indicated that a one-seventh power law was not representative of the temperature distribution in the inner layer. A 1/14 power law relationship provided a better fit of their data. They also observed a greater spread of the temperature profile than that of the velocity profile. Similarity of the temperature profiles did hold in the inner layer.

No references were found concerning the similarity problem for temperature profiles in the outer layer of a wall jet in a still medium. However, Seban and Back (1961) investigated the problem for a wall jet injected into a moving stream. The test conditions were the same as those mentioned in the discussion of their findings for the velocity case (see section in Literature Review on Maximum Velocity Decay). The jet was heated and the wall was adiabatic. By means of an energy balance procedure they were able to derive an expression for the effectiveness. The effectiveness was defined as the ratio of local adiabatic wall temperature to the temperature of the injection air. The following relationship was derived:

$$\bar{T}_{w}/\bar{T}_{s}=7.7(x/L)^{-0.6}$$
 (2.18)

 $\bar{\mathbf{T}}_{\mathbf{w}}$ =wall temperature

 $\bar{T}_S=$ the free stream temperature When \bar{T}_W/\bar{T}_S was plotted versus y/ δ similarity of temperature profiles was indicated.

2.4 Wall Jet Shearing Stress

Although the results of the various investigators show close agreement for the decay of maximum velocity and the growth of the wall jet, there is considerable disagreement between their findings concerning the shearing stress at the wall.

Sigalla (1958) obtained shear data by the method of Preston (1954) which involves the use of pitot tubes. He took data out to 65 slot widths for a Reynolds number range from 22,800 to 52,000. The following equation was found to fit his data:

$$C_{f}=0.0565(\bar{U}_{m}\delta/\gamma)^{-\frac{1}{4}}$$
 (2.19)

where:

 C_f =the friction factor

 δ =the lateral distance to where $U/U_m=1/2$

Y = the kinematic viscosity

Schwarz and Cosart (1960) obtained their wall shearing stress information by applying momentum-integral techniques to their measured velocity profiles. Their results
showed values of the wall jet friction factor to be at most
a slowly varying function of Reynolds number and independent

of the downstream position. The average value for their experimental conditions was, $C_f=1.109 \times 10^{-2}$.

Forthmann (1934) also used the momentum-integral method to obtain the shear distribution normal to the flat surface but did not show a variation along the plate.

As part of an investigation of a wall jet with an external stream. Bradshaw and Gee (1960) obtained some shear stress results for the ordinary wall jet. They found friction factors about 6% higher than those of Sigalla.

Myers et al (1963) used a hot film technique for measuring the wall shear stress. They obtained values about 15% higher than those of Sigalla's but 50% lower than those of Schwarz and Cosart. They comment on these differences by noting that the method of Preston has been found to be in error by about 12 to 14% below accepted flat plate data. This would bring the results of Sigalla more in line with their own. They also state that measuring wall shear stress by the momentum-integral technique is not an accurate means since a small error in the determination of the derivative of the velocity profile would be greatly magnified in the final answer for the wall shear stress.

2.5 Eddy Diffusivity For Momentum

Although considerable research has been undertaken with wall jets to determine relationships for velocity decay, jet growth, wall shear stress and heat transfer, little has been done in the way of determining the turbulence properties

of a wall jet. Perhaps the most important property of the turbulent flow regime is the eddy diffusivity for momentum, $\epsilon_{\rm m}$.

Glauert (1956) assumed that $\varepsilon_{\rm m}$ was proportional to $\overline{\rm U}^6$ in the inner layer and remained constant in the outer layer much like a free jet. Since any reasonable assumption of the behavior for $\varepsilon_{\rm m}$ will result in a solution of the mean flow parameter which fit the data reasonably well, Glauerts assumed variation of $\varepsilon_{\rm m}$ remains to be tested against experimental data.

Schwarz and Cosart (1960) derived an expression for ϵ_m in terms of their universal velocity profile. This expression necessitated differentiation and integration of the universal profile for the determination of ϵ_m . They did this for the outer portion of the wall jet as represented by their experimental data. The values obtained showed that ϵ_m was fairly constant in the middle portion, diminishing towards the outer edge. Thus their results tend to verify Glauert's assumed behavior of ϵ_m in the outer portion of the wall jet. It is well to note that Schwarz and Cosart mention that such a method for the determination of the eddy diffusivity for momentum often produce results which are moderately inaccurate even when exceptional care is taken.

2.6 Turbulent Prandtl Number

The process of turbulent mixing causes the transfer of properties of fluid in a lateral direction of the stream.

Analogous to the eddy diffusivity for momentum which appears in the turbulent form of the momentum equation, there is a eddy diffusivity for heat (e.g. $\varepsilon_{\rm H}$) which appears in the turbulent form of the energy equation (Eckert and Drake, 1959, pg. 219).

Initially it was believed that the mechanisms of momentum transfer and heat transfer in turbulent flow were identical. However, measurements by Reichardt (1944) in a two-dimensional free jet showed that the temperature profiles are wider than the velocity profiles. This result has, been confirmed by Corrsin (1950), Hinze (1948) and Forstall and Shapiro (1950). An entirely satisfactory explanation for this phenomenon has not yet been found.

The ratio $\varepsilon_{\rm m}/\varepsilon_{\rm H}$ is called the turbulent Prandtl number, Prt, and its determination has been the subject of numerous researchers. Forstall and Shapiro (1950) found a value of 0.70 for the turbulent Prandtl number in their investigation of coaxial free jets. They indicated the value to be substantially independent of the nature of the experiment.

Nottage, Slaby and Gojsza (1952) in their investigation of a chilled, free jet also found a value for the turbulent Prandtl number of 0.70.

Reichardt (1940 and 1951) made an extensive investigation of the heat transfer across turbulent boundary layers and found a value of 0.77 for the turbulent Prandtl number.

The problem of the determination of the turbulent Prandtl number for wall jets has apparently received very

little attention to this time. The only reference to be found in the review of literature concerning this subject was that of Myers et al (1963_b) . They hypothesized as to the behavior of the value of the turbulent Prandtl number and assumed an average value across the entire wall jet.

3. ANALYTICAL CONSIDERATIONS

The analysis phase of this investigation will be undertaken in two steps. They are:

- 1. A dimensional analysis of the governing equations will be carried out. This will provide some information about the magnitude of the buoyancy forces relative to the magnitude of the inertia and viscous forces.
- 2. A similarity approach will be used on the energy equation to determine relationships for maximum temperature decay and the thermal boundary layer growth.

Before proceeding further one assumption will be made. This is, that the fluid properties can be assumed to be independent of temperature. Schlichting (1962), pg. 295, states that fluid properties may be assumed constant for temperature differences less than 50°C. The temperature differences encountered in this investigation are well below this limit.

Since buoyancy forces arise from density changes produced by temperature differences it appears that the assumption of constant properties implies negligible buoyancy forces. This is not necessarily true (Eckert and Drake, 1959, pg. 327) and further development will proceed under the premise of constant fluid properties and appreciable buoyancy forces.

3.1 Dimensional Analysis of the Governing Equations

In non-isothermal ventilation it is important to know whether the buoyancy forces have an effect on the velocity field and if they do. the magnitude of that effect.

As mentioned in the Literature Review, non-isothermal free jet trajectories have been found to be affected by the buoyancy forces which result from the temperature differences.

The dimensional analysis of the governing equations will be carried out in two steps. They are:

- 1. The governing differential equations will be made dimensionless for the purpose of determining the dimensionless groups which govern the solution of the problem.
- 2. The resulting dimensionless equations will be examined by an order of magnitude approach to attempt to gain some insight into the importance of the various forces in the flow field.

The dimensional analysis approach outlined above is discussed in Schlichting (1962) and Kline (1965).

3.1a Analysis of the boundary layer equations

Prandtl's approximation to the equations of motion for the case of steady, plane, turbulent, incompressible, two-dimensional flow with constant physical properties and with buoyancy forces may be written as (Eckert and Drake, 1959, pg. 218):

for the x-direction

$$\overline{U}\frac{\partial\overline{U}}{\partial x} + \frac{\partial\overline{U}}{\partial y} = \frac{1}{2} \frac{\partial\overline{p}}{\partial x} + \gamma \frac{\partial^2\overline{U}}{\partial y^2} - \frac{\partial\overline{u}\overline{v}}{\partial y} + g_x \beta\theta$$
 (3.1)

for the y-direction

$$\frac{\partial \bar{\mathbf{p}}}{\partial \mathbf{y}} = \rho g_{\mathbf{y}} \beta \theta \tag{3.2}$$

The barred quantities are mean values and the lower case letters denote the fluctuating component of the instantaneous velocity. Also:

p=the density before heating or cooling g_{x} and g_{y} =the vectors of gravitational acceleration β =the coefficient of expansion of gas

0 =a characteristic temperature difference However, the x-direction for this case, is perpendicular to the direction of gravitational acceleration thus the buoyancy force term is zero for equation 3.1.

Now according to Boussinesq (1877)

$$-\overline{u}\overline{v} = \varepsilon_{m}\frac{\partial\overline{U}}{\partial y} \tag{3.3}$$

and thus equation 3.1 becomes

$$\overline{\overline{U}}\frac{\partial\overline{\overline{U}}}{\partial x} + \overline{V}\frac{\partial\overline{\overline{U}}}{\partial y} = \frac{1}{\sqrt{2}}\frac{\partial\overline{\overline{p}}}{\partial x} + \gamma \frac{\partial^2\overline{\overline{U}}}{\partial y^2} + \frac{\partial}{\partial y}\varepsilon_{m}\frac{\partial\overline{\overline{U}}}{\partial y}$$
(3.4)

The pressure term $\frac{\partial \bar{p}}{\partial x}$, may be neglected for the case of a wall jet, Glauert (1956), Schwarz and Cosart (1961) and Myers et al (1963_a). Also the term representing the viscous shear stress may be neglected in the turbulent case since it is negligible compared to the turbulence shear stresses.

Equations 3.2 and 34 may be transformed into a dimensionless form. To do this, dimensionless quantities are defined as follows:

$$\overline{\overline{U}} = \frac{\overline{\overline{U}}}{\overline{U}_c}; \ \overline{\overline{V}} = \frac{\overline{\overline{V}}}{\overline{U}_c}; \ x = \frac{x}{h}; \ y = \frac{y}{h}; \ \varepsilon_m = \frac{\varepsilon_m}{\gamma}; \ \overline{p} = \frac{\overline{\overline{p}}}{\sqrt{U_c^2}}$$

where:

 $\overline{\mathbf{U}}_{\mathbf{c}}$ =a characteristic velocity

h =a characteristic length

Substituting into equations 3.2 and 3.4 for the dimensional variables in terms of the dimensionless quantities and simplifying, the following dimensionless form of equations 3.2 and 3.4 are obtained.

$$\overline{U} \cdot \frac{\partial \overline{U} \cdot \mathbf{i}}{\partial x \cdot \mathbf{i}} + \overline{V} \cdot \frac{\partial \overline{U} \cdot \mathbf{i}}{\partial y \cdot \mathbf{i}} = \frac{\gamma}{\gamma} \cdot \frac{\partial y}{\partial x} \epsilon_m \cdot \frac{\partial \overline{U} \cdot \mathbf{i}}{\partial y \cdot \mathbf{i}}$$
(3.5)

$$\frac{\partial \bar{\mathbf{p}}^{\dagger}}{\partial \mathbf{v}^{\dagger}} = g_{\mathbf{y}} \beta \Theta h / U_{\mathbf{c}}^{2}$$
 (3.6)

The body force term of equation 3.2 now appears as $g_y \beta \theta h/U_c^2$. This term is equal to the Grashoff number divided by the square of the Reynolds number as shown below.

$$\frac{g_{\mathbf{y}}\beta\Theta h}{U_{\mathbf{c}}^{2}} = \left(\frac{g_{\mathbf{y}}\beta\Theta h^{3}}{\gamma^{2}}\right)\left(\frac{\gamma}{U_{\mathbf{c}}h}\right)^{2} = Gr/Re^{2}$$
 (3.7)

Thus equation 3.6 may be written as:

$$\frac{\partial \overline{D}^{\,2}}{\partial y^{\,2}} = Gr/Re^2 \tag{3.8}$$

Prandtl's approximation to the turbulent energy equation of the boundary layer is given by Eckert and Drake (1959), pg. 219, as:

$$\overline{U}\frac{\partial \overline{I}}{\partial x} + \overline{V}\frac{\partial \overline{I}}{\partial y} = \frac{k}{\rho c_p} \frac{\partial^2 \overline{I}}{\partial y^2} - \frac{\partial}{\partial y} \overline{vt}$$
(3.9)

Boussinesq (1877) gives the relationship

$$-\overline{vt} = \varepsilon_{H\overline{\partial y}}^{\overline{d}}$$
 (3.10)

which when substituted into the boundary layer equation gives:

$$\frac{\vec{U}\frac{\partial\vec{T}}{\partial x} + \vec{V}\frac{\partial\vec{T}}{\partial y} = \frac{k}{\rho c_p} \frac{\partial^2\vec{T}}{\partial y^2} + \frac{\partial}{\partial y} \varepsilon_{H\partial y}^{H\partial y}$$
(3.11)

Indicating dimensionless quantities by primes as follows

$$\vec{\mathbf{U}} = \frac{\vec{\mathbf{U}}}{\vec{\mathbf{U}}_{\mathbf{C}}}; \vec{\mathbf{V}} = \frac{\vec{\mathbf{V}}}{\vec{\mathbf{U}}_{\mathbf{C}}}; \vec{\mathbf{T}} = \frac{\vec{\mathbf{T}}}{\Theta}; \vec{\mathbf{y}} = \frac{\mathbf{y}}{\mathbf{h}}; \mathbf{x} = \frac{\mathbf{x}}{\mathbf{h}}; \boldsymbol{\varepsilon}_{\mathbf{H}} = \frac{\boldsymbol{\varepsilon}_{\mathbf{H}}}{\alpha}$$

where:

0=a characteristic temperature difference and introducing these dimensionless quantities into the above equation we have after some simplification

$$\vec{\mathbf{U}}^{\dagger} \frac{\partial \vec{\mathbf{T}}^{\dagger}}{\partial \mathbf{x}} + \vec{\mathbf{V}}^{\dagger} \frac{\partial \vec{\mathbf{T}}^{\dagger}}{\partial \mathbf{y}^{\dagger}} = \frac{\alpha}{h \mathbf{U}_{\mathbf{C}}} \frac{\partial^{2} \vec{\mathbf{T}}^{\dagger}}{\partial \mathbf{y}^{\dagger 2}} + \frac{\alpha}{h \mathbf{U}_{\mathbf{C}}} \frac{\partial}{\partial \mathbf{y}} \varepsilon_{\mathbf{H}}^{\dagger} \frac{\partial \vec{\mathbf{T}}^{\dagger}}{\partial \mathbf{y}^{\dagger}}$$
(3.12)

where:

 $\alpha=k/\rho c_p$ =the thermal diffusivity

k=the thermal conductivity

c_p=the specific heat

The dimensionless group α/hU_c can be further simplified as shown below.

$$\alpha/hU_{c} = (\alpha/\gamma)(\gamma/hU_{c}) = 1/RePr$$
 (3.13)

where:

Pr=the Prandtl number

3.1b Order of magnitude analysis of the momentum equations

As was mentioned previously the body force term in the dimensionless form of equation 3.2 appears as the ratio Gr/Re^2 . This suggests that if the magnitudes of all the terms of the momentum equations could be determined, then it might be possible to predict the effect of the body

forces on the velocity field.

In order to carry out an order of magnitude analysis it is first necessary to evaluate the Reynolds number and Grashoff number. They are represented in the dimensionless form of the momentum equations as:

Re=
$$\overline{U}_c h/\gamma$$

Gr= $g_v \beta \theta h^3/\gamma^2$

 $\overline{\mathtt{U}}_{c}$, h and θ remain to be defined and the ratio Gr/Re^2 will depend strongly on their definition.

One way of defining \overline{U}_c , h and θ is:

h=L

$$\Theta = \triangle \overline{T}_1$$

Thus the Reynolds number and Grashoff number would be evaluated at the inlet. This is a convenient method. However, there is no reason to be certain that this will provide a representative ratio Gr/Re^2 .

Another way of evaluating Re and Gr is to define $\bar{\mathbb{U}}_{c}$, h and θ as follows:

$$\overline{U}_{c} = \overline{U}_{m}$$

$$h=\delta$$
t

$$\Theta = \triangle \overline{T}_m$$

where:

 δ_t =the thermal boundary layer thickness and the subscript m refers to the maximum value at any given longitudinal position. This would permit an order of magnitude

analysis at any particular longitudinal location in the wall jet and hopefully provide an indication of the body force effect on the velocity field. Since this system necessitates knowing values from experimental results, evaluation must follow experimentation. Therefore this system cannot be used for prediction but only as a tool for analyzing experimental results.

The method mentioned first, will be used in facilitating an order of magnitude analysis of the momentum equations.
Thus for the dimensionless quantities the following orders
of magnitudes could be expected.

<u>v</u> '=v/v	and	o≤Ū/Ū ₁ ≤1
⊽'= ⊽ /Ū ₁	and	o≤v/ū ₁ ≤.1
$x^{\dagger}=x/L$	and	0 <u>≤</u> x/L≤100
y • = y/L	and	0 ≤ y/L≤10
$\epsilon_{\mathbf{m}}^{\bullet} = \epsilon_{\mathbf{m}} / \gamma$	and	$\epsilon_{\rm m}/\gamma \approx 2 \times 10^3$

It is necessary to determine values of the Grashoff and Reynolds numbers to determine the order of magnitude of the buoyancy force term. This will be done for three different conditions. They are

1.
$$\bar{U}_1$$
=400 ft/min. and $\triangle \bar{T}_1$ =50°F

2.
$$\overline{U}_{i}=600$$
 ft/min. and $\triangle \overline{T}_{i}=50$ oF

3.
$$\overline{U}_1=800$$
 ft/min and $\triangle \overline{T}_1=50$ or

The value of the Grashoff number for all three conditions is 13,640 and the values of the Reynolds numbers are as follows:

$$Re_{12}=3140$$

$$Re_{13} = 5830$$

The ratios of the Grashoff number to the square of the Reynolds number are:

Condition 1 .00271

Condition 2 .00129

Condition 3 .00040

Equations 3.5 and 3.6 are written again with the estimates of the order of magnitude of each term indicated underneath.

$$\overline{U} \cdot \frac{\partial \overline{U} \cdot \mathbf{i}}{\partial \mathbf{x}} + \overline{V} \cdot \frac{\partial \overline{U} \cdot \mathbf{i}}{\partial \mathbf{y}} = \frac{1}{\text{Re}} \cdot \frac{\partial}{\partial \mathbf{y}} \mathbf{c}_{\mathbf{m}} \cdot \frac{\partial \overline{U} \cdot \mathbf{i}}{\partial \mathbf{y}}$$

1
$$\frac{1}{100}$$
 •1 $\frac{1}{10}$ $\frac{1}{Re_1}$ $\frac{2000}{10}$ $\frac{1}{10}$

$$\frac{\partial \vec{p}^{\dagger}}{\partial y^{\dagger}} = Gr/Re_1^2$$

Thus compared to the magnitude of the terms of the momentum equation the buoyancy force term has a magnitude; of the same order for condition 1, about one degree less for condition 2 and considerably less for condition 3. Therefore from this analysis it appears that buoyancy forces may be neglected for inlet velocities of approximately 800 ft/min and greater and inlet temperature differences of 50°F and less. Below 800 ft/min and at the higher temperature differences buoyancy forces may be appreciable.

3.2 Maximum Temperature Difference Decay and Thermal Boundary Layer Growth

For the case of a chilled ventilation wall jet it would be convenient to determine a relationship between the maximum temperature difference at any longitudinal position and the distance from the inlet. Such a relationship might provide a measure of the "cooling potential" of the wall jet for a given distance from the inlet.

Before proceeding further, another assumption in addition to the one of constant fluid properties, will be made. This assumption is that buoyancy forces can be neglected. As shown in the dimensional analysis, the validity of this assumption is dependent on the test conditions. However, most of the test conditions of this investigation will be within the limits prescribed for assuming negligible buoyancy effects.

In the general case of non-isothermal flow the momentum and heat energy equations mutually interact. When buoyancy forces are neglected and fluid properties are assumed to be independent of temperature, the velocity field no longer depends on the temperature field although the inverse of this statement does not apply. If similarity of velocity profiles applies for the case of the chilled wall jet it seems reasonable that similarity of temperature profiles might also apply.

The following development of a similarity solution of the turbulent energy equation closely parallels the similarity solution of the turbulent momentum equation by Schwarz and Cosart (1961).

Prandtl's approximation to the turbulent heat energy equation for steady, two-dimensional, turbulent and incompressible flow is given as:

$$\overline{U}\frac{\partial\overline{T}}{\partial x} + \overline{V}\frac{\partial\overline{T}}{\partial y} = \alpha \frac{\partial^2\overline{T}}{\partial y^2} - \frac{\partial \overline{V}\overline{V}}{\partial y} \tag{3.14}$$

Assuming that similarity of temperature profiles applies, similarity functions and a similarity transformation variable may be defined as follows.

$$\vec{\mathbf{U}} = \vec{\mathbf{U}}_{\mathbf{m}} \mathbf{f}(\mathbf{\eta}) \tag{3.15}$$

$$\bar{\mathbf{T}} = \bar{\mathbf{T}}_{\mathbf{m}} \mathbf{g}_{1} (\eta) \tag{3.16}$$

$$\overline{\mathbf{v}} \mathbf{t} = \overline{\mathbf{T}}_{\mathbf{m}} \overline{\mathbf{U}}_{\mathbf{m}} \mathbf{g}_{2}(\eta) \tag{3.17}$$

$$\eta = y/\delta_{+} \tag{3.18}$$

tethe thermal boundary layer thickness (not yet defined)

Tethe temperature difference between a point in the

wall jet and the ambient temperature in the venti-

lated space

Making use of the similarity functions and the similarity transformation the partial derivatives of the energy equation are evaluated as follows.

$$\frac{d\overline{T}}{dx} = g_1(\eta) \frac{\partial \overline{T}_m}{\partial x} - \frac{\overline{T}_m}{\delta_+} \frac{d\delta_t}{\partial x} \frac{\partial g_1(\eta)}{\partial \eta} \eta \qquad (3.19)$$

$$\frac{d\overline{T}}{dy} = \frac{\partial \overline{T}}{\partial g_1(\eta)} \frac{\partial g_1(\eta)}{\partial \eta} \frac{\partial \eta}{\partial y} = \overline{T}_m(\frac{1}{\delta_t}) \frac{\partial g_1(\eta)}{\partial \eta}$$
(3.20)

$$\frac{\mathrm{d}^2 \bar{\mathbf{T}}}{\mathrm{d}\mathbf{y}^2} = \frac{\partial}{\partial \mathbf{y}} \frac{\partial \bar{\mathbf{T}}}{\partial \mathbf{y}} = \frac{\partial}{\partial \eta} \frac{\partial \eta}{\partial \mathbf{y}} \frac{\partial \bar{\mathbf{T}}}{\partial \mathbf{y}} = \frac{\bar{\mathbf{T}}_{m}}{\delta_{+}^2} \frac{\partial^2 g_1(\eta)}{\partial \eta^2}$$
(3.21)

$$\frac{\partial \overline{\mathbf{v}} \mathbf{t}}{\partial \mathbf{y}} = \frac{\partial \overline{\mathbf{v}} \mathbf{t}}{\partial \mathbf{g}_{2}(\eta)} \frac{\partial \mathbf{g}_{2}(\eta)}{\partial \eta} \frac{\partial \eta}{\partial \mathbf{y}} = \frac{\overline{\mathbf{T}}_{m} \overline{\mathbf{v}}_{m}}{\delta_{\mathbf{t}}} \frac{\partial \mathbf{g}_{2}(\eta)}{\partial \eta}$$
(3.22)

 \vec{V} may be found in terms of \vec{U} by making use of the equation of continuity which is:

$$\frac{\partial o \overline{U}}{\partial x} + \frac{\partial o \overline{V}}{\partial y} = 0 \tag{3.23}$$

However the density is assumed to be constant thus the continuity equation becomes:

$$\frac{\partial \overline{U}}{\partial x} + \frac{\partial \overline{V}}{\partial y} = 0 \qquad \text{or} \qquad \frac{\partial \overline{V}}{\partial y} = -\frac{\partial \overline{U}}{\partial x} \qquad (3.24)$$

Integrating both sides yields:

$$\overline{V} = -\int_{0}^{Y} \frac{\partial}{\partial x} \overline{U} \partial y \tag{3.25}$$

Changing variables gives:

$$\overline{V} = -\frac{d}{dx}\overline{U}_{m}\delta_{t}\int_{0}^{\pi}f(\eta)\partial\eta \qquad (3.26)$$

The energy equation after making appropriate substitutions is:

$$\overline{U}_{\underline{m}} \frac{d\overline{T}_{\underline{m}}}{dx} f(\eta) g_{\underline{1}}(\eta) - \frac{\overline{U}_{\underline{m}} \overline{T}_{\underline{m}}}{\delta_{\underline{t}}} \frac{d\delta_{\underline{t}}}{dx} f(\eta) \frac{dg_{\underline{1}}(\eta)}{d\eta} \eta - (3.27)$$

$$\frac{\bar{T}_{m}}{\delta_{t}} \frac{dg_{1}(\eta)}{d\eta} \frac{d}{dx} \bar{U}_{m} \delta_{t} \int_{0}^{\eta} f(\eta) d\eta = \frac{\alpha \bar{T}_{m}}{\delta_{t}^{2}} \frac{d^{2}g_{1}(\eta)}{d\eta^{2}} - \frac{\bar{T}_{m}}{\delta_{t}} \bar{U}_{m} \frac{d}{d\eta} g_{2}(\eta)$$

And finally after some simplification the energy equation becomes:

$$\frac{\delta_{\mathbf{t}}}{\overline{\mathbf{T}}_{\mathbf{m}}} \frac{d\overline{\mathbf{T}}_{\mathbf{m}}}{d\mathbf{x}} \mathbf{f}(\eta) \mathbf{g}_{1}(\eta) - \frac{d\delta_{\mathbf{t}}}{d\mathbf{x}} \mathbf{f}(\eta) \frac{d\mathbf{g}_{1}(\eta)}{d\eta} \eta - \frac{\delta_{\mathbf{t}}}{d\mathbf{x}} \frac{d\mathbf{g}_{1}(\eta)}{d\eta} \int_{0}^{\eta} \mathbf{f}(\eta) d\eta - \frac{\delta_{\mathbf{t}}}{\overline{\mathbf{U}}_{\mathbf{m}}} \frac{d\overline{\mathbf{U}}_{\mathbf{m}}}{d\mathbf{x}} \frac{d\mathbf{g}_{1}(\eta)}{d\eta} \int_{0}^{\eta} \mathbf{f}(\eta) d\eta = \frac{\alpha}{\delta_{\mathbf{t}}} \frac{d^{2}\mathbf{g}_{1}(\eta)}{d\eta^{2}} - \frac{d}{d\eta} \mathbf{g}_{2}(\eta)$$

For a turbulent flow condition the first term on the right hand side of the equation can be neglected as molecular heat diffusion is of a considerable smaller magnitude than the diffusion due to the eddy diffusivity for heat.

If the flow is similar the functions $f(\eta)$, $g_1(\eta)$ and $g_2(\eta)$ are independent of x thus the solution of 3.28 requires that the coefficients of the universal functions be either non-zero constants or zero. The coefficients are:

$$\frac{\delta_t}{T_m} \frac{dT_m}{dx}$$
, $\frac{d\delta_t}{dx}$ and $\frac{\delta_t}{\bar{U}_m} \frac{d\bar{U}_m}{dx}$

For a non-trivial solution the coefficients may be equated to constants and the resulting differential equations are solved as follows.

$$\frac{\mathrm{d}\delta}{\mathrm{d}x} = \mathrm{C}_{\mathrm{o}} \tag{3.29}$$

Therefore:

$$\delta_{t} = C_{0}x + C_{1} \tag{3.30}$$

This may be rewritten as:

$$\delta_{t} = C_{0}(x + C_{3}) \tag{3.31}$$

where:

$$C_0C_3 = C_1 \tag{3.32}$$

Thus C_3 may be viewed as the distance to the virtual origin or $C_3=x_0$ where x_0 is the distance to the virtual origin. Figure 3.1 shows the relationship between δ_t , x and x_0 . Therefore:

$$\delta_{t} = C_{o}(x + x_{o}) \tag{3.33}$$

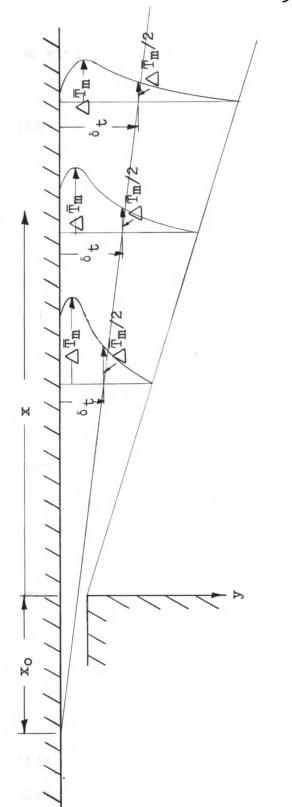


Figure 3.1 -- A schematic view of the thermal boundary layer of the wall jet

and a simple transformation where:

$$\mathbf{x}^* = \mathbf{x} + \mathbf{x}_0 \tag{3.34}$$

yields:

$$\delta_{t} = C_{0}x^{\dagger} \tag{3.35}$$

Now let:

$$\frac{\delta_{t}}{\overline{T}_{m}} \frac{d\overline{T}_{m}}{dx^{*}} = C_{\mu} \tag{3.36}$$

Substituting the relationship for δ and separating variables yields:

$$\frac{d\bar{T}_{m}}{\bar{T}_{m}} = \frac{C_{4}}{C_{o}} \frac{dx^{\dagger}}{x^{\dagger}} \tag{3.37}$$

Let

$$C_{4}/C_{0} = b$$
 (3.38)

Performing the integration yields:

$$ln\bar{T}_{m} = blnx^{\dagger} + lnC_{5}$$
 (3.39)

This simplifies to:

$$ln\bar{T}_{m} = lnC_{5}x^{\dagger b}$$
 (3.40)

Therefore:

$$\bar{\mathbf{T}}_{\mathbf{m}} = \mathbf{C}_{5} \mathbf{x}^{*b} \tag{3.41}$$

Now let:

$$\frac{\delta_{t}}{\overline{U}_{m}} \frac{d\overline{U}_{m}}{dx} = C_{6} \tag{3.42}$$

Substituting for $^{\delta}$ _t, separating variables, integrating and simplifying the results yields:

$$\overline{U}_{m} = C_{7}x^{*a} \tag{3.43}$$

This is the relationship derived by Schwarz and Cosart (1961)

from the momentum boundary layer equation.

Under the previous assumption, that buoyancy forces are negligible, the above similarity analysis applies to flow in either the horizontal or vertical direction. It would also apply equally well to a chilled or a heated jet of air.

Boundary conditions have not been explicitly included in the above development. However the assumption that the coefficients of equation 3.28 are constant with respect to x, implies that the wall temperature is constant in the x-direction. The validity of this assumption remains to be checked from the experimental data.

From the analysis of the energy equation and assuming that similarity holds for the temperature profiles, it may be seen that the growth of the temperature boundary layer is a linear function of x while the decay of the maximum temperature difference is a power function of x. The constants and exponent must be determined experimentally.

4. EXPERIMENTAL PROCEDURE

AND EQUIPMENT

4.1 Equipment

All tests were conducted in a large room where the temperature could be held to within $\pm 2^{\circ}F$ during any one test period. An overall view of the experimental equipment is shown in Figure 4.1.

An arrangement consisting of a slotted inlet adjacent to a section of ceiling provided the simulated ventilation system which was investigated. This is shown in Figure 4.2.

A schematic view of the nozzle-plenum assembly which formed the two-dimensional inlet is shown in Figure 4.3. The perforated sheets used in the assembly were made of 11 gauge material. The open area of the sheet constituted 25% of the total area and the diameter of the perforations was 0.20 inches. The nozzle consisted of two sections made of carefully rounded sheet metal and mounted on a wooden frame. The lips of the nozzle were formed by bars of cold rolled steel thus providing a sharp corner for the nozzle exit. The nozzle height was .49 inches and its width was 48 inches.

The velocity profiles at the nozzle were measured at three locations along the length of the nozzle. These locations were two inches from either end and midway between the ends. No significant difference could be found in either the



Figure 4.1 -- Overall view of the experimental equipment



Figure 4.2-- Ceiling with adjacent slotted inlet, thermocouples indicated by lighter areas in the center

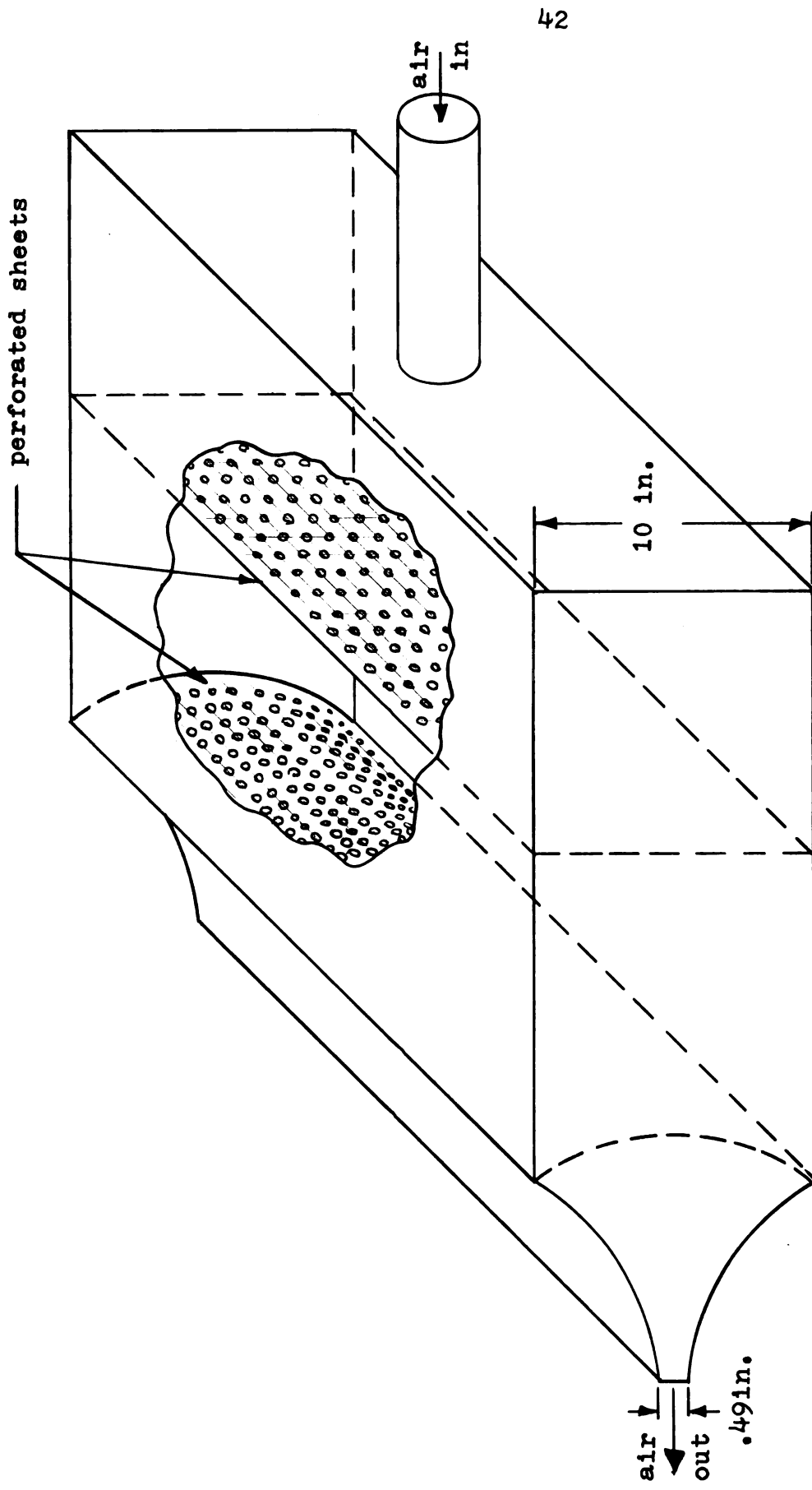


Figure 4.3-- A schematic view of the nozzle-plenum assembly

shape of the velocity profiles or the velocity magnitude, between these positions. This was done for three different inlet velocities. Thus it was believed that this indicated a very good representation of two-dimensional flow.

The ceiling was formed with one and one-half 4x8 sheets of 3/4 inch thick plywood which were fastened by screws to a ceiling stud assembly. The plywood was finished with three coats of plane Dura Seal and sanded after each coat to provide a relatively smooth surface. The 2x4 ceiling studs were constructed by gluing and nailing together 2 inch wide by 8 foot strips of 1/2 inch thick plywood. The edges of each laminated 2x4 were then run over a jointer to insure as straight an edge as possible. A screw jack was mounted on each leg for leveling the ceiling assembly.

Sides four feet high were provided to insure the maintenance of two-dimensional flow conditions.

A centrifugal type fan with a constant speed 5 h.p. electric motor was used to provide the air flow. The air velocity at the inlet was controlled by a slide arrangement at a mixing box. The inlet air velocity was determined by measuring the flow rate through a venturi. The venturi was calibrated using a Meriam Laminar Flow Meter, Model 50MC2-4P. A total head pitot tube was used at the inlet as a means of checking the inlet velocity. Micro-manometers each with an accuracy of ±.001 inches of water were used to measure the pressure. The venturi and manometer are shown in Figure 4.4.



Figure 4.4-- Venturi and manometer used in measuring the air-flow rates

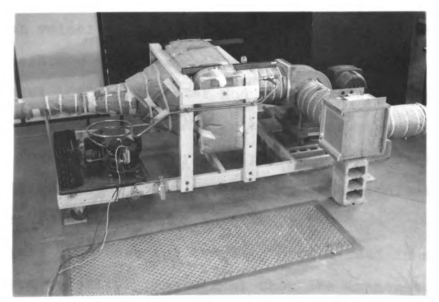


Figure 4.5-- Temperature control units, fan and mixing box

The inlet air temperature was controlled by connecting a commercial ceiling type evaporator unit, with accompanying compressor, to the outlet side of the fan. It was found necessary to connect the fan inlet, via a mixing box, to the cold outside air source for the lowest temperature tests.

The mixing box enabled either cold outside air, warm room air or a mixture of the two to be the source air depending on the test being run. Figure 4.5 shows a view of this part of the equipment. All ducts, the fan, the evaporator and the nozzleplenum assembly were insulated with two inches of Owens-Corning Fiberglas bat-type insulation (k=.125 BTU/hr-in-OF).

Mean velocity was measured with a Thermo-Systems constant temperature anemometer (Model 1051 Monitor and Power Supply, Model 1053A Anemometer Module). The sensor element was of the hot-film type. All velocity measurements were corrected for temperature by multiplying the anemometer bridge voltage output by an appropriate dimensionless temperature ratio (see Appendix, section A.1).

Figure 4.6 shows the complete system used in measuring the mean velocity. The signal from the anemometer was fed to a Hickock digital voltmeter (Model DMS-3200) with an accuracy of ±1 for the last digit. At each transverse position with respect to the ceiling, ten readings were taken over a 20 second period. Since the digital voltmeter reads the instantaneous velocity the following relationship was

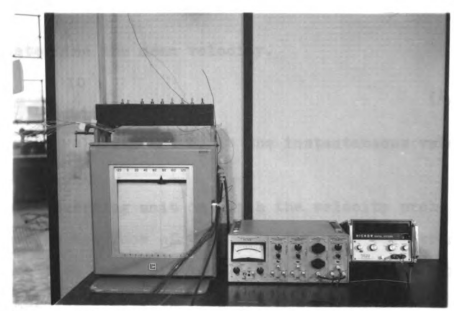


Figure 4.6 -- Temperature and velocity instrumentation



Figure 4.7-- Traversing mechanism with velocity probe and temperature sensing unit

used to determine the mean velocity.

$$\bar{U} = \frac{1}{10} \sum_{i=1}^{10} U_i$$
 (4.1)

 \overline{U} is the mean velocity and U_{1} is the instantaneous velocity at time i.

The traversing unit on which the velocity probe was mounted had an accuracy of $\pm .5$ mm in the vertical (transverse) direction and $\pm 1/16$ inch in the longitudinal direction. Figure 4.7 shows the traversing mechanism.

4.1b Mean temperature profiles

The mean temperature profiles were measured using nineteen. 30 gauge. copper-constantan thermocouples in a stack arrangement (Figure 4.8) plus an additional thermocouple imbedded in the ceiling surface for the ceiling surface temperature. The thermocouple junctions extended one inch beyond the wood support strips. Another thermocouple was placed on the traversing mechanism itself at a point where it was well outside of the thermal boundary layer for any particular flow situation studied. This temperature was considered to be the ambient temperature. Since temperature profiles were measured at eight stations with respect to the longitudinal distance from the inlet it was necessary to use a switching box to handle the eight thermocouples which were imbedded in the ceiling. All temperatures were recorded on a Leeds and Northrup Speedomax G, 24 point recording potentiometer with a print speed of 4 seconds, a temperature range of -20°F to 125°F and an accuracy of ±.25%

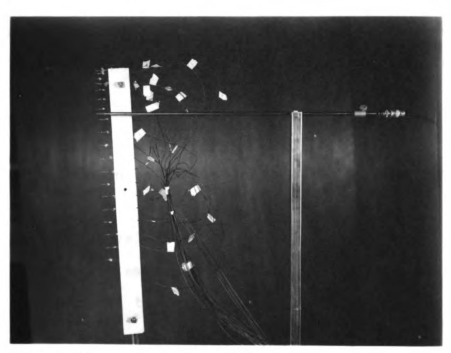


Figure 4.8-- Closeup view of velocity probe and thermocouple stack

of full scale reading.

All thermocouples were calibrated against a certified mercury in glass thermometer.

A means was provided for measurement of the heat transfer through the ceiling. A thermocouple was placed on the top side of the ceiling at station one. This provided the temperature differential at that point. The heat transfer rate was then determined from the temperature differential.

4.2 Scope of Tests

The independent variables studied in this investigation were:

- a. inlet velocity
- b. inlet temperature difference between the inlet air and the ambient air.

4.3 Experimental Procedure

Five inlet velocities were selected as being representative of those encountered in ventilation practices. These five were 1200, 1000, 800, 600 and 400 ft per min. For each velocity the isothermal case and those of 3 different temperature differences between the space air and the incoming air were investigated. The largest temperature differential case could not be reached for the 400 ft per min inlet velocity. Thus a total of nineteen tests were run.

All velocity and temperature profiles were measured

in a plane perpendicular to and midway from either end of the inlet. Eight stations were selected at distances of 8, 14, 22, 32, 44, 58, 72 and 90 inches from the inlet. Velocity and temperature profiles were determined at these stations only. These stations will be referred to henceforth as station numbers 1, 2, 3, 4, 5, 6, 7 and 8 respectively.

For the non-isothermal cases velocity and temperature profiles were measured simultaneously by placing the temperature and velocity sensing probes two inches apart and at the same longitudinal distance from the inlet (Figure 4.8).

The exact procedure was as follows. First the velocity profiles were measured for the isothermal case. Room, ambient (space), inlet and venturi air temperatures were monitored throughout the test to insure as close as possible, isothermal conditions. The venturi pressure differential and pitot tube pressure readings were taken throughout the test to insure a constant inlet velocity. Next the velocity and temperature profiles were measured for each of three different temperature differences between the space air and inlet air and at approximately the same velocity as used in the isothermal test. The temperature differences (henceforth reffered to as $\triangle T$) were:

 $\triangle \bar{\mathbf{T}}_1 \approx 20^{\circ} \mathrm{F}$, $\triangle \bar{\mathbf{T}}_2 \approx 40^{\circ} \mathrm{F}$ and $\triangle \bar{\mathbf{T}}_3 \approx 50^{\circ} \mathrm{F}$. As mentioned previously the $\triangle \bar{\mathbf{T}}_3$ condition could not be reached for the lowest inlet velocity of 400 ft per min. As implied above the inlet air velocity was not identical between the isothermal case and each of those for the non-isothermal cases.

however they were reasonably close. The largest velocity difference was 10.5% and the lowest was 0.25%. The average difference was 6.15%.

Only one transverse traverse was made to determine the velocity profile for each of the eight longitudinal stations. Three complete temperature profiles were measured during this same time for each station.

A considerable amount of time was allowed before each non-isothermal run in order for steady state temperature conditions to be reached. This condition was affirmed by noting when certain reference temperatures had reached steady state. These reference temperatures were the venturi air temperature, inlet air temperature and the ceiling temperature.

During preliminary non-isothermal tests it was noted that the experimental space temperature ran from two to four degrees Fahrenheith below that of the room air temperature. It seemed logical therefore to use the space temperature rather than the room temperature as a reference for taking into account any possible buoyancy effects.

The relative humidity of the ventilation air was not measured.

Table 4.1 indicates the inlet velocity, the inlet temperature difference, the slot inlet Reynolds number and the inlet Grashoff number, for each test.

Table $\psi_{\bullet}1$ Velocity and temperature conditions for all tests

Test No.	<pre>Inlet Velocity (ft/sec)</pre>	Inlet Temperature Difference (°F)	Inlet Reynolds Number	Inlet Grashoff Number
たつ ひよ	22.8 20.6 20.4 20.5	1sothermal 20.7 41.8 52.3	5620 5690 6030 6140	4,130 9,890 12,820
87.60	116.0 16.6 16.6 16.6	1sothermal 21.3 40.0 54.8	4220 4410 4930 5050	3,990 9,600 13,430
1100	11122	1sothermal 21.8 41.4 55.1	3380 3490 3730 3810	4,200 9,410 13,650
1111 64 <i>7</i> 20	10 90.5 10.3 6.3	1sothermal 21.9 38.5 50.1	1840 2580 2650 3090	4.170 8.640 12.280
17 18 19	7.5	1sothermal 18.2 40.8	1840 1830 2120	3,350 9,030

5. EXPERIMENTAL RESULTS

5.1 Mean Velocity Results

The mean velocity profiles indicated some scattering occurring with increased distance from the inlet. This condition was accentuated with decreasing slot inlet velocities. It was felt that the major contributing factor for this was a probable increased scale of turbulence occurring at the lower mean velocities. Figure 5.1 shows a mean velocity profile typical of those which were on the least end of the scatter spectrum. Figure 5.2 shows a mean velocity profile representative of those exhibiting a greater degree of scatter.

A previous assumption was made that the velocity fields of this two-dimensional, chilled wall jet conformed to the similarity conditions of a two-dimensional, turbulent wall jet. The theory of Schwarz and Cosart (1961) will be used to check this assumption.

Schwarz and Cosart found a number of conditions to characterize the velocity field of a two-dimensional, turbu-lent wall jet. Two of them were:

- 1. The mean velocity profiles, at different longitudinal positions with respect to the inlet, were similar when $\overline{U}/\overline{U}_m$ was plotted versus y/δ_m .
- 2. The decay of maximum velocity was described by a

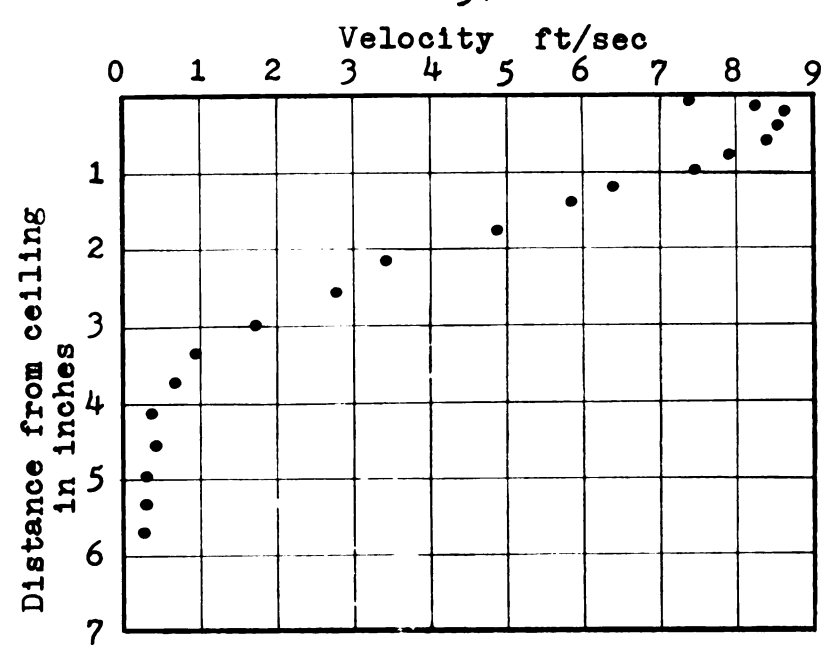


Figure 5.1-- Mean velocity profile for station 3, test 2, \bar{U}_1 =1225 ft/min

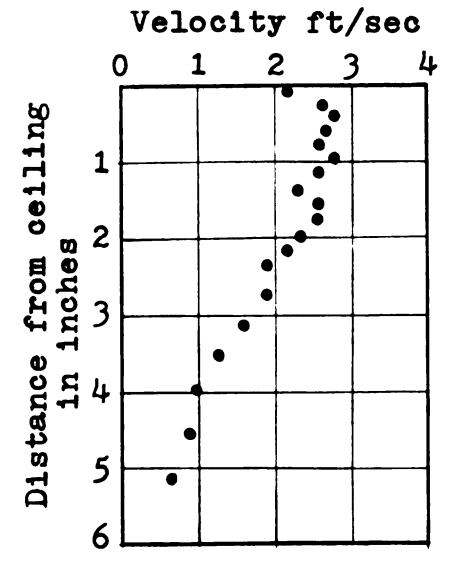


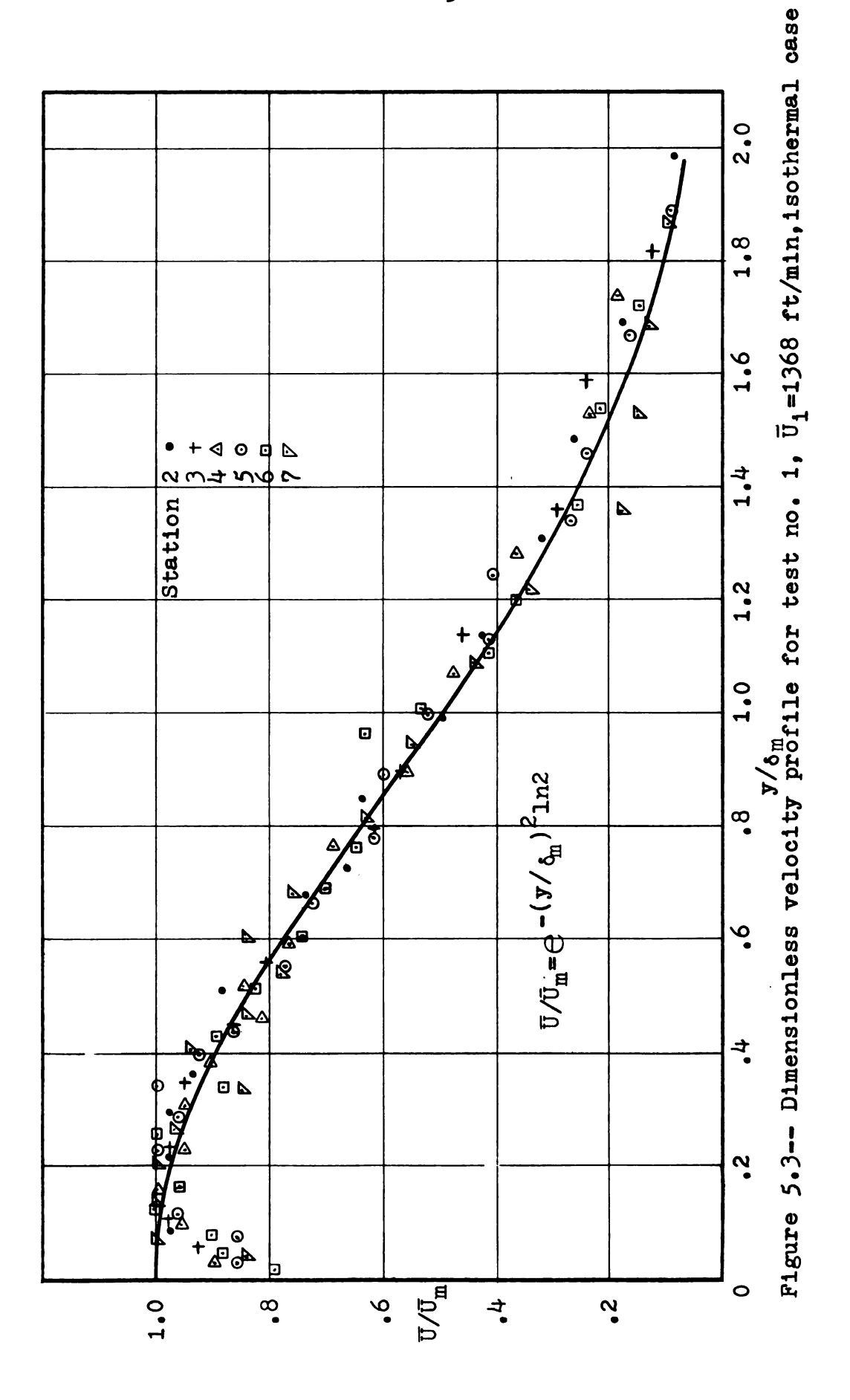
Figure 5.2-- Mean velocity profile for station 3, test $17,\overline{U}_1=450$ ft/min

power law of the form $\bar{U}_m/\bar{U}_1=C_7(x^*/L)^a$. If the velocity fields of this investigation can be characterized as a turbulent wall jet then they should exhibit the above characteristics.

The mean velocity profiles from the various stations for each test were plotted on a dimensionless basis, that is, by plotting $\overline{U}/\overline{U}_m$ versus y/δ_m . \overline{U}_m and δ_m were determined by observation from the measured mean velocity profiles. Figure 5.3 indicates such a plot for the results of Test no.1 (1200 ft/min inlet velocity range, isothermal). The velocity profiles from stations 2, 3, 4, 5, 6 and 7 are congruent. There is a reasonably close grouping of the experimental points. The value of y/δ_m for which $\overline{U}=\overline{U}_m$, appears to be approximately .2 which concurs with the findings of Schwarz and Cosart. Thus from the standpoint of congruency of velocity profiles, similarity of the mean velocity profiles does apply for Test no. 1.

Attempts have previously been made to fit various types of curves to the dimensionless velocity profiles. Schwarz and Cosart (1961) tried fitting two types of curves to the outer portion of their measured profile. Neither curve described their data particularly well. However, the basic assumption made by investigators of wall jets, that the outer portion behaves much like a free jet, encourages trying to fit a known solution of a free jet. To this end an exponential curve due to Reichardt (1941) was tried.

Reichardt's inductive theory of free turbulence has



often been used by researchers in their investigations of free jets. For a thorough discussion of his theory, Schlichting (1962) or Hinze (1959) may be consulted. Reichardt's theory offers an exponential relationship,

$$\frac{\overline{U}}{\overline{U}_{m}} = \exp\left(\frac{y}{2 c_{m} x}\right)^{2} \tag{5.1}$$

as representing the mean velocity profiles in free jet flow. C_m is a velocity spreading coefficient, y is the transverse distance and x is the longitudinal distance. If $y = \delta_m$ is defined as the transverse distance to where $\bar{U} = \bar{U}_m/2$, it follows that:

$$\exp - \left(\frac{\delta^{\frac{2}{m}}}{2c_{m}^{2}x^{2}}\right) = \frac{1}{2}$$
 (5.1a)

from which

$$2C_{\rm m}^2 x^2 = \frac{\delta_{\rm m}^2}{3n^2} \tag{5.2}$$

Substitution of this expression into equation 5.1 yields

$$\frac{\overline{U}}{\overline{U}_{m}} = \exp -(\frac{y^{2}}{\delta_{m}^{2}} \ln 2)$$
 (5.3)

This expression for $\overline{\mathbb{U}}/\overline{\mathbb{U}}_m$ does not contain any arbit-rary constants.

Schwarz and Cosart attempted to fit an exponential curve to their data points by matching them at the points where $\overline{U}/\overline{U}_m=1$. However, if the exponential curve represented by equation 5.3 above is matched to the experimental data of Figure 5.3 by placing the $\overline{U}/\overline{U}_m=1$ ordinate of the exponential curve, at the ceiling, the data points from $y/\delta_m=0.3$ and

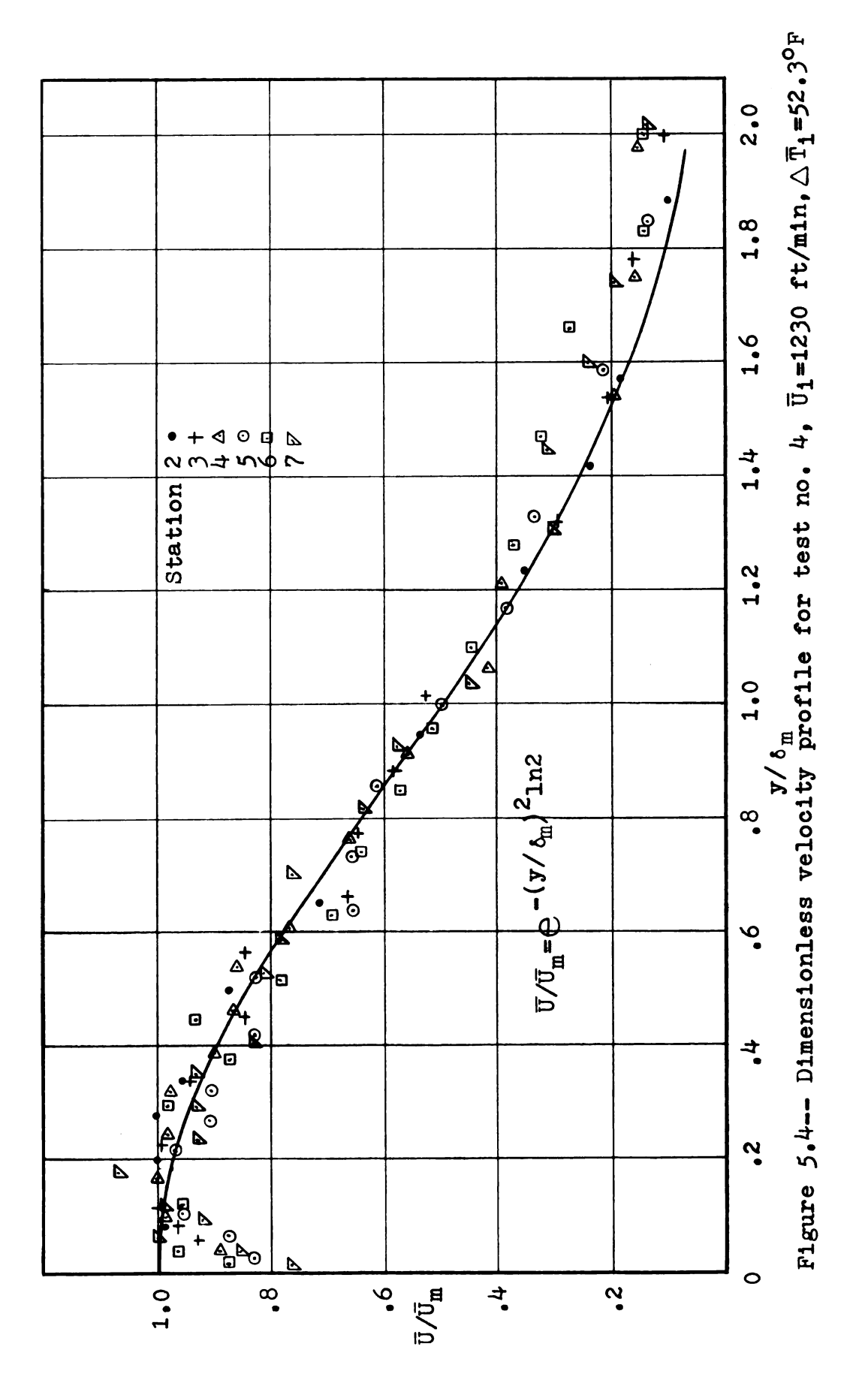
greater are represented quite well. Reichardt's form of the velocity profile implies a constant coefficient of the eddy diffusivity for momentum. Therefore, based on the close fit between the exponential curve of Reichardt and the data points for the outer part of the wall jet, it appears that Glauert's (1956) assumption of a constant eddy diffusivity for momentum in this area, is indicated for Test no. 1.

Figure 5.4 shows the dimensionless velocity profile for Test no. 4 (1200 ft/min inlet velocity range, $\Delta \bar{T}=52.3^{\circ}F$). The conclusions reached concerning Test no. 1 apply equally well to the results of this test, with one exception. The exception is, that there is some deviation between the exponential curve due to Reichardt and the data points beyond $y/\delta_m=1.4$. However, this region is the intermittant region of the boundary layer and no corrections were made for intermittancy.

In comparing Figures 5.3 and 5.4 it appears that there was little temperature effect on the shape of the dimension-less velocity profile for the 1200 ft/min inlet velocity range.

The remarks concerning the dimensionless velocity profiles of Test nos. 1 and 4 can be extended to include Test nos. 2 and 3 ($\triangle \overline{T}=20.7^{\circ}F$ and $\triangle \overline{T}=41.8^{\circ}F$ respectively), the two remaining non-isothermal tests of the 1200 ft/min inlet velocity range.

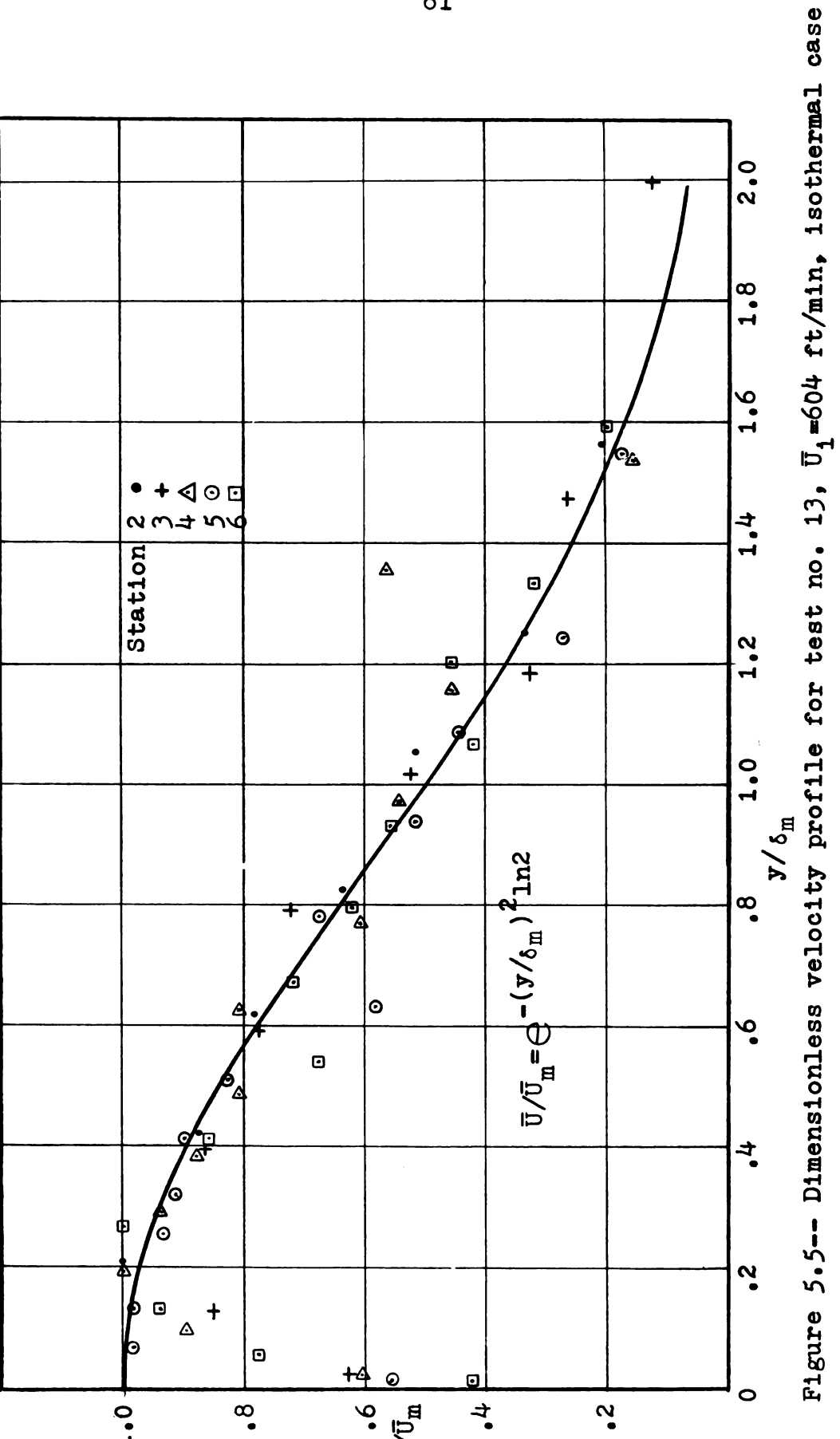
For the 1000 ft/min velocity range (Test nos. 5, 6, 7 and 8), the above remarks apply with one exception. There

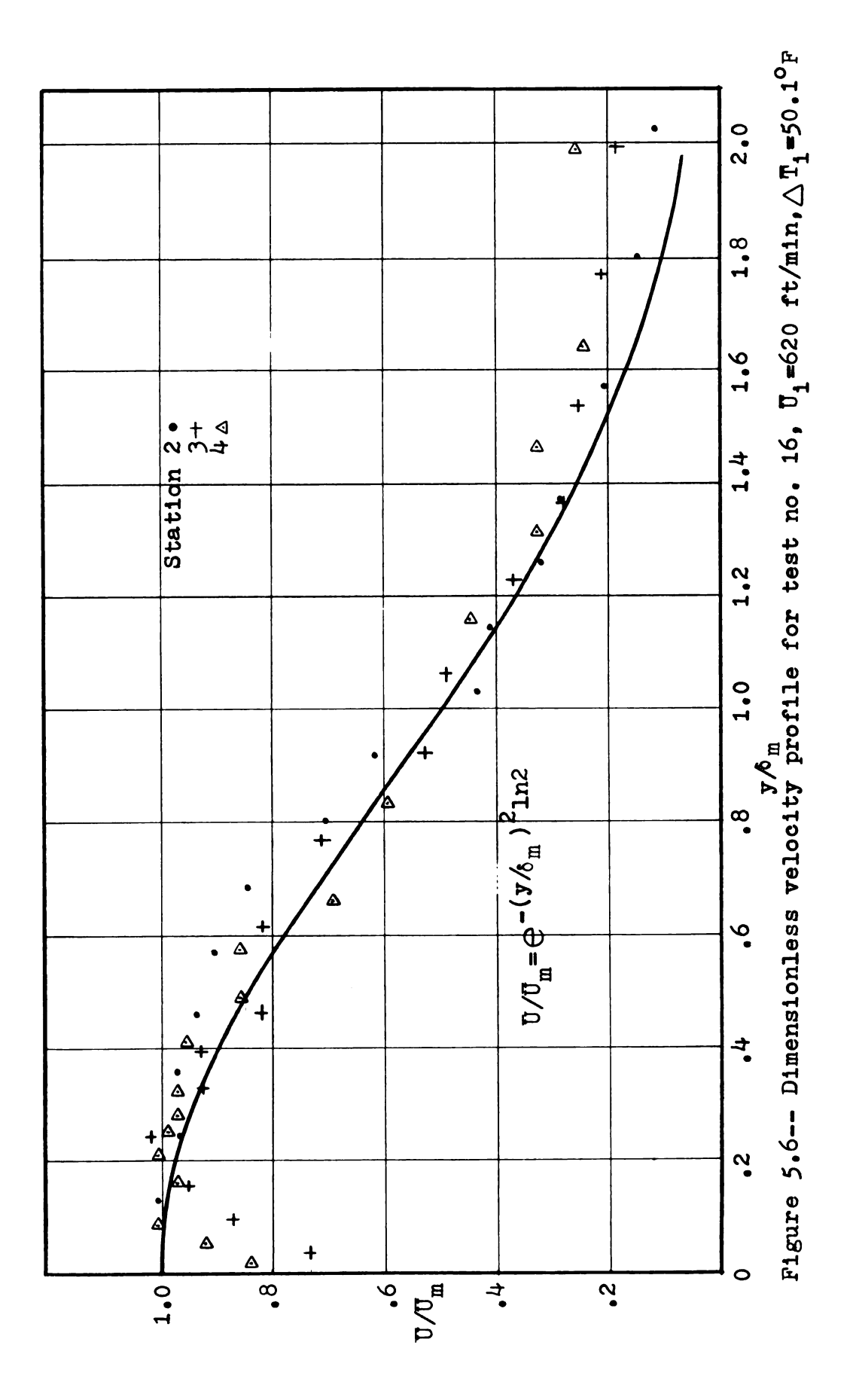


was slightly more scattering of the data points for these tests. The data for these tests, as well as that for all tests not presented in graphical form, are given in tabular form in the Appendix.

The dimensionless velocity profiles of Test nos. 9, 10, 11 and 12 (800 ft/min inlet velocity range), gave the same results as those of the 1200 and 1000 ft/min velocity ranges. However, there was slightly more scattering of the data points and the velocity profiles from stations 2, 3, 4, 5 and 6 only, were similar.

Figures 5.5 and 5.6 show the dimensionless velocity profiles from Tests 13 and 16 (600 ft/min inlet velocity range, isothermal case and $\Delta \overline{T} = 50.1^{\circ} F$ respectively). For Test 13 the velocity profiles at stations 2, 3, 4, 5 and 6 indicated that similarity applies. However for Tests 14. 15 and 16, only the velocity profiles from stations 2, 3 and 4 indicated similarity. The mean velocity profiles for stations 5 and 6 of Tests 14. 15 and 16 exhibited too much scatter to be able to determine with any reasonable accuracy a representative profile. Thus it was impossible to plot dimensionless profiles for these tests. The exponential curve provides a reasonable fit to the data of Test no. 13. However, it appears that the data of Test no. 16 deviates somewhat from the exponential curve for the region $.2 \le y/\delta_m \le$ The reason for this deviation cannot be ascertained exactly although a likely reason is, that it is due to temperature effects. Deviation of the data from the





exponential curve was also indicated for Tests 14 and 15 ($\triangle \bar{T}$ = 21.9°F and $\triangle \bar{T}$ =38.5°F respectively) although it was not quite as great as it was for Test 16. Further evidence of a possible temperature effect on the velocity field was the fact that the air flow became detached from the ceiling at station 7 for Tests 14, 15 and 16, while this was not true for Test 13. The 600 ft/min inlet velocity range was the highest one for which a temperature effect was indicated.

The dimensionless velocity profile for Test 17 (400 ft/min inlet velocity range, isothermal) indicated similarity for the velocity profiles from stations 2, 3, 4 and 5. The exponential curve provided a reasonably good fit of the data. The amount of scatter was greater than that found at the higher velocities. Dimensionless plots were not made for Tests 18 and 19 ($\Delta \bar{T}$ =18.2°F and $\Delta \bar{T}$ =40.8°F respectively). Although velocity profiles were measureable to station 7 for Test 17, the air flow became detached after station 5, for Tests 18 and 19. This detachment appears to indicate a temperature effect on the flow field.

The theory of Schwarz and Cosart (1961) indicated that the decay of maximum velocity follows a power law relationship of the form $\overline{U}_m = C_7 x^{*a}$. The determination of values for a, necessitates knowing the location of the virtual origin. The location of the virtual origin can be obtained from analyzing the data for the growth of the momentum boundary layer (e.g. using $\delta_m = C_1(x + x_0)$). However, it was felt that

the amount of scatter in the velocity profiles precluded an accurate determination of the location of \mathbf{x}_0 by this method. For this reason x instead of x' was used in analyzing the velocity decay data. Myers et al (1963_a) used this method for determining a in their investigation. In addition Kruka and Eskinazi (1964) arrived at a prediction equation for velocity decay of the same form as that of Schwarz and Cosart but used x in the actual determination of a.

 $\overline{U}_m/\overline{U}_1$ was plotted versus x/L on log-log paper for Tests 1 through 17. The data were handled in this dimensionless form because of its more universal applicability. The resulting plots indicated that for each test, most of the data points appeared to be well represented by a straight line. Accordingly a least squares method was used to determine best fit lines through the data points. A representative sample of the plots with their best fit lines are shown in Figures 5.7,5.8,5.9, and 5.10. The values of C_7 and the exponent a for the rest of the tests, along with the number of points used in determining the best fit lines is shown in Table 5.1.

The average value of the exponent a for all the tests is -.530. This compares with a value of -.49 found by Myers et al (1963_a) and a value of -.55 by Schwarz and Cosart (1961). The higher value of Schwarz and Cosart cannot be compared directly with the values found by Myers et al or this investigator. The reason for this is that using x' (adding the virtual origin to x) for determining a, auto-

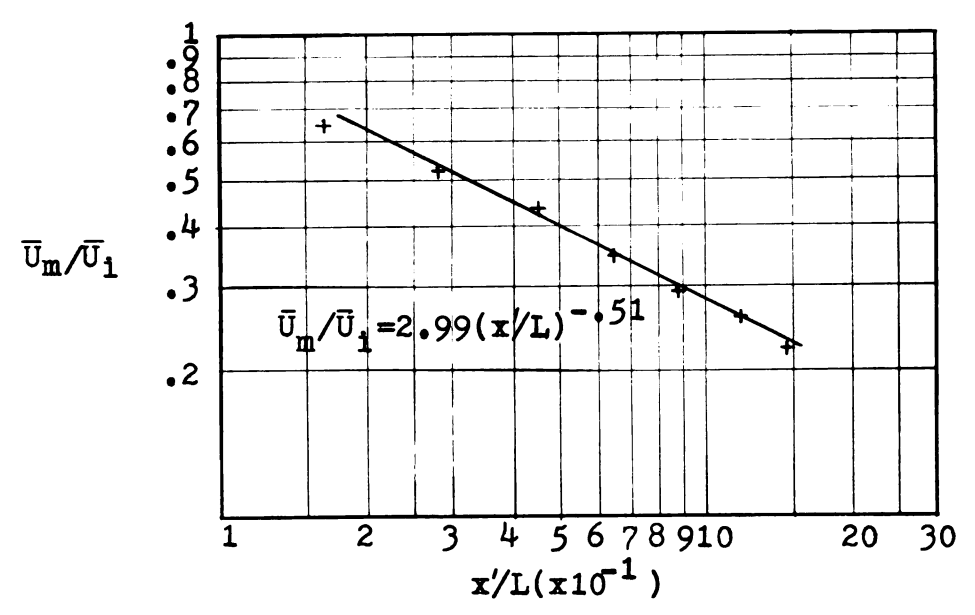


Figure 5.7-- Velocity decay results for test no. 8, \overline{U}_1 =1015 ft/min, $\triangle \overline{T}_1$ =54.8°F

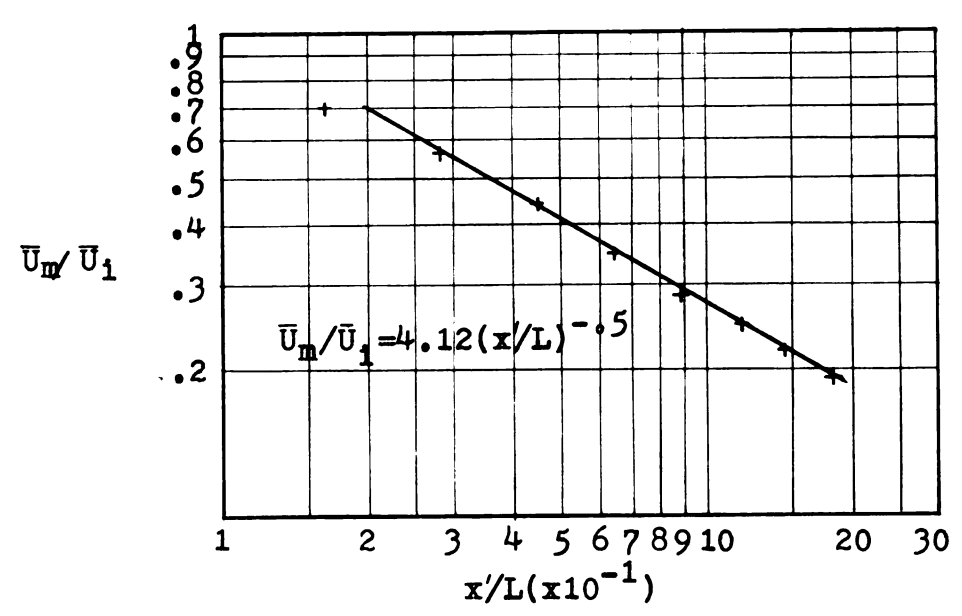


Figure 5.8-- Velocity decay results for test no. 1, \overline{U}_1 =1370 ft/min, isothermal case

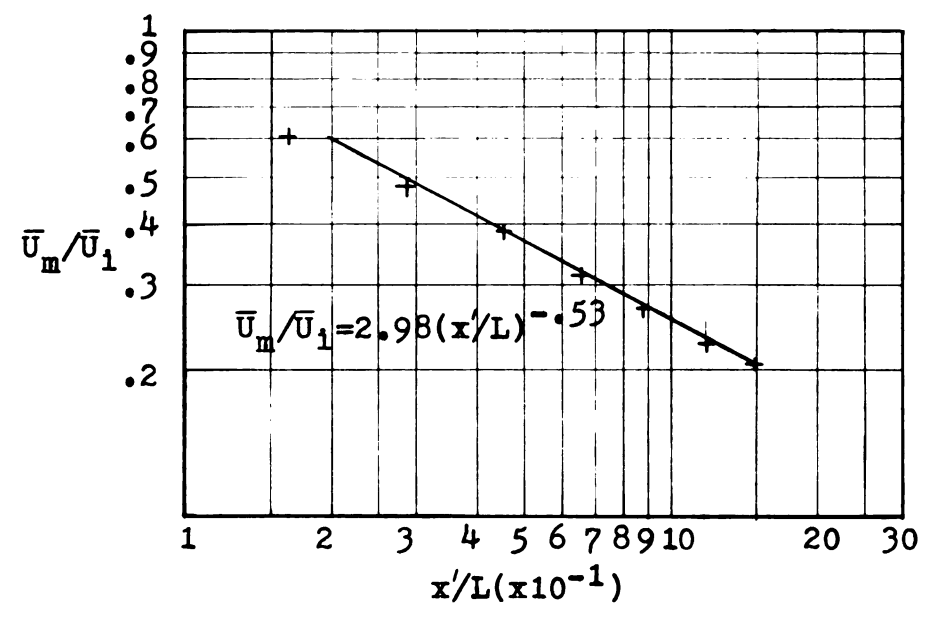


Figure 5.9-- Velocity decay results for test no. 9, \bar{U}_1 =767 ft/min, $\Delta \bar{T}_1$ =21.8°F

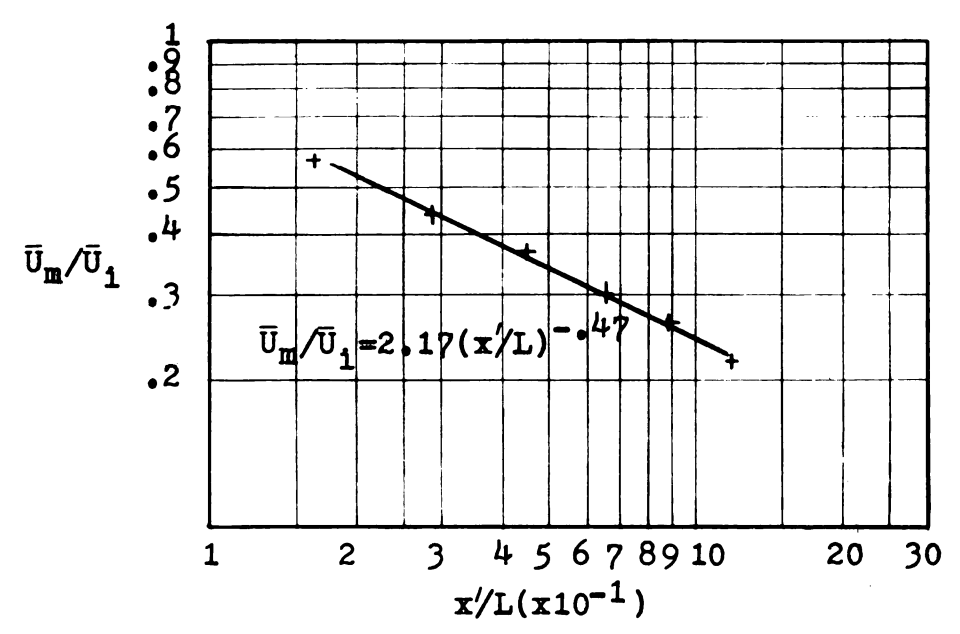


Figure 5.10-- Velocity decay results for test no. 17, \overline{U}_1 =450 ft/min, isothermal case

Table 5.1 Experimentally determined constants for velocity decay

Test No.	c ₇	а	Number of Points Used
1	4.12	 588	7
2	3.43	 553	7 ·
3	3.41	544	7
4	3.12	514	7
5	3.13	 526	7
6	3.69	572	7
7	3.16	547	7
8	2.99	514	6
9	3.08	 536	6
10	2.98	531	6
11	2.81	520	5
12	2.29	470	5
13	3.01	530	6
14	3.82	623	4
15	2.29	498	4
16	2.07	465	4
17	2.17	474	6

matically increases the value of a.

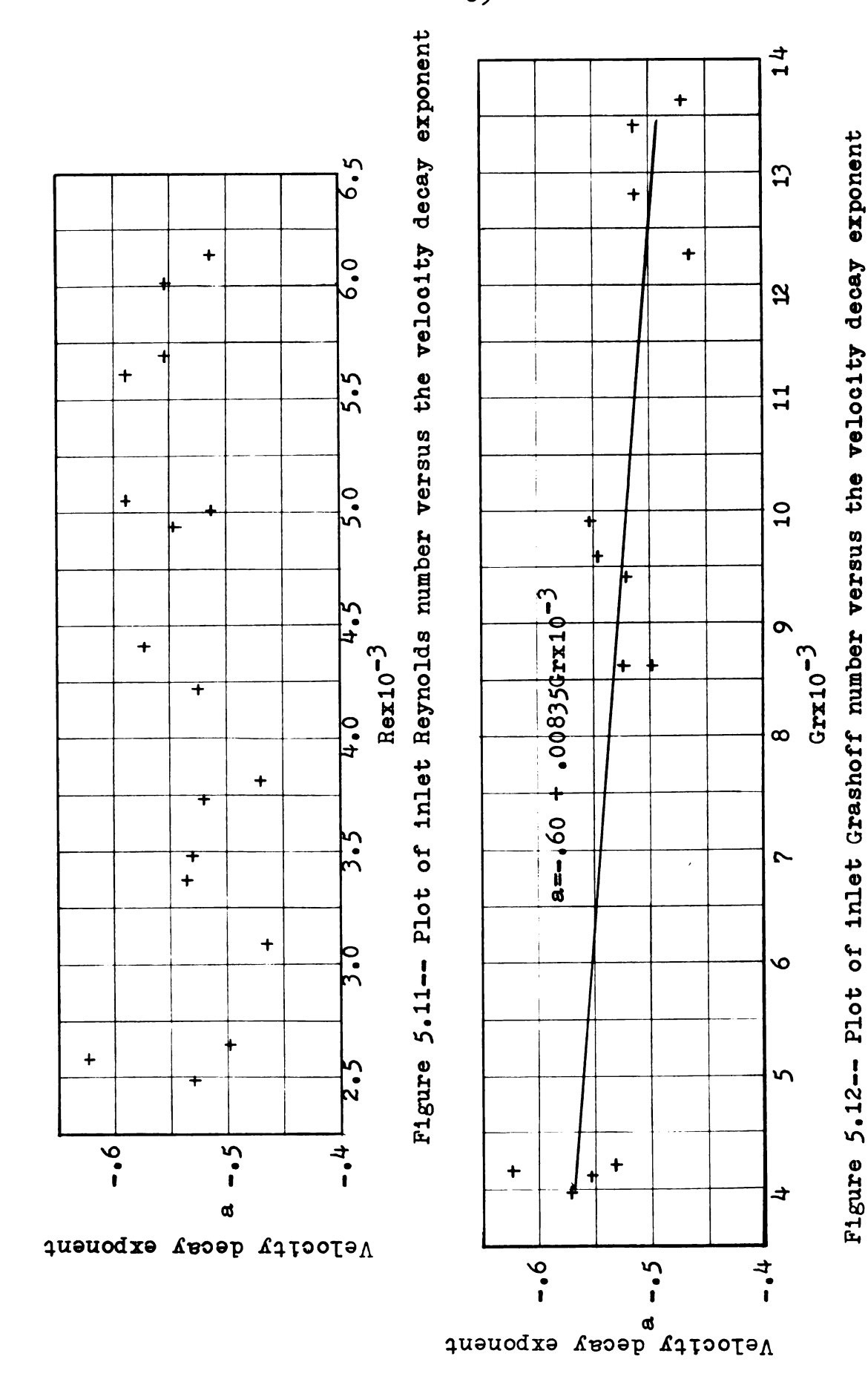
Figure 5.11 shows a plot of the exponent a versus the inlet Reynolds number. A best fit straight line was determined, however the correlation coefficient was very low indicating that a linear relationship was not applicable. It appears from the data that over the range of Reynolds numbers tested there was no functional relationship between the exponent a and the inlet Reynolds number.

A plot of the exponent a versus the inlet Grashoff number is shown in Figure 5.12. A least squares, best fit straight line is also indicated. The correlation coefficient was .73, indicating that the data were reasonably well correlated by a straight line. The data seemed to indicate a slight Grashoff number effect with lower values of the exponent occurring at the higher Grashoff number. This means that the rate of maximum velocity decay decreased with increasing temperature differences, for the range of inlet Reynolds numbers tested. No explanation was found in the literature which could provide any reason for such a result.

The results indicate that the velocity fields of these tests exhibited the characteristics of a two-dimensional, turbulent wall jet. This observation appears to apply better at the higher inlet Reynolds numbers.

5.2 Similarity of Mean Temperature Profiles

In the analysis phase of this investigation, the assumption was made that similarity applied for the mean



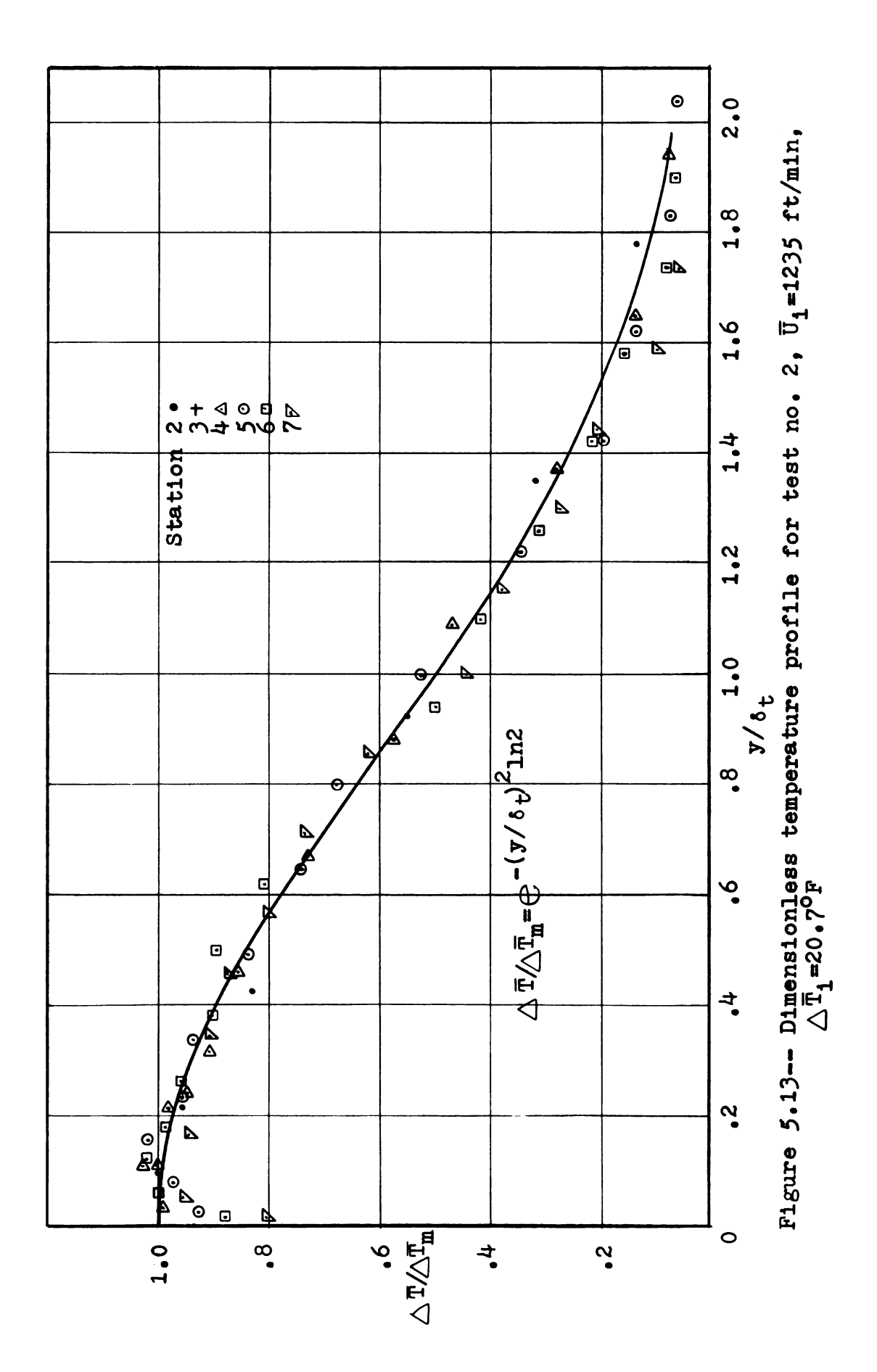
temperature profiles. If this assumption is true the mean temperature profiles at different longitudinal positions with respect to the inlet (e.g. stations) will be congruent when plotted in a dimensionless form. The arbitrarily defined similarity function and similarity variable, $\mathbf{g}_1(\eta) = \Delta \overline{\mathbf{T}}/\Delta \overline{\mathbf{T}}_{m}$ and $\eta = \mathbf{y}/\delta_t$ respectively, were used in obtaining the dimensionless plot. The selection of a definition for δ_t is arbitrary. It was defined to equal the transverse distance \mathbf{y} , where $\Delta \overline{\mathbf{T}} = \Delta \overline{\mathbf{T}}_{m}/2$. This is analogous to the mean velocity case.

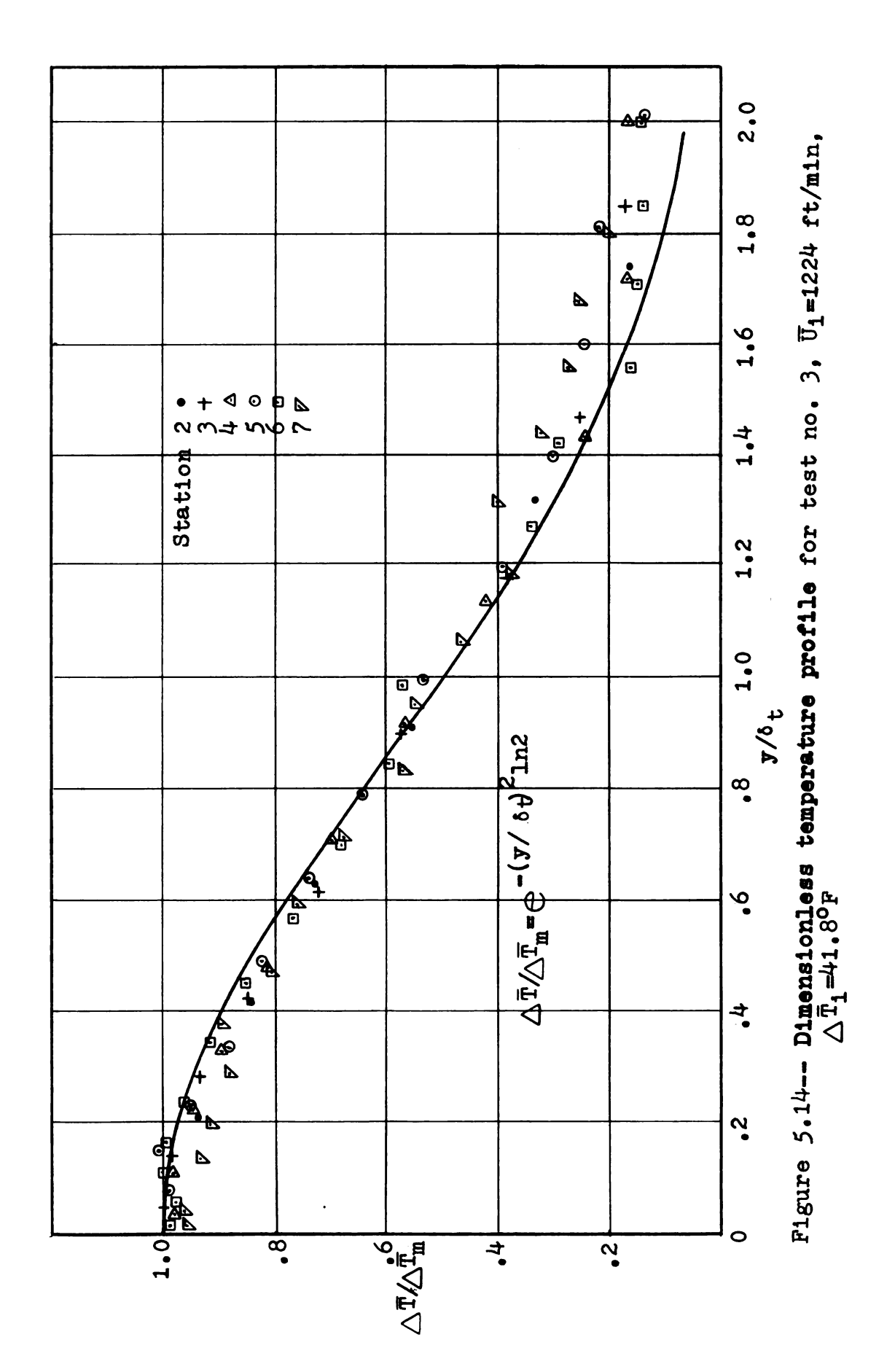
Using the above definition of δ_t , dimensionless plots of $\triangle \bar{T} /\!\!\! \triangle \bar{T}_m$ versus y/δ_t were made for non-isothermal tests, 2 through 19.

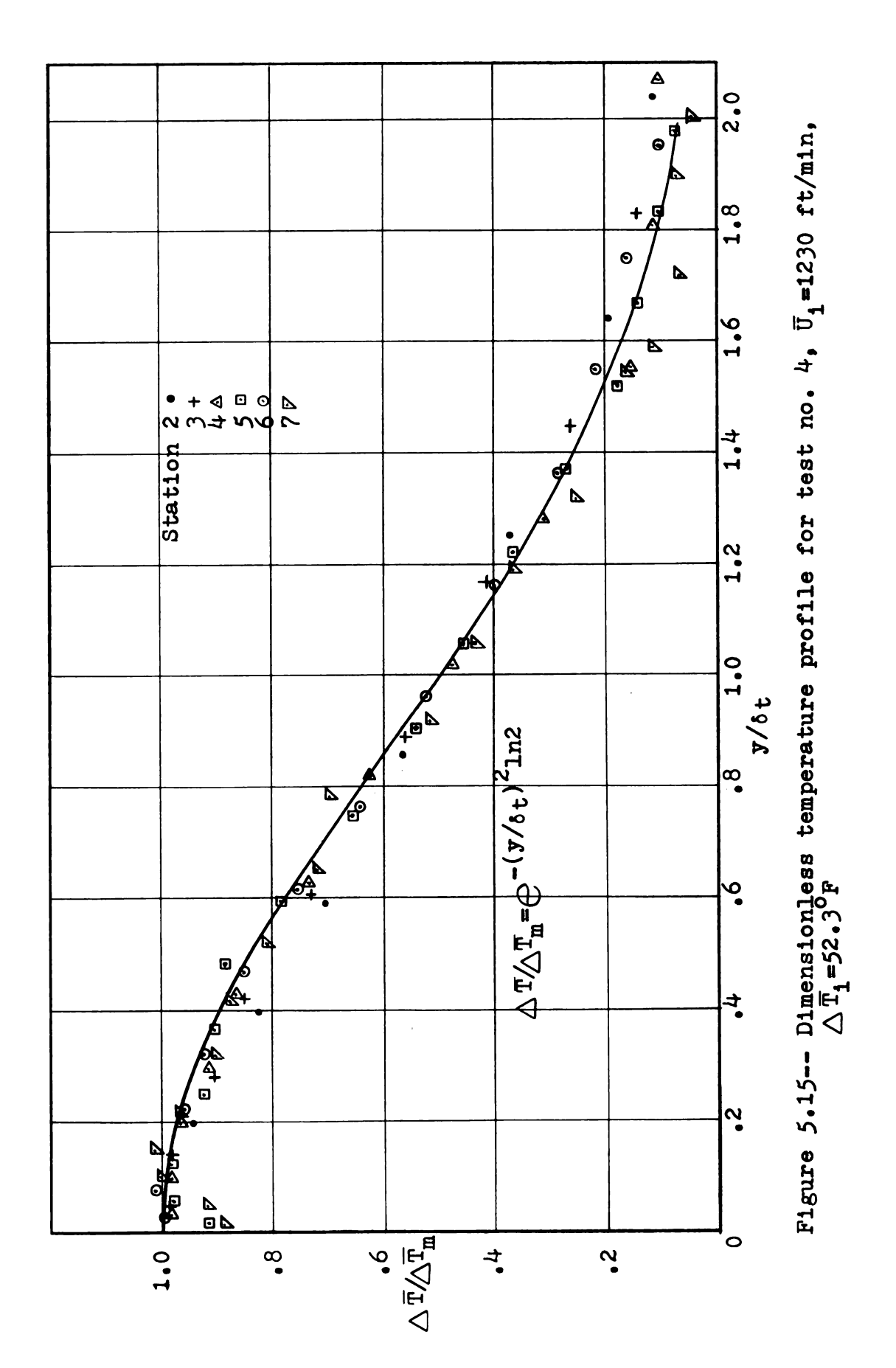
For the 1200 ft/min inlet velocity range (Tests 2, 3, and 4) the dimensionless profiles from stations 2, 3, 4, 5, 6 and 7 appear to be similar. There was a reasonably tight grouping of the data for these three tests. Figures 5.13, 5.14 and 5.15 show the data.

It would be advantageous to be able to describe the dimensionless temperature profile with some type of curve. It was found that an exponential curve due to Reichardt (1941) approximated the data points in the outer portion of the dimensionless velocity profiles quite well, for nearly all of the tests. Reichardt further hypothesized the following relationship describing the mean temperature profile for a free jet.

$$\frac{\triangle \bar{T}}{\triangle \bar{T}_{m}} = \exp -\left(\frac{y}{2 c_{m} x}\right)^{2} \tag{5.4}$$







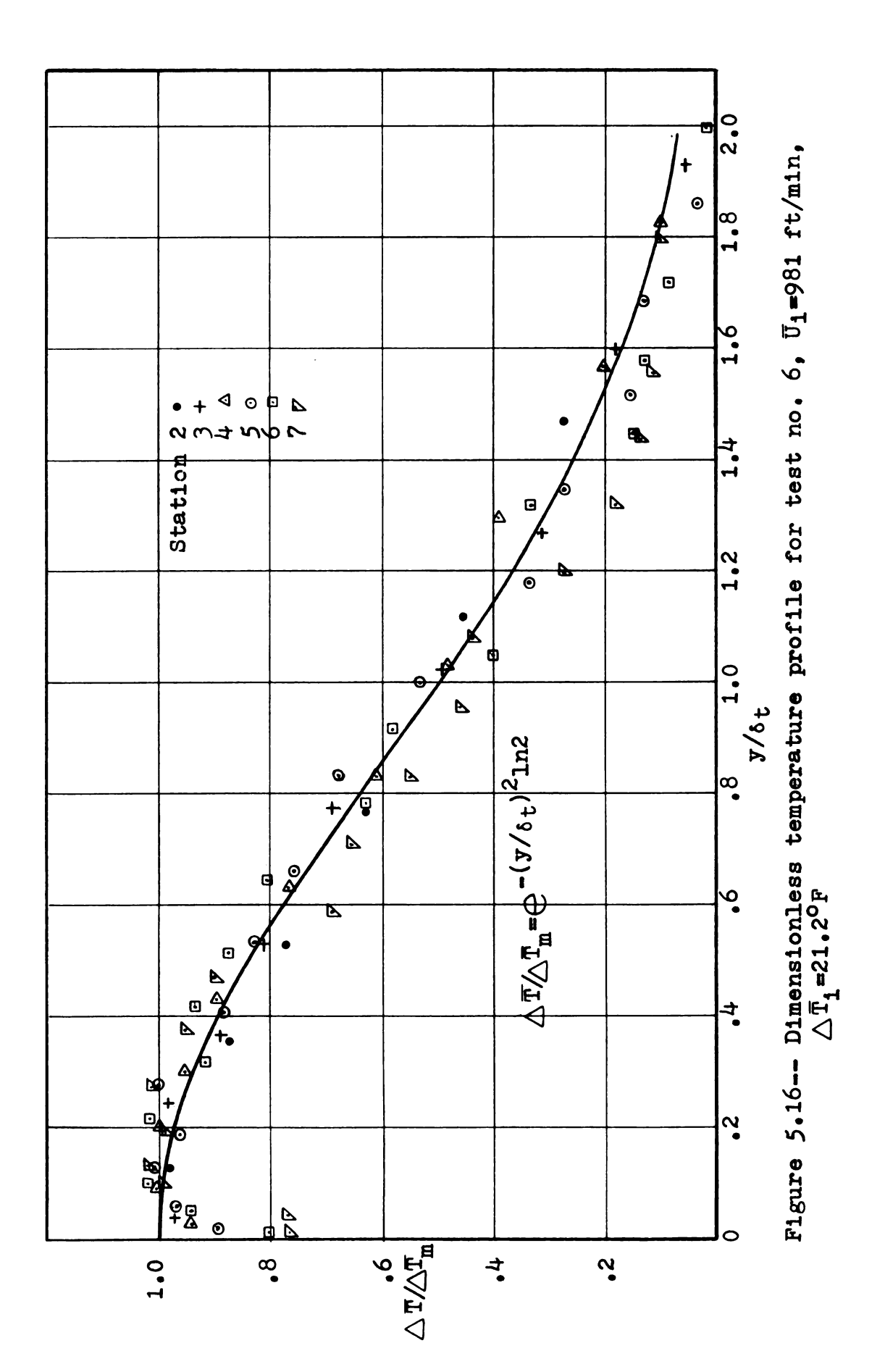
 $C_{\overline{T}}$ is a temperature spreading coefficient analogous to the velocity spreading coefficient. By defining $y=\delta_{\overline{t}}$ as the transverse distance to where $\triangle \overline{T}=\triangle \overline{T}_m/2$ the following form of equation 5.4 is obtained.

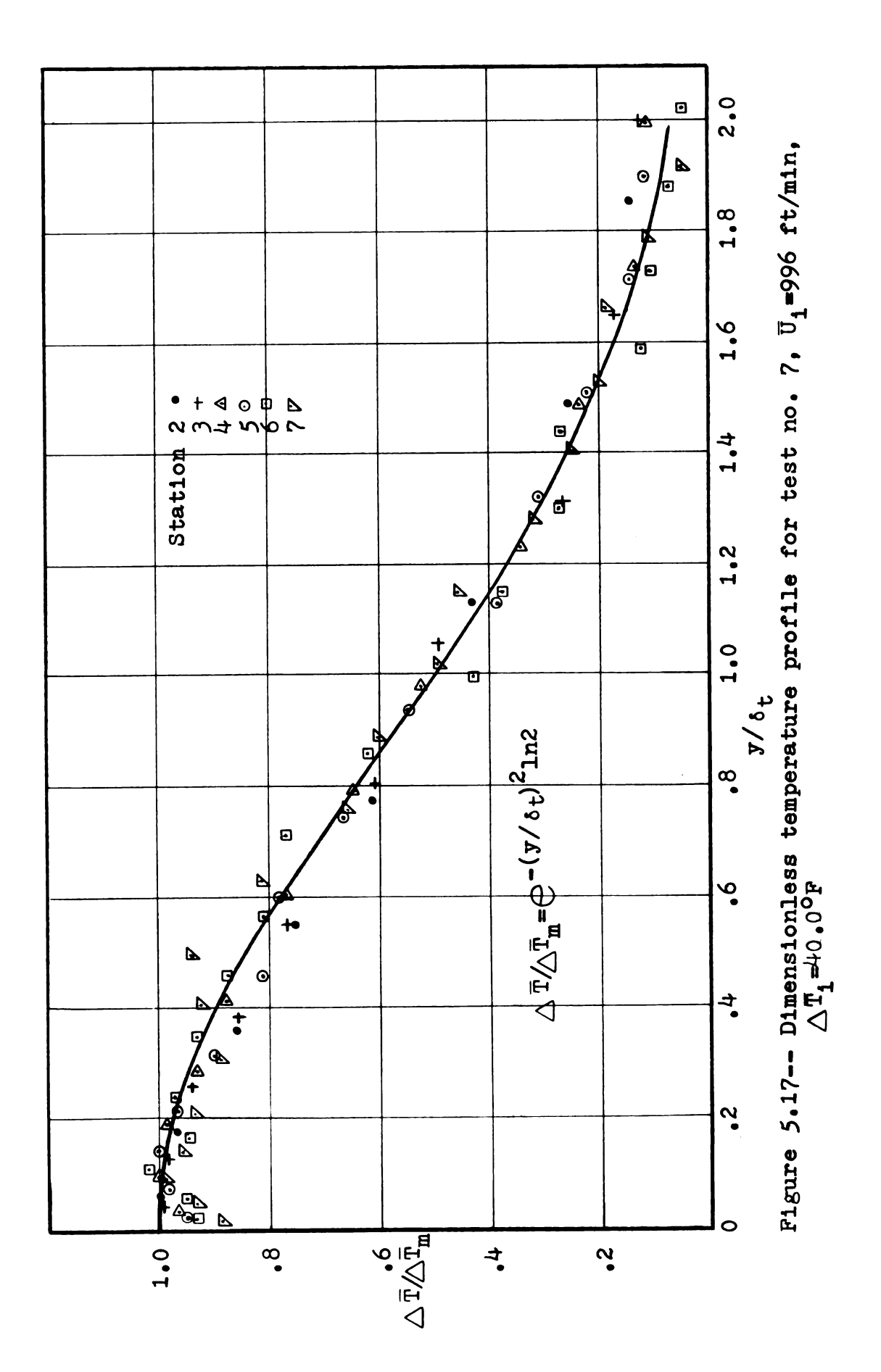
$$\frac{\triangle \overline{T}}{\triangle \overline{T}_{m}} = \exp -(\frac{y^{2}}{\delta_{t}^{2}} \ln 2)$$
 (5.5)

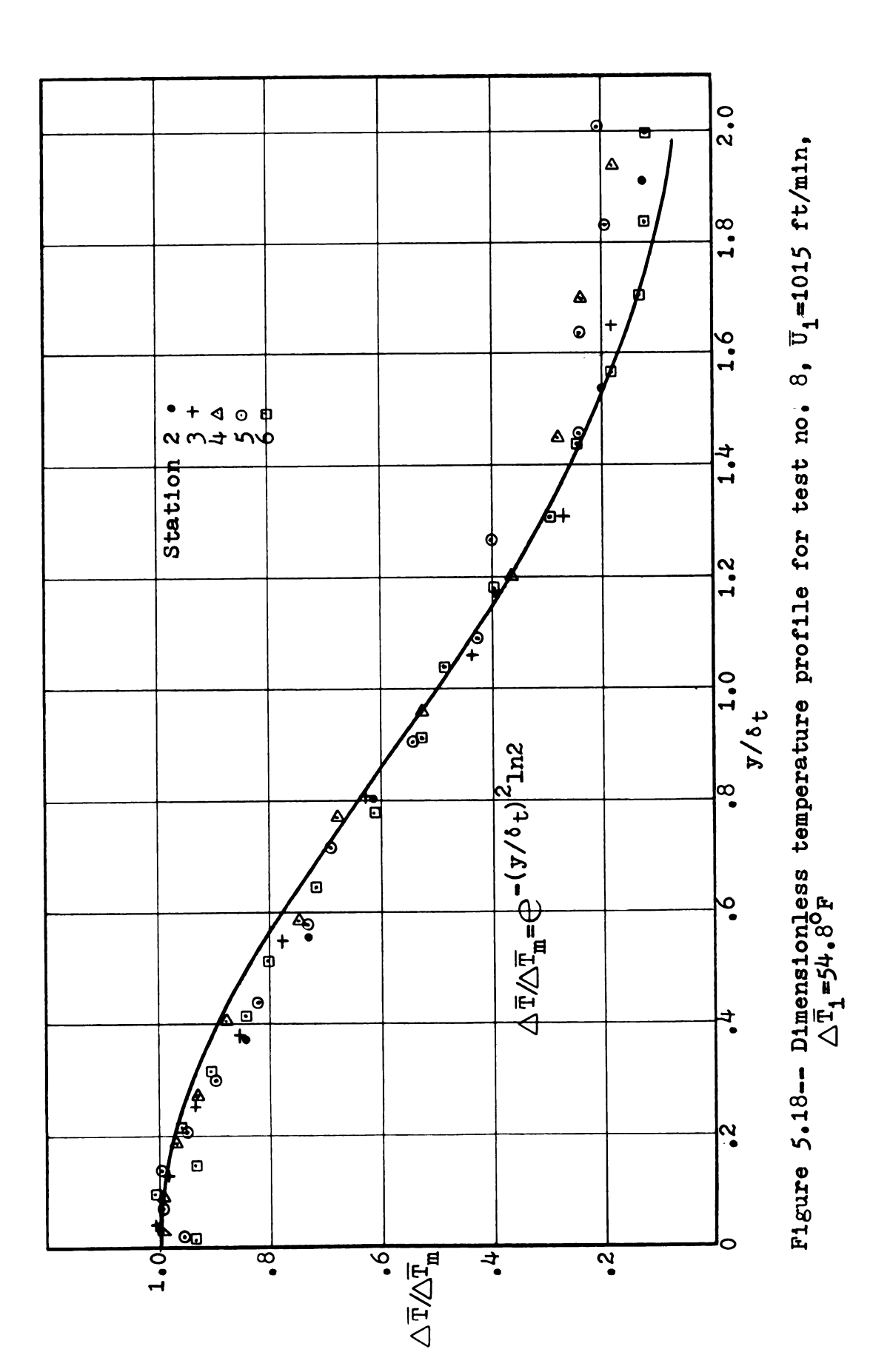
This equation is shown in Figures 5.13, 5.14, and 5.15. It is apparent that it represents the data points of Test no. 2 $(\triangle \overline{T}=20.7^{\circ}F)$ reasonably well for $y/\delta_{t}^{\geq}.2$. However, the exponential curve deviates slightly from the data of Test no. 3 $(\triangle \overline{T}=41.8^{\circ}F)$. The deviation is even more for Test no. 4 $(\triangle \overline{T}=52.3^{\circ}F)$. Thus there appears to be some temperature effect on the shape of the dimensionless temperature profiles in the 1200 ft/min velocity range.

Figures 5.16, 5.17, and 5.18 show the dimensionless temperature profiles for Tests 6, 7 and 8 (1000 ft/min velocity range, $\Delta T=21.3^{\circ}F$, $\Delta T=40^{\circ}F$ and $\Delta T=54.8^{\circ}F$ respectively). There is greater scatter of the data for these tests than for the data of the tests in the 1200 ft/min velocity range. The exponential curve appears to be a reasonable fit to the data for y/δ_t^{\geq} .3 for both Tests 6 and 7. However, there is some deviation of the data for Test no. 8, from the exponential curve.

Tests 10, 11 and 12 (800 ft/min inlet velocity range, $\triangle \bar{T}$ =21.8°F, $\triangle \bar{T}$ =41.4°F and $\triangle \bar{T}$ =55.1°F respectively) indicated that the exponential curve was a reasonably good representation for the mean temperature profiles, in the outer layer.







In fact the data for Test 12 were represented better by the exponential curve than were the $\triangle \bar{T} \approx 50^{\circ} F$ cases of the higher velocity ranges. For Tests 10,11 and 12 the velocity profiles from stations 1, 2, 3 and 4 exhibited similarity. Figures 5.19, 5.20 and 5.21 show the dimensionless temperature profiles for these tests.

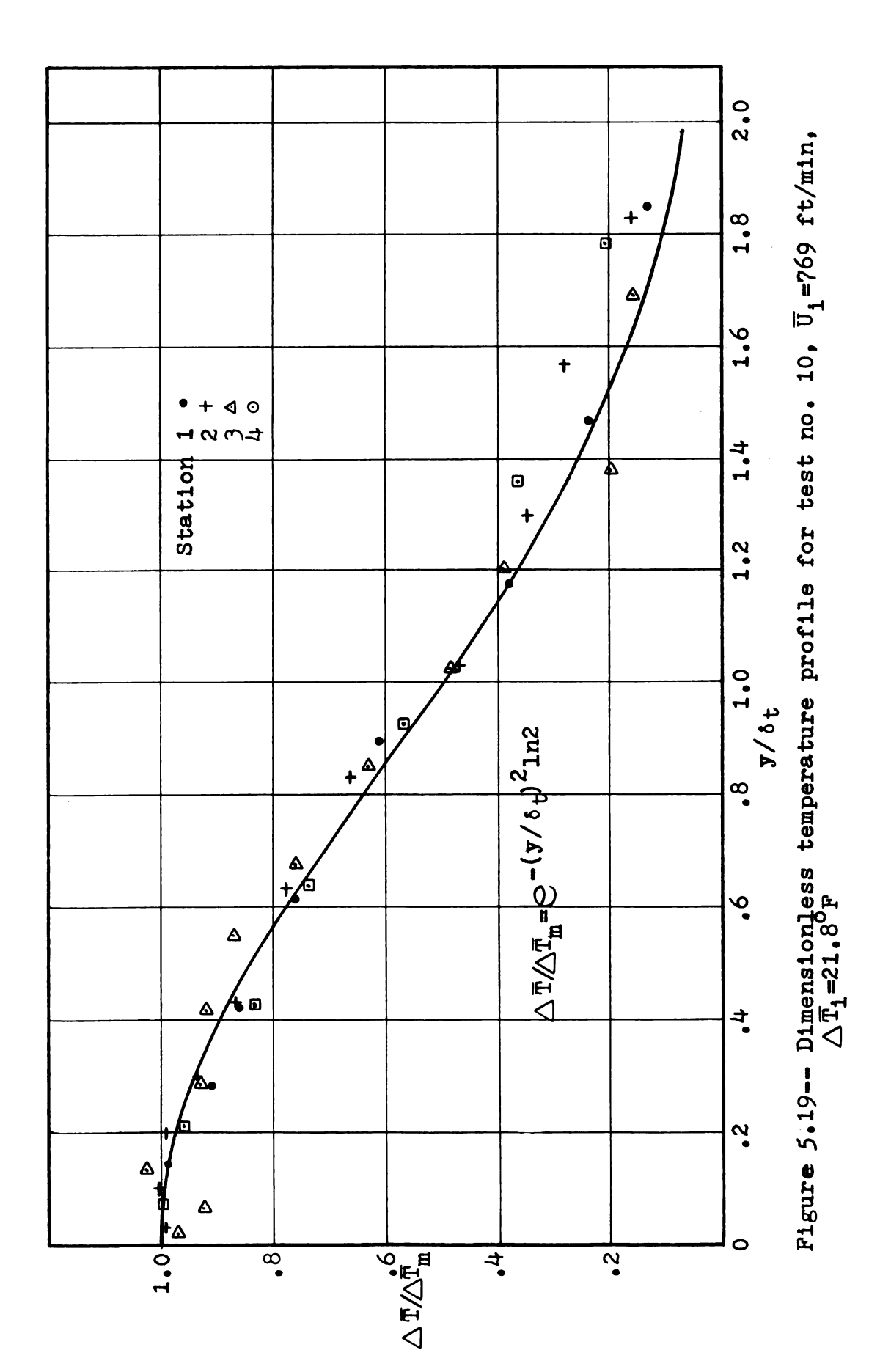
The exponential curve was a reasonable representation for the data in the outer layer, for Test 14 and 15. For these tests the temperature profiles from stations 1, 2, 3 and 4 exhibited similarity. For Test no. 16 the temperature profiles from stations 1, 2 and 3 were similar. The dimensionless temperature profiles for these tests are shown in Figures 5.22, 5.23 and 5.24.

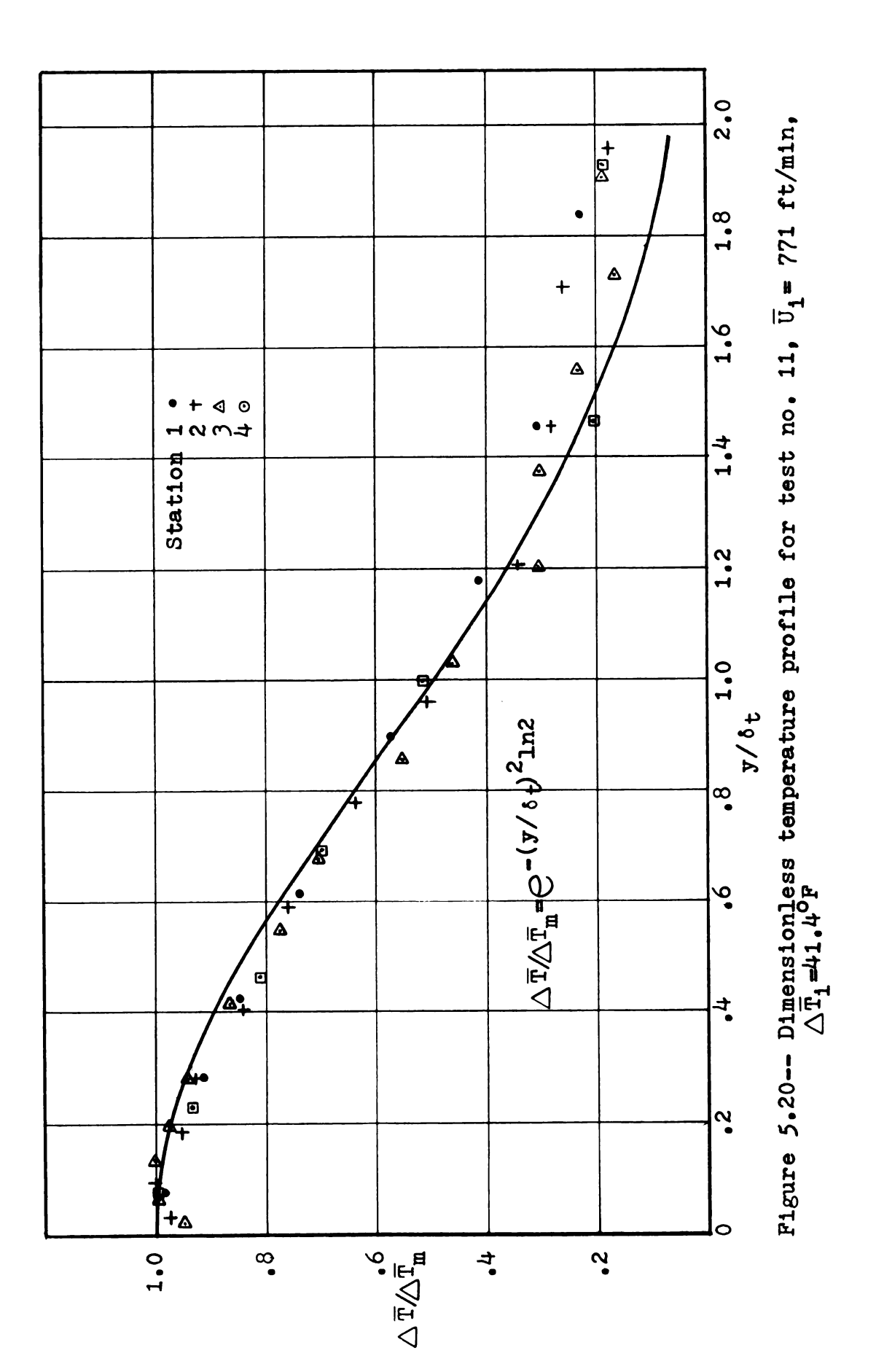
In the 400 ft/min inlet velocity range there was no apparent similarity of the temperature profiles.

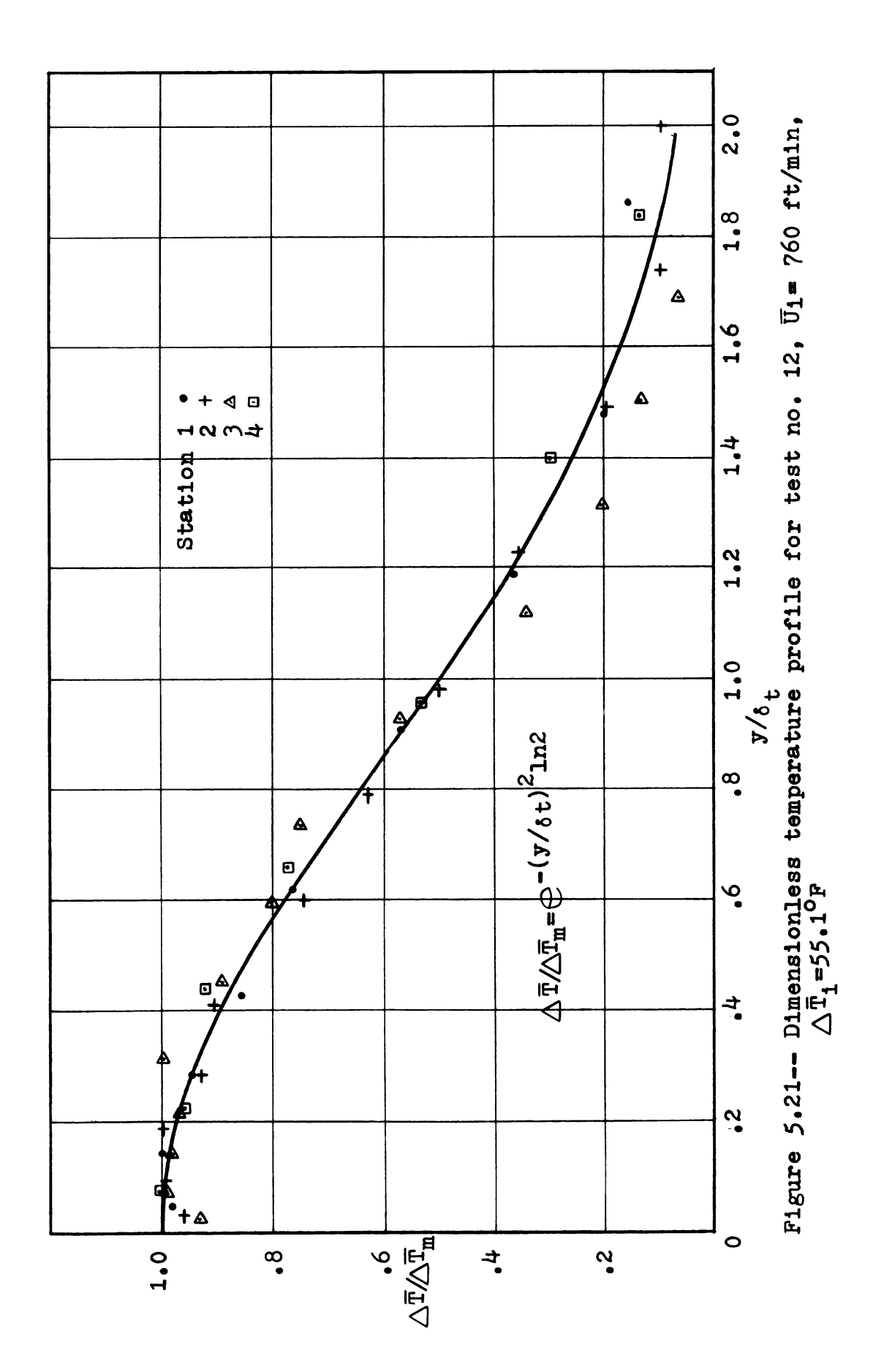
The assumption of similarity of temperature profiles appears to be a valid one for the range of Reynolds numbers and temperature differences investigated. This vindicates the selection of $\delta_{\,t}$ as the y-value at which $\triangle\,\overline{T} = \triangle\,\overline{T}_m/2$.

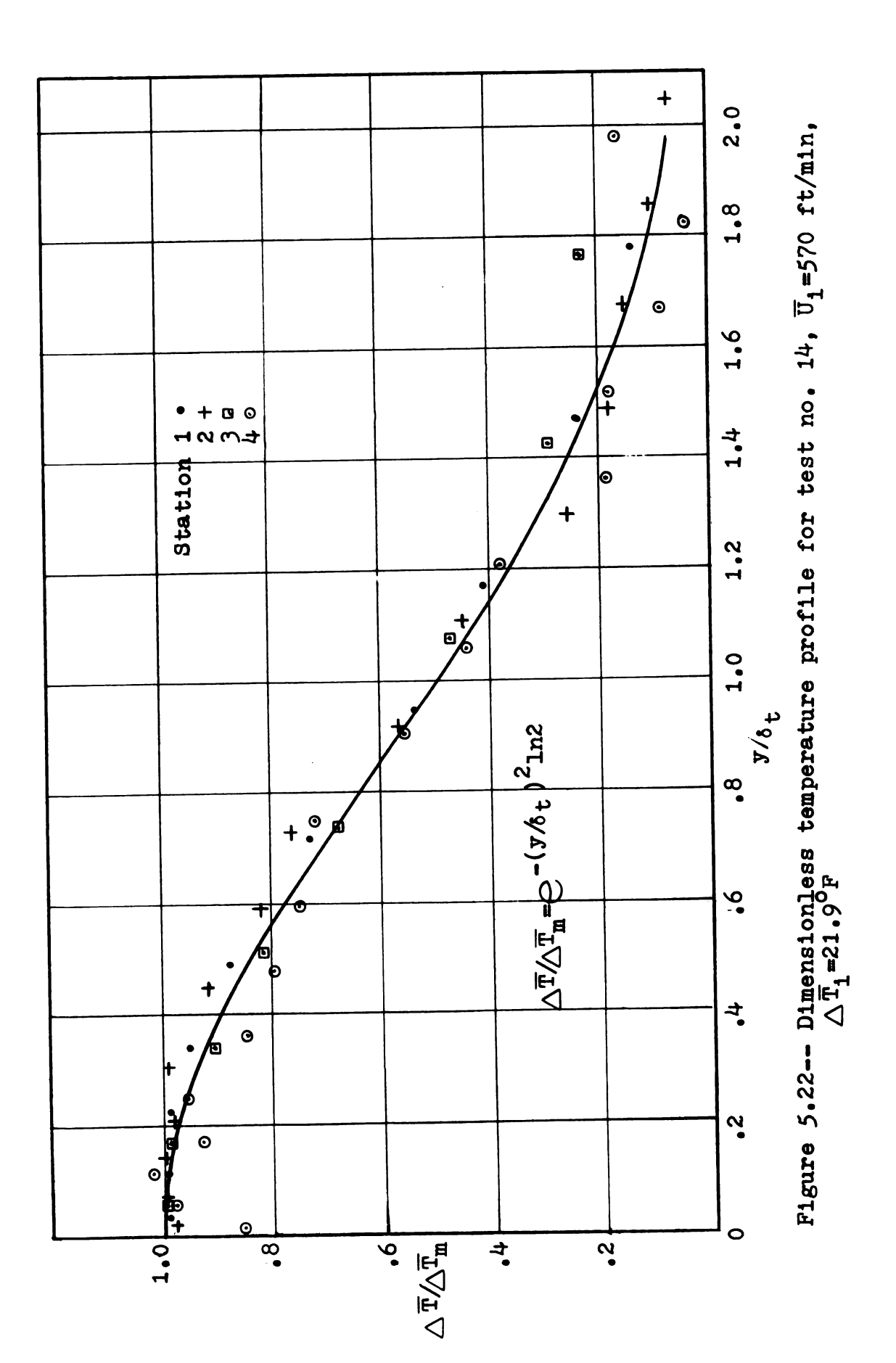
No attempt was made to fit a curve to the inner layer of the thermal boundary layer although it appears that a power law relationship of the form used by Myers et al (1963_b) would apply.

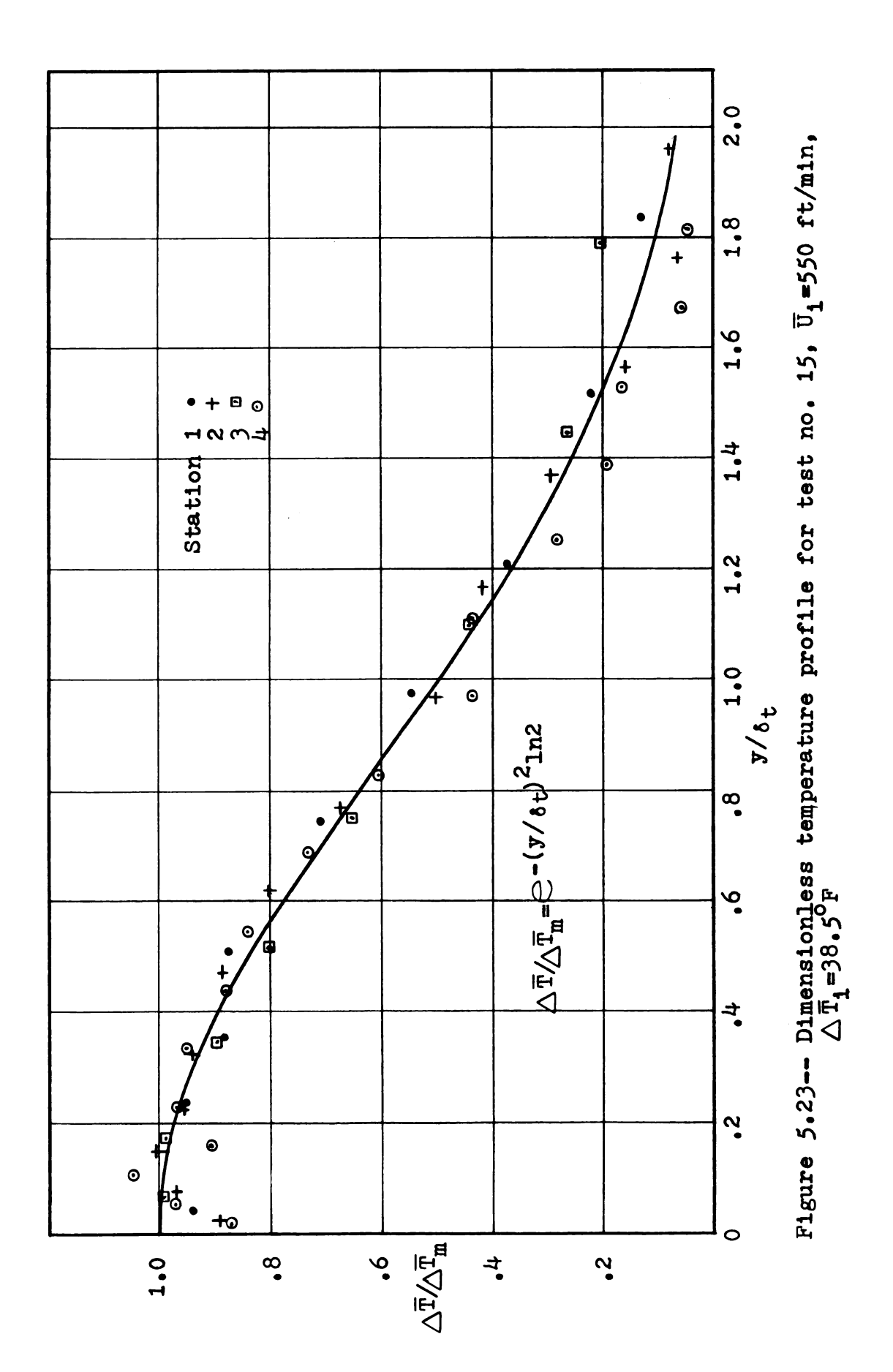
The similarity analysis of the energy equation was based on the implicit assumption that the ceiling temperature was constant in the x-direction. Actual measurements showed that the ceiling temperature varied considerably in the

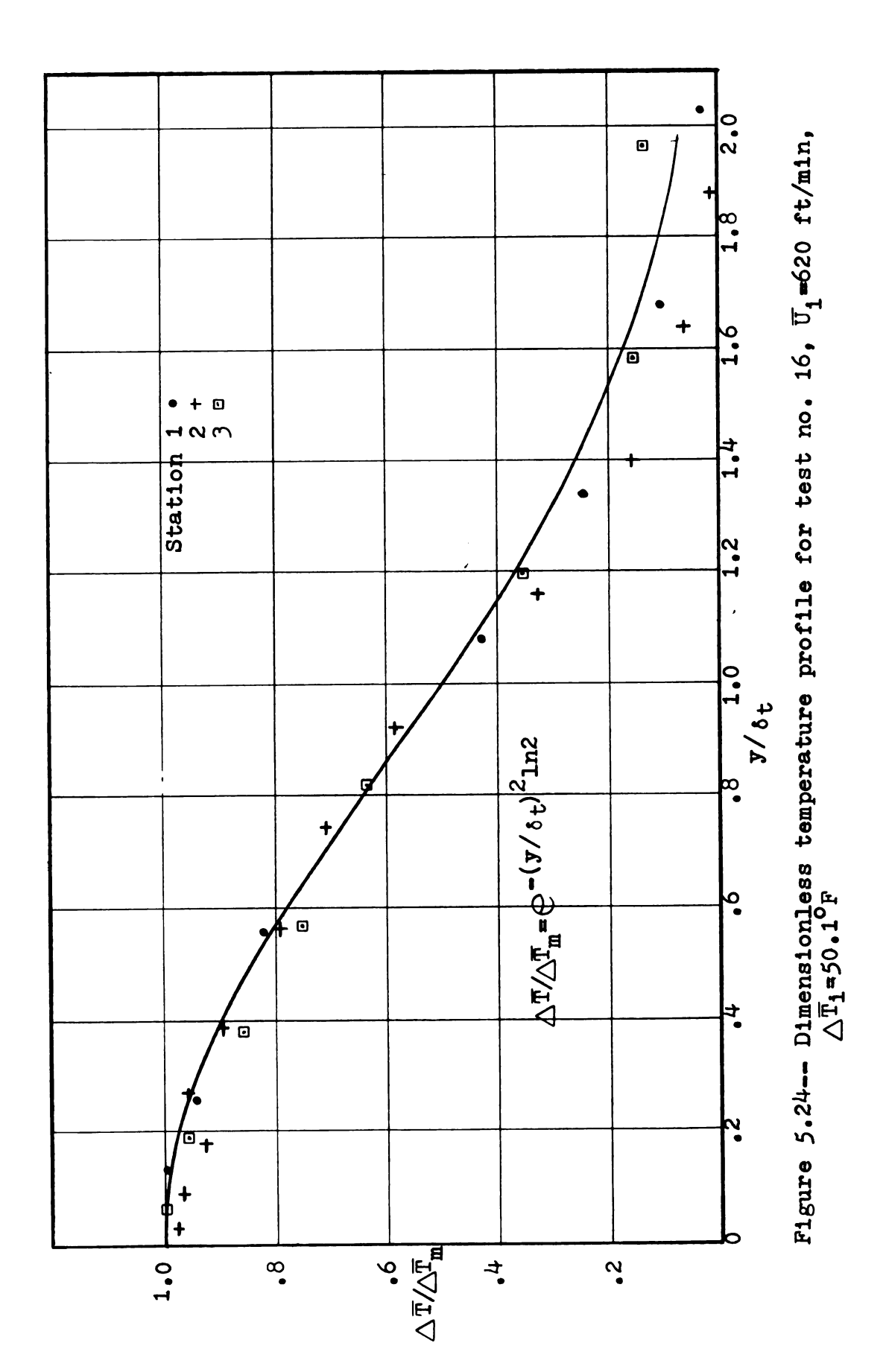












x-direction. Thus while the boundary condition at the ceiling does not conform to the conditions for analytical similarity, experimental similarity is indicated by the measured mean temperature profiles. This apparent discrepancy could be due to a number of reasons. One reason could be this. The dimensionless temperature profiles are "force fitted" and this creates congruency at one section of the profile. In this particular case the section in question would be at the point where $y/\delta_{\pm}=1.0$ or what is the same point, where $\triangle \overline{T}/\!\!\!\triangle \overline{T}_m=0.5$. Another reason could be this. Experimental errors in the temperature measurement would hinder the attempt to verify whether similarity does exist. A third explanation might be this one. Recall that Myers et al (1963) concluded that the outer region, which closely resembles a free jet, dominates the hydrodynamics of the turbulent wall jet. In this free jet region of the wall jet, turbulent mixing of the cold jet air with the warmer ambient air occurs through the entrainment process and the ensuing turbulent diffusion. Now it is shown in the appendix that the percentage of heat added to the wall jet by heat transfer through the ceiling is at most 6% of the total heat, transferred to the wall jet. Thus it seems reasonable that the effect of a varying ceiling temperature would not be indicated in the temperature profile of the outer region. Rather, it appears logical to expect that the varying ceiling temperature would be reflected in the temperature measurements of the inner layer. Table A.20 in the Appendix gives the temperature difference at the ceiling along the maximum temperature difference, for each test.

The width of the thermal boundary layer was greater than the width of the momentum boundary layer, for all tests.

5.3 Thermal Boundary Layer Growth

The similarity analysis of the turbulent energy equation of the boundary layer has indicated that the growth of the thermal boundary layer is a linear function of the longitudinal distance x, from the inlet. This functional relationship may be written as $\delta_{\,t} = C_{\,o}(x\,+\,x_{\,o})$ where $x_{\,o}$ is the distance to the virtual origin and $\delta_{\,t}$ has been previously defined as the transverse distance to where $\triangle \, \overline{t} = \! \triangle \, \overline{t}_{m}/2$.

The determination of C_0 and x_0 for each test was carried out in several steps. First the values of δ_t were determined by observation, from the mean temperature profiles. A plot of δ_t vs. x, was then made. From this plot it was determined whether the data points appeared to describe a straight line. This was done without regard to similarity of the mean temperature profiles. In only two cases, were the values of δ_t not used in determining a best fit line describing the growth of the thermal boundary layer. These two locations were station eight for Tests 4 and 11. The reason they were not used was that they deviated appreciably from the trend established by the rest of the points of the

test. The method of least squares was used in determining the best fit lines.

In order to make the data applicable to other systems the thermal boundary layer thickness was made dimensionless by dividing it by the slot height L and the same procedure was used for x. Thus the equations of the best fit lines are of the form $\delta_{\rm t}/{\rm L=A} + C_{\rm o}({\rm x/L})$ or in terms of the virtual origin, $\delta_{\rm t}/{\rm L=C_o}[{\rm x/L} + ({\rm x_o/L})]$.

Table 5.2 gives the values of C_0 and x_0 for each test. Also given is the number of stations used in the determination of the best fit lines and the values of the correlation coefficient, for each test. The correlation coefficients indicate that the data points are described quite well by a straight line for all tests. As a further check on the validity of the apparent linear relationship between δ_t and x, the best fit lines were drawn through the data. In all cases the data indicated no apparent curvature with respect to the best fit line. The standard deviation of the observed values of δ_t from the best fit line is also given in Table 5.2.

The values of the virtual origin and C_0 were plotted against both the inlet Reynolds number and the inlet Grashoff number to try and determine if any functional relationship existed between them. Although there was considerable scattering of the data, there nevertheless appeared to be a definite trend between the inlet Reynolds number and both the virtual origin and C_0 . Best fit lines were determined through the data points by the method of least squares.

Table 5.2 Experimentally determined constants for thermal boundary layer growth

Test No.	Number of Points Used	ပိ	x _o (ft)	Correlation Coefficient	Standard Deviation of $\delta_{\mathbf{t}}$ from Best Fit Line (ft)
ત્ય	80	260•	04.	.9957	420°
6	ω	060°	.73	.9920	• 030
†	2	.111	.15	.9961	.028
9	ω	.117	•39	.9953	240.
2	ω	.101	•59	9866*	• 035
∞	ω	.120	.23	4866.	• 026
10	∞	.116	.85	.9961	•038
11	2	.128	• 59	.9929	.058
12	2	.142	. 48	.9961	7700
14	9	.146	.82	.9891	.053
15	9	.164	.57	.9913	.055
16	5	.126	*54	9466•	.023

The best fit lines along with their equations are shown in Figures 5.25 and 5.26. The correlation coefficient for the relationship between Reynolds number and C_0 was .8345 which indicates a straight line to be a reasonable approximation. Thus over the range of inlet velocities tested, it appears that the slope of the line describing the growth of δ_t , decreases with increasing inlet Reynolds number. In other words, at the higher inlet velocities (e.g. Reynolds numbers), there appears to be less spreading out in the transverse direction of the mean temperature profile or less mixing of the cold air with the warm air.

The correlation coefficient for the equation describing the relationship between the virtual origin and the inlet Reynolds number was .5848 thus making the assumption of a linear relationship between them, rather tenuous.

The correlation coefficients for Grashoff number versus \mathbf{x}_0 and the Grashoff number versus \mathbf{C}_0 were both well below .5 indicating that a linear relationship did not exist. No other type of curve fitting was attempted.

The fact that the growth of the thermal boundary layer was well represented by a linear relationship for all tests, implies that the buoyancy forces were negligible compared to the inertia and viscous forces. If the buoyancy forces had been significant, the line describing $\delta_{\mathbf{t}}$ would have been curved, not straight. However, for the 600 ft/min inlet velocity range the air flow became detached from the

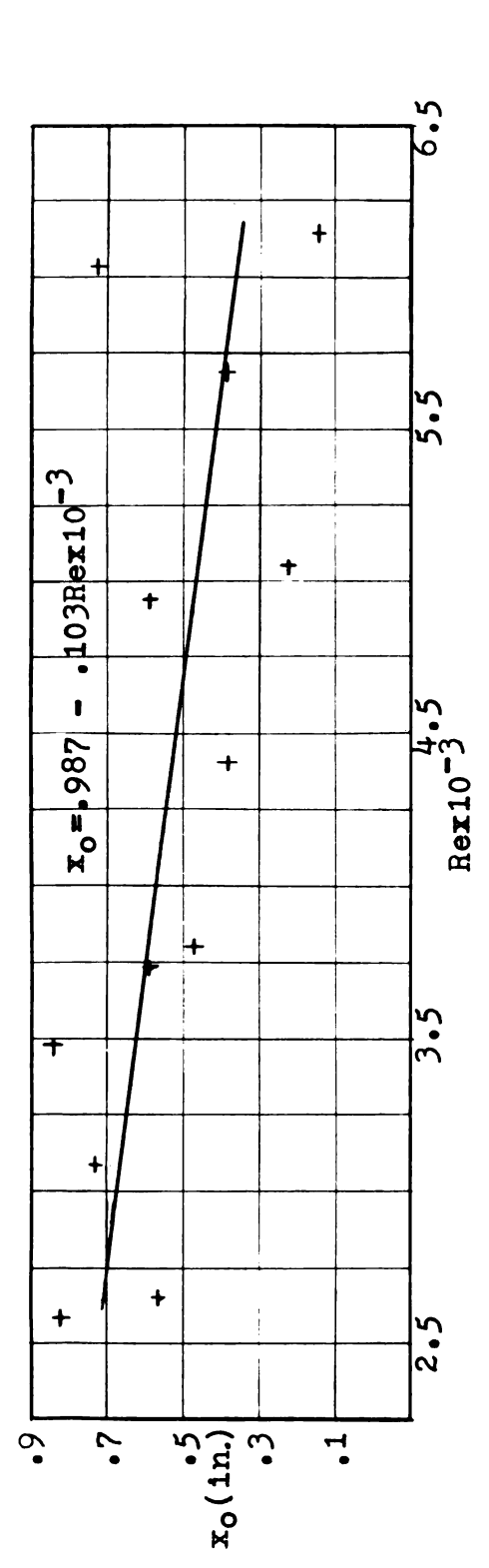


Figure 5.25 -- Inlet Reynolds number versus the virtual origin

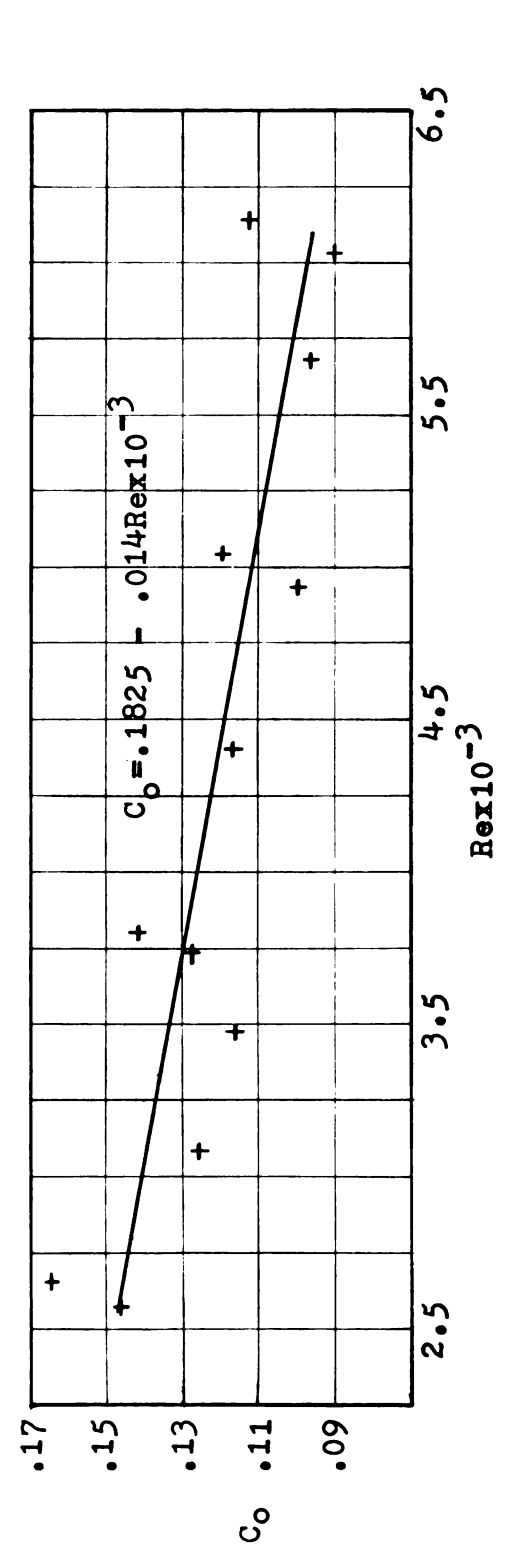


Figure 5.26-- Inlet Reynolds number versus $C_{\rm O}$, the coefficient representing the slope of the thermal boundary layer

ceiling at station 7 for the three non-isothermal tests. This was not the case for the isothermal test. This same phenomenon occurred for the 400 ft/min inlet velocity range. This detachment appears to indicate buoyancy force effects, which contradicts the results of the thermal boundary layer growth data. In light of these observations it is interesting to note that the order of magnitude analysis of the momentum equations indicated that buoyancy force effects would be important at both the 600 ft/min and 400 ft/min inlet velocity ranges. This may be fortuitous since the order of magnitude analysis at best, is approximate.

It appears that for the range of velocities and temperature differences tested, and within the range of experimental accuracy, buoyancy forces were found to have a negligible effect on the growth of the thermal boundary layer.

5.4 Results of Temperature Decay Measurements

Analysis has predicted that, based on assumed similarity of temperature profiles, a power law relationship of the form $\triangle \overline{T}_m = C_5 x^{\, i \, b}$ will describe the decay of maximum temperature difference. It has already been shown that the mean temperature profiles of this investigation do exhibit similarity. It remains now to examine the data in order that the validity of the analysis concerning the maximum temperature decay, may be either proven or disproven.

If the power law relationship holds then a log-log plot of $\Delta \overline{\mathbf{T}}$ versus x' should describe a straight line. Such

plots for four of the five velocity ranges investigated, are shown in Figures 5.27 through 5.38. The 400 ft/min inlet velocity cases are not shown, the reason being that the temperature profiles could not be measured at enough stations for this inlet velocity. The data is presented in dimensionless form. This allows wider application of the results to similar systems without changing the basic functional relationship between $\triangle \overline{\mathbf{T}}$ and \mathbf{x}^* . A look at the resultant plots indicates that at least part of the points appear to describe a straight line. Using the method of least squares, best fit straight lines were found for the data.

In determining a best fit straight line through the data points it was necessary, at the lower velocities and higher temperature differences, to exclude some of the data points from the stations farthest from the inlet. These points were rejected on an arbitrary basis. The criteria for rejection was, observing when a point seemed to deviate markedly from a trend established by the closer stations. Thus the resultant best fit lines describe only a portion of the data points with the number of data points used in each case, indicated by the range over which the best fit lines are drawn, in the figures. In some cases, data points from stations whose temperature profiles did not indicate similarity were used, however the inverse was not true. It is questionable whether a straight line is the best representation of the data, for all the tests. This

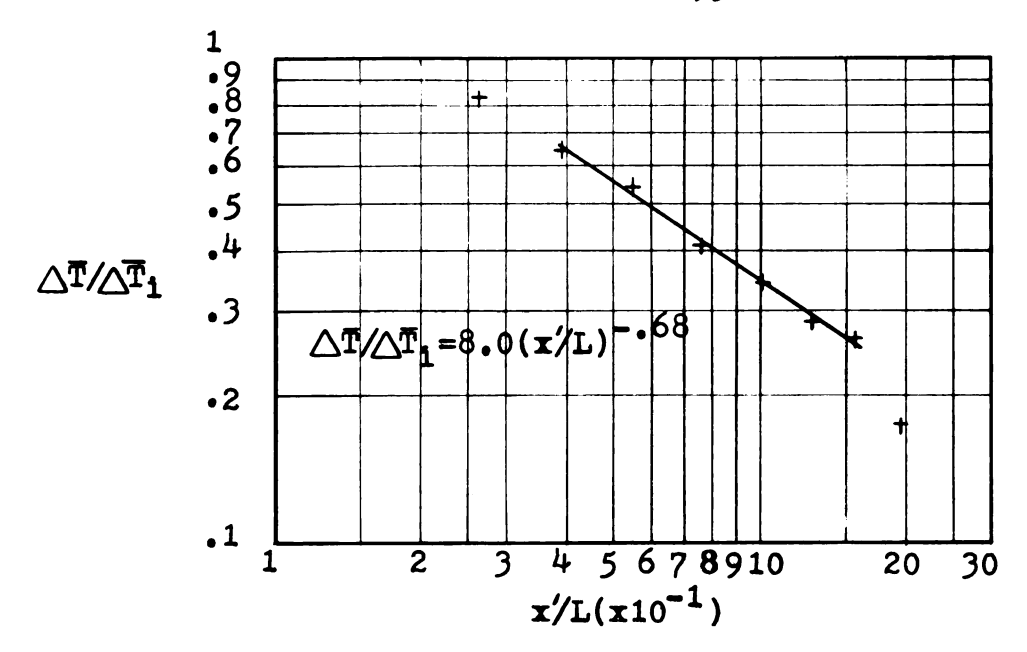


Figure 5.27-- Maximum temperature difference decay results for test no. 2, \bar{U}_1 =1236 ft/min, $\Delta \bar{T}_1$ =20.7°F

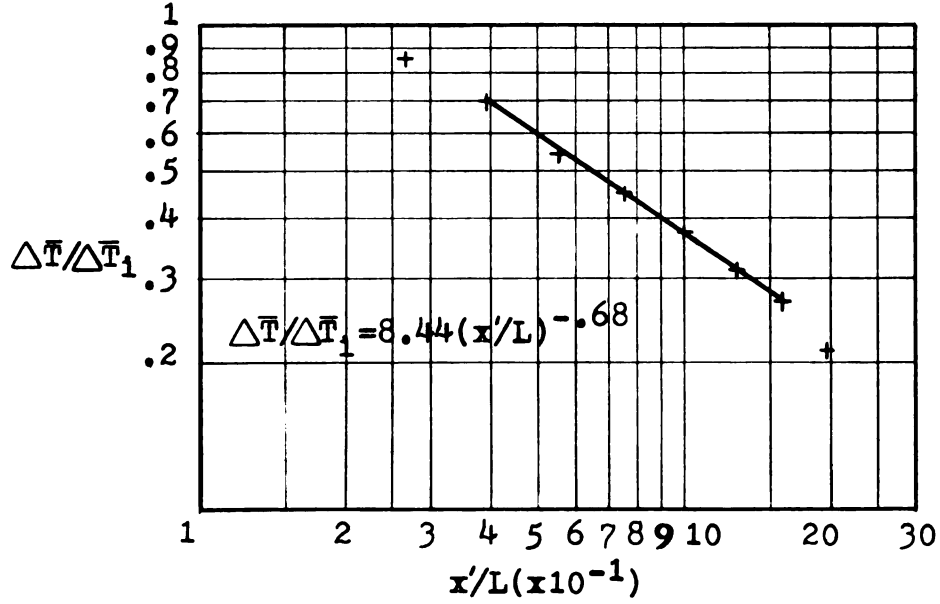


Figure 5.28-- Maximum temperature difference decay results for test no. 3, $\overline{U}_1=1225$ ft/min, $\sqrt{T}_1=41.8$ °F

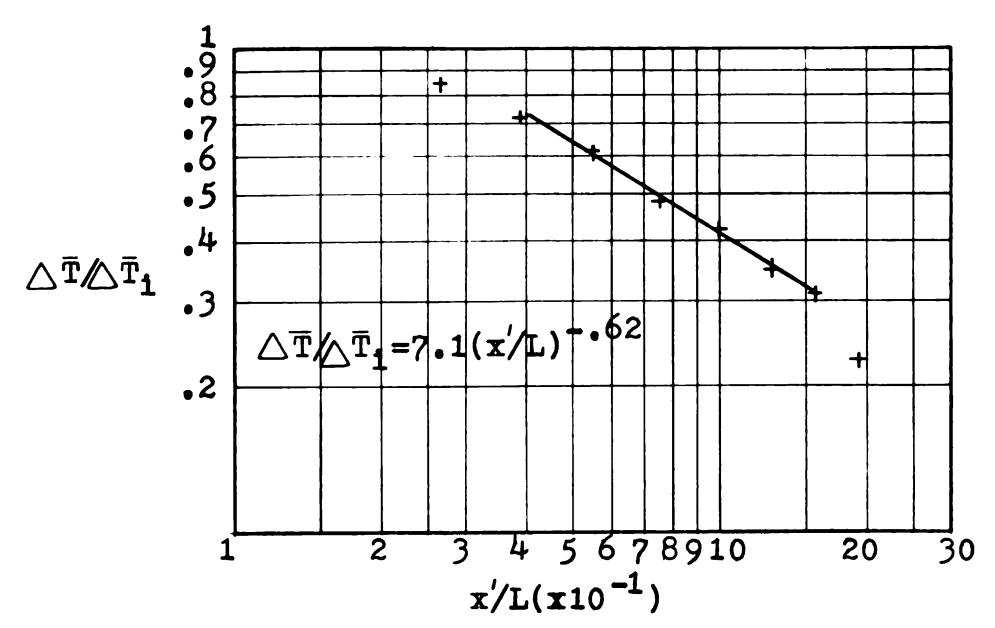


Figure 5.29-- Maximum temperature difference decay results for test no. 4, \overline{U}_1 = 1230 ft/min $_1$ =52.3°F

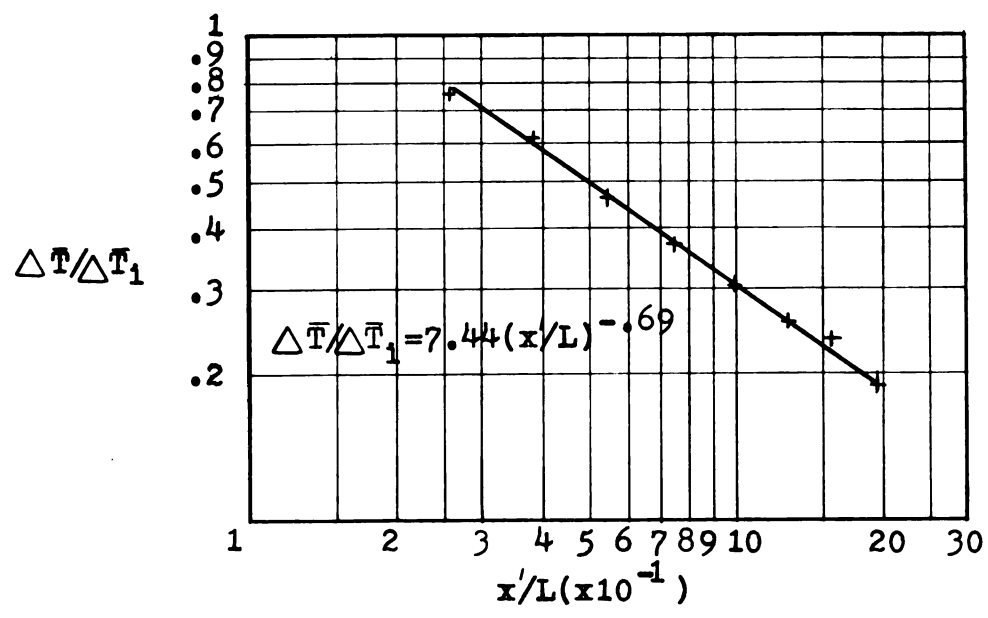


Figure 5.30-- Maximum temperature difference decay results for test no. 6, $U_1=981$ ft/min $T_1=21.3$ °F

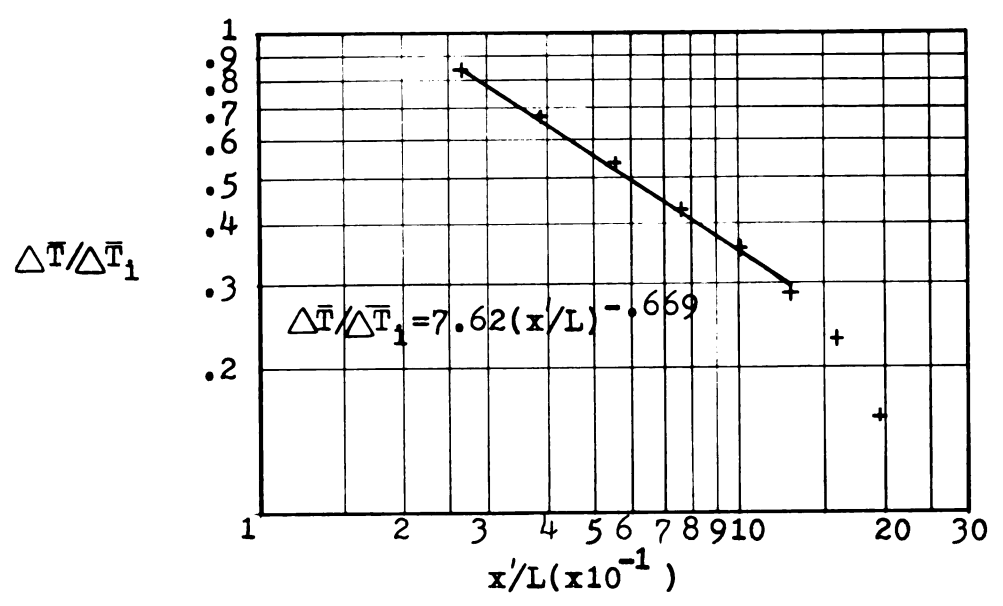


Figure 5.31-- Maximum temperature difference decay results for test no. 7, \bar{U}_1 =996 ft/min, $\Delta \bar{T}_1$ =40°F

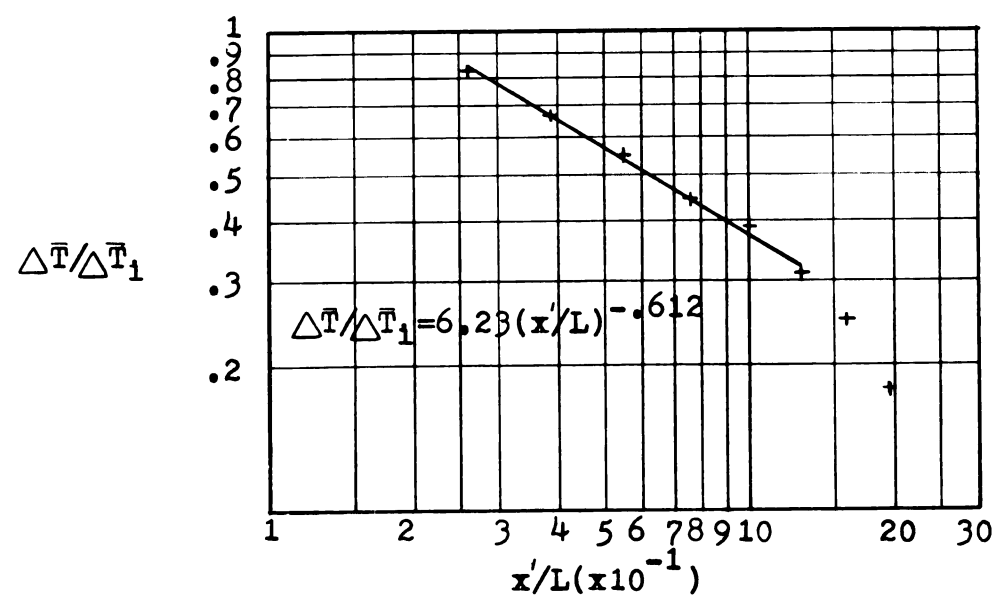


Figure 5.32-- Maximum temperature difference decay results for test no. 8, \bar{U}_1 =1015 ft/min, $\triangle \bar{T}_1$ =54.8°F

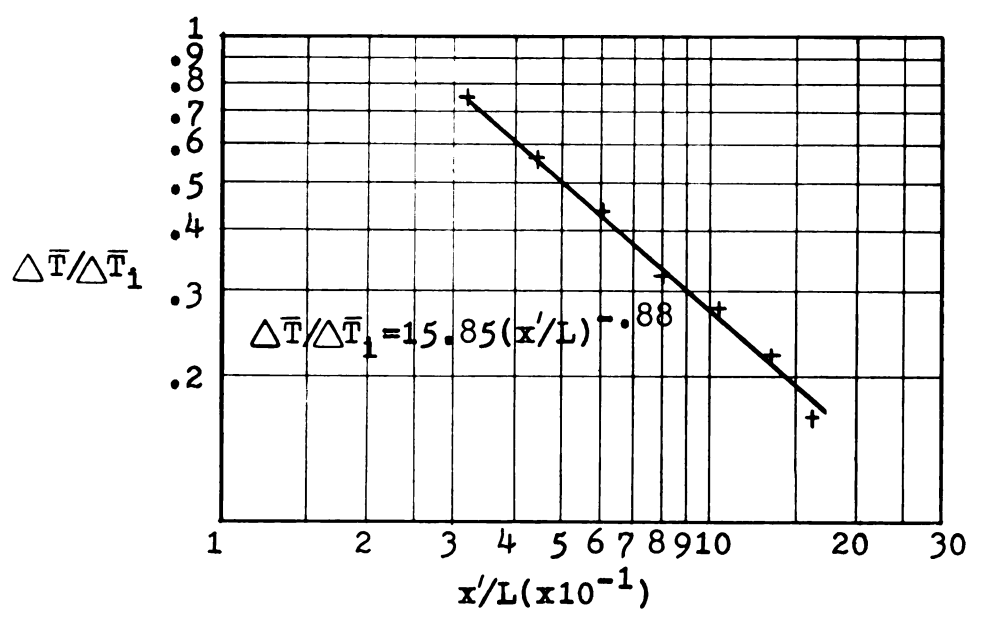


Figure 5.33- Maximum temperature difference decay results for test no. 10, \overline{U}_1 =769 ft/min, $\triangle \overline{T}_1$ =21.80F

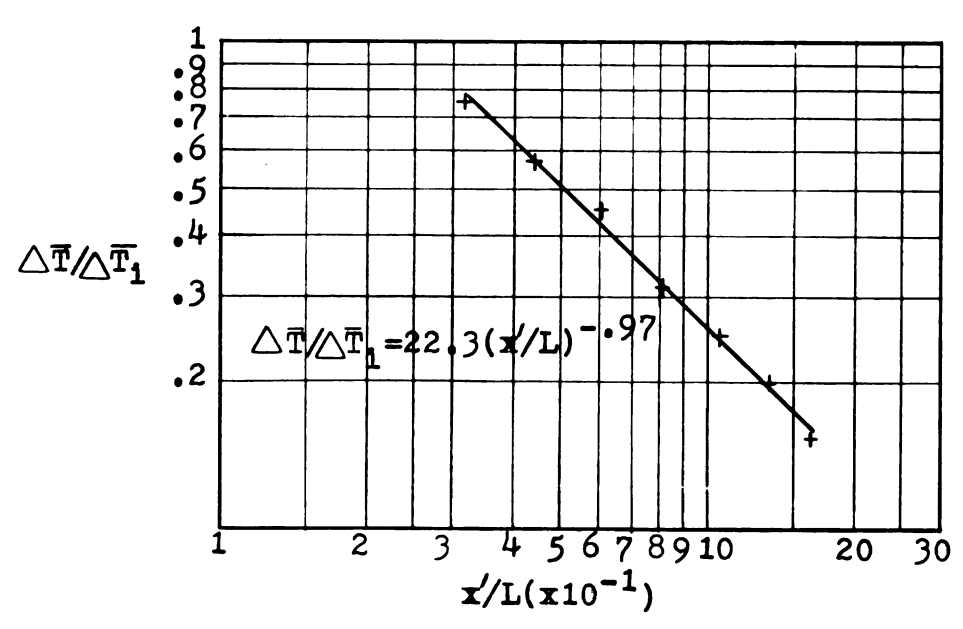


Figure 5.34-- Maximum temperature difference decay results for test no. 11, \bar{U}_1 =771 ft/min, $\Delta \bar{T}_1$ =41.40F

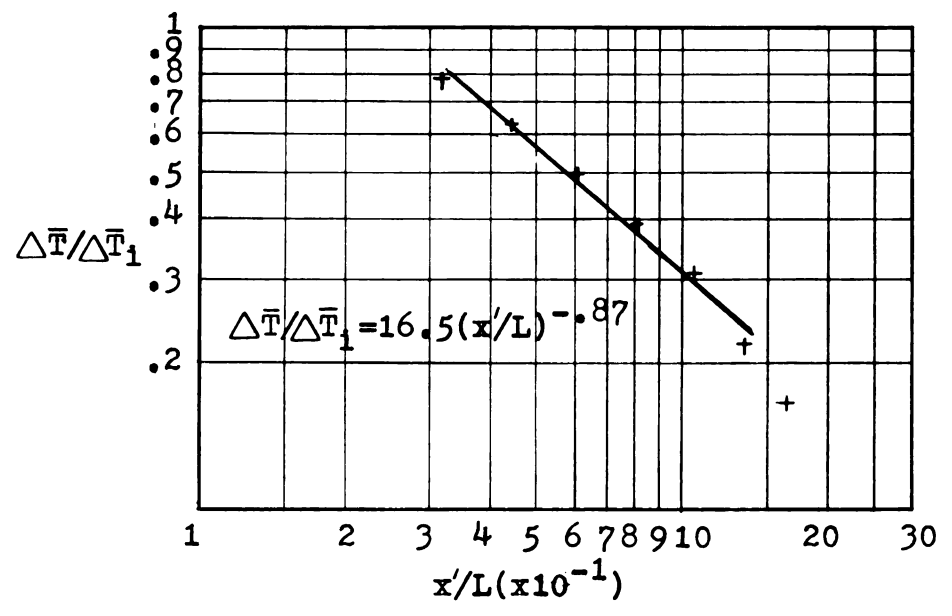


Figure 5.35-- Maximum temperature difference decay results for test no. 12, \overline{U}_1 =760 ft/min, $\triangle \overline{T}_1$ = 55.1°F

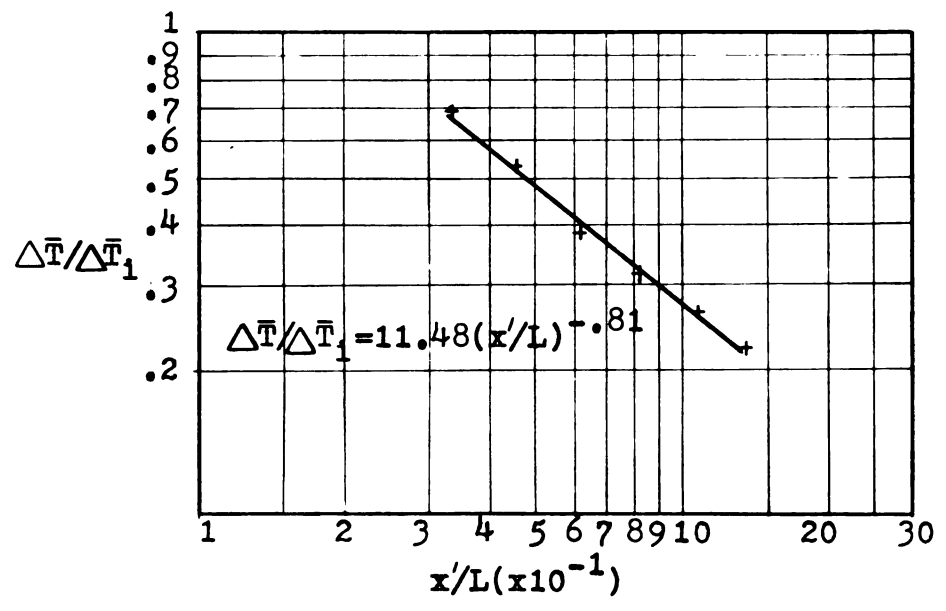


Figure 5.36--Maximum temperature difference decay results for test no. 14, \bar{U}_1 =570 ft/min, $\triangle \bar{T}_1$ =21.9°F

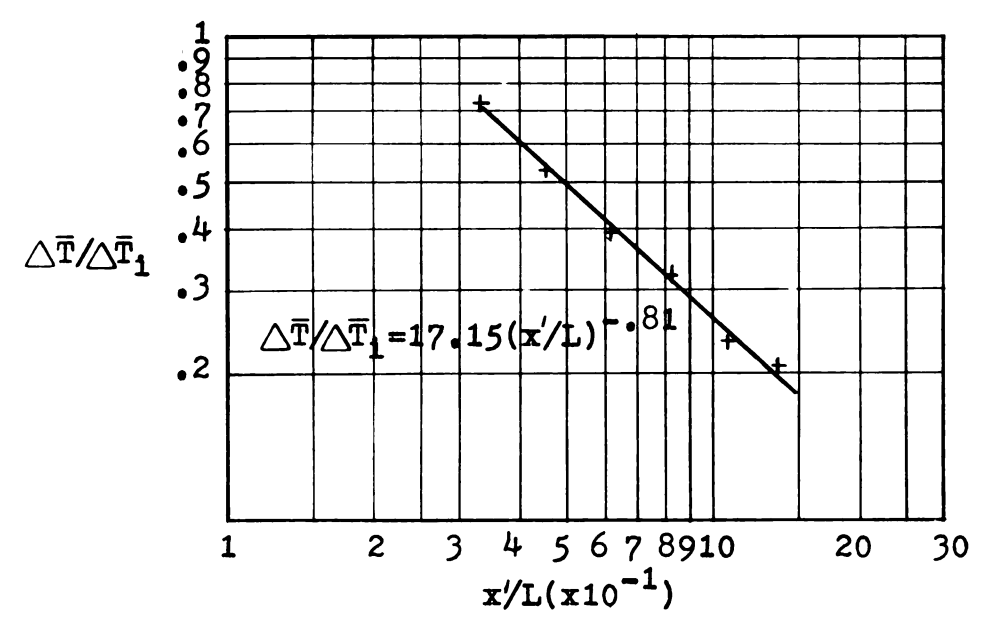


Figure 5.37-- Maximum temperature difference decay results for test no. 15, \overline{U}_1 =550 ft/min, $\triangle \overline{T}_1$ =38.5°F

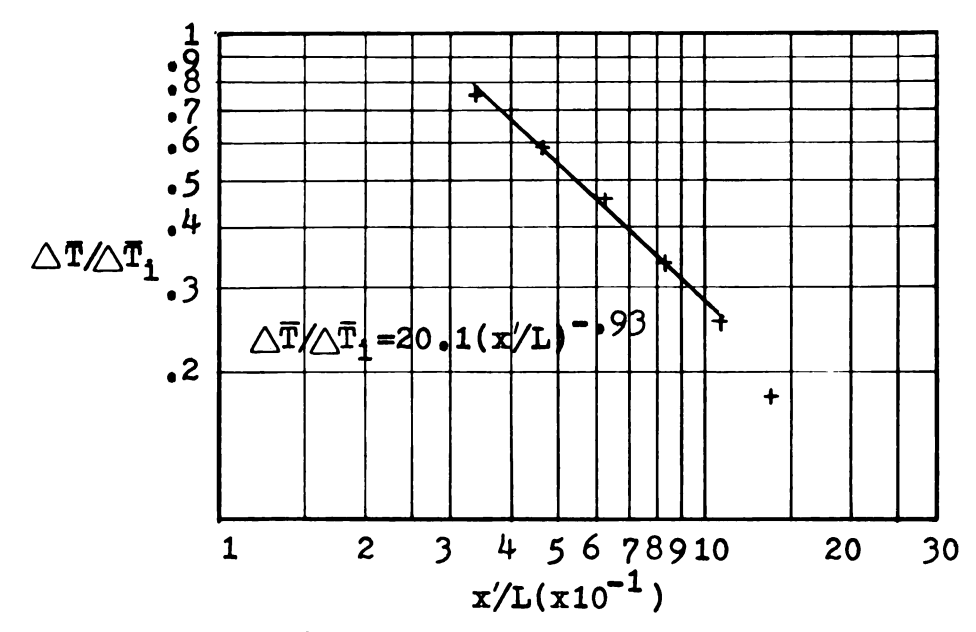


Figure 5.38-- Maximum temperature difference decay results for test no. 16, \overline{U}_1 =620 ft/min, $\triangle \overline{T}_1$ =50.1°F

can be seen by observing the data and best fit lines of Tests 7, 8, 12 and 16. For these four tests there is a curving of the data with respect to the lines, at the larger x^{*}/L values.

Table 5.3 shows the values of C_5 and b as determined by the least squares best fit line of the data. The correlation coefficient for each case is also given in Table 5.3. The average value of the exponent b for all the tests was -.768. This is considerably greater than the average value of the exponent a from the velocity decay data. However, the exponent a was determined by using x for the abcissa of the log-log plot, instead of $(x + x_0)$. Thus direct comparison is impossible.

Over the range of inlet Reynolds numbers tested, an apparent functional relationship existed between them and the exponent b. The rate of decay of the temperature difference appeared to be inversely proportional to the inlet Reynolds number. This result indicates that there is less thermal mixing of the cold incoming air with the warm air, at the higher inlet Reynolds numbers. This observation agrees with the results of the thermal boundary layer growth data, which indicated that the growth was inversely proportional to the inlet Reynolds number.

A plot of inlet Reynolds number versus b, along with a best fit line to the data, is shown in Figure 5.39. The correlation coefficient was .767.

There appeared to be no functional relationship between b and the inlet Grashoff number. A least squares, straight

5.3 Experimentally determined constants for temperature decay

	+ x)	$x + x_0$) as	abc1ssa			x used	d as abclssa
Test No.	c ₅	٩	Corr. Coeff.	$c_{\mathcal{S}}$	ф	Corr. Coeff.	x/L range for which eqn. of best fit line applies
7	ω	682	266•	4.98	593	66•	28 ≤ x/L ≤ 150
6	44.8	•• 68	666•	86.4	581	866.	28 ≤ x/L ≤ 150
†	7.1	619	666•	4.39	529	266.	28 ≤ x/L ≤ 150
9	44.6	169	866.	84.4	598	666.	28 ≤ x/L ≤ 150
2	7.62	699	266.	5.12	598	.995	28 ≤ x/L ≤ 125
ω	6.23	612	.998	90.4	534	966•	28 ≤ x/L ≤ 125
10	15.85	883	266.	5.05	653	.998	28 ≤x/L≤1 25
11	22.3	967	866•	49.6	761	.995	28 ≤ x/L ≤ 125
12	16.5	866	.993	7.52	725	.987	28 ≤x/L≤1 25
14	11.48	812	266.	3.8	599	666•	28 ≤ x/L≤125
15	17.15	807	266.	19.9	717	.993	28 ≤ x/L ≤ 100
16	20.1	927	266•	5.08	673	966•	28 ≤ x/L≤ 90

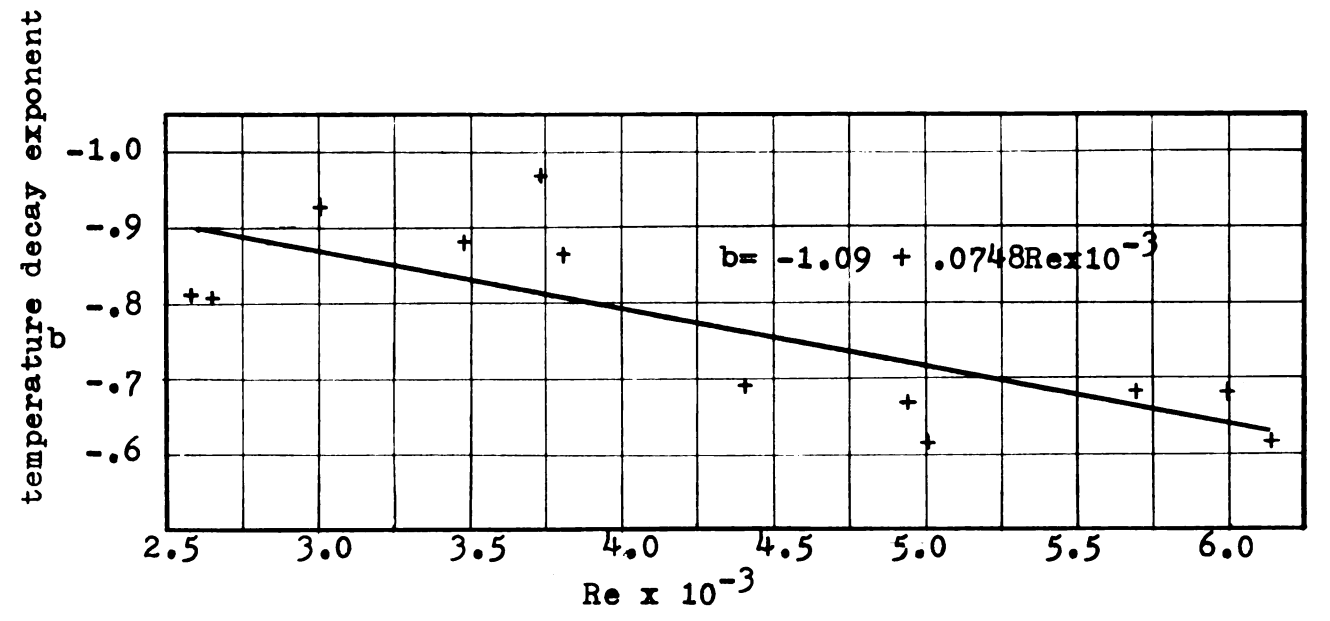


Figure 5.39-- Plot of inlet Reynolds number versus the temperature decay exponent

line fit was attempted. However, the correlation coefficient was well below .1 indicating that a linear relationship did not exist.

In order that the maximum temperature difference decay rate might be compared with the velocity decay rate, the temperature data were replotted, using x instead of $(x + x_0)$ as the abcissa. Best fit straight lines were then determined for each test. The values of C_5 and b as found from the best fit lines are given in Table 5.3. Also shown is the range of x/L for which the equation of the best fit line applies. The average value of b was -.63. This compares to a value of -.53 for the velocity decay exponent. The larger value for the exponent of the temperature decay agrees with the observations that the thermal boundary layer was wider than the momentum boundary layer for all tests.

The value of the exponent b, found using x as the abcissa, was 22% smaller than the value using $(x + x_0)$ as the abcissa. This large discrepancy points out the apparent sensitivity of b, to the value found for the virtual origin. Thus any error which might occur in the determination of x_0 would also affect the value found for b.

Generally the maximum temperature decay was reasonably well represented by a power law relationship, over the range of inlet Reynolds numbers and inlet temperature differences tested.

6. APPLICATION

Having an expression for the decay of the maximum temperature difference and also an expression for the temperature distribution, it is possible to obtain an expression for the temperature at any point in the thermal boundary layer.

The expression for the decay of the maximum temperature was found to be:

$$\triangle \bar{T}_{m} / \triangle \bar{T}_{i} = C_{5}(x/L)^{b}$$
(6.1)

Therefore

$$\triangle \bar{T}_{m} = \triangle \bar{T}_{i} C_{5}(x/L)^{b}$$
 (6.1a)

Reichardt's representation of the temperature distribution was seen to approximate reasonably well the temperature data in the outer layer. It is:

$$\triangle \bar{\mathbf{T}} / \!\!\! \triangle \bar{\mathbf{T}}_{m} = \exp(y/\delta_{t})^{2} \ln 2 \qquad (6.2)$$

Thus

$$\triangle \bar{\mathbf{T}} = \triangle \bar{\mathbf{T}}_{m} \exp -(\mathbf{y}/\delta_{t})^{2} \ln 2 \qquad (6.2a)$$

Substituting equation 6.1a for $\triangle \bar{T}_m$ into equation 6.2a results in the following.

$$\triangle \bar{T}_{m} = \triangle \bar{T}_{1} C_{5} (x/L)^{b} \exp -(y/\delta_{t})^{2} \ln 2 \qquad (6.3)$$

However

$$\delta_{t} = C_{o}(x + x_{o}) = C_{o}x^{\dagger} \tag{6.4}$$

Therefore

$$\Delta \bar{\mathbf{T}} = \Delta \bar{\mathbf{T}}_{\mathbf{1}} \mathbf{C}_{5} (\mathbf{x/L})^{b} \exp -(\mathbf{y/C_{o}}\mathbf{x}^{\dagger})^{2} \ln 2 \qquad (6.5)$$

Taking the log of both sides of equation 6.5 gives:

$$\ln \triangle \bar{\mathbf{T}} = \ln \triangle \bar{\mathbf{T}}_1 + \ln \mathbf{C}_5 + \ln \left(\frac{\mathbf{x}}{\mathbf{L}}\right)^b + \ln \mathbf{C} - \left(\frac{\mathbf{y}}{\mathbf{C}_0 \mathbf{x}^*}\right)^2 \ln 2$$
(6.6)

Simplification yields:

$$\ln \triangle \bar{\mathbf{T}} = \ln \triangle \bar{\mathbf{T}}_1 + \ln C_5 + \ln \left(\frac{\mathbf{x}}{\mathbf{L}}\right)^b - \ln^2 \left(\frac{\mathbf{y}}{\mathbf{C_0} \mathbf{x}^*}\right)^2 \tag{6.7}$$

Taking the anti-logs of both sides results in the following:

$$\triangle \bar{\mathbf{T}} = \triangle \bar{\mathbf{T}}_{1} \mathbf{C}_{5} \left(\frac{\mathbf{x}}{\mathbf{L}}\right)^{b} / 2^{\left(\frac{\mathbf{y}}{\mathbf{C}_{0} \mathbf{x}^{\dagger}}\right)^{2}}$$
(6.8)

 C_5 , b, C_0 and x_0 are determined experimentally. Therefore for a given outlet velocity (e.g., x_0 , C_0 , C_5 and b are Reynolds number dependent) and a known inlet temperature difference, the temperature at any point in the outer portion of the thermal boundary layer can be determined. This assumes that the inlet Reynolds number and the inlet temperature difference are within the range covered in this investigation.

Example calculations are given in the Appendix.

7. CONCLUSIONS

- 1. The velocity fields of the chilled wall jets of this investigation conformed to the characteristics of a turbulent wall jet. The velocity profiles exhibited similarity. The decay of maximum velocity was inversely proportional to x^a where the average value of a for this investigation was, -.53.
- 2. Generally the mean temperature profiles of the chilled wall jets were congruent when plotted in a dimensionless form. This better applies at the higher inlet Reynolds numbers. The dimensionless temperature scale was $\triangle \bar{T}/\!\!\triangle \bar{T}_m$ and the dimensionless distance scale was y/δ_t . The temperature distribution in the outer layer, was described reasonably well by an exponential relationship (e.g. $\triangle \bar{T}/\!\!\triangle \bar{T}_m = \exp -(y/\delta_t)^2 \ln 2$).
- 3. The maximum temperature difference was inversely proportional to x^b, where b was a function of the inlet Reynolds number. The average value of b for all the tests was -.63. Thus the rate of maximum temperature difference decay was greater than the maximum velocity decay. This is a reasonable result in light of the fact that the thermal boundary layer was always wider than the momentum boundary layer.
- 4. The growth of the thermal boundary layer, as described by

a characteristic length dimension $\delta_{\mathbf{t}}$, was a linear function of x. The rate of growth of the thermal boundary layer was inversely proportional to the inlet Reynolds number. This agrees with the results on the relationship between the maximum temperature difference decay and the inlet Reynolds number.

- 5. In general, buoyancy forces effects were found to be negligible. This is based primarily on the fact that the thermal boundary layer growth was always linear. However, for the non-isothermal cases of the lower inlet Reynolds numbers, the air flow was observed to be detached from the ceiling, at the further distances from the inlet. Thus it appears that there were some buoyancy forces effects at the lower velocities but they could not be determined from the measurements taken.
- 6. The following relationship was found for determining the temperature at any position in the outer layer of the thermal boundary layer, of the chilled wall jets of this investigation.

$$\triangle \bar{T} = \triangle \bar{T}_1 c_5(x/L)^b/2^{y/c_0(x+x_0)^2}$$

Calculations made using this relationship agreed reasonably well with measured temperatures.

8. RECOMMENDATIONS FOR FUTURE WORK

The results of this investigation indicate the need for additional work in the following areas.

- Additional work is needed at the lower inlet velocities to further attempt to determine any possible buoyancy effects.
- 2. Measurements should be made of the turbulence shear stresses. This would permit evaluation of the eddy diffusivity for momentum. The effect of inlet Reynolds number and temperature on the eddy diffusivity for momentum might then be investigated.
- 3. Measurements of the correlation between the fluctuating components of temperature and velocity (e.g. vt) should be made. Thus the eddy diffusivity for heat could be determined. Knowing the diffusivities for heat and momentum, the turbulent Prandtl number could then be determined. The effect of the inlet Reynolds number and temperature on the turbulent Prandtl number should be investigated.
- 4. The effect of different types of ceiling configurations, such as a corrugated ceiling material, on the characteristics of the momentum and thermal boundary layers, should be investigated.
- 5. An attempt should be made to solve the turbulent form of

the momentum equation, with the boundary conditions of this problem, by the method of finite differences.

This would involve assuming values for the eddy diffusivities for momentum which would in effect be a way of determining such values.

APPENDIX

A.1 Correcting for Error in Velocity Measurements Due to Fluid Property Changes

A constant temperature anemometer instantaneously measures fluid flow parameters by sensing the heat transfer rate (heat flux) between an electrically heated sensor and the flow medium. The basic signal depends on the fluid composition, mass flow and temperature difference. For many measurements, density is constant and the instrument measures velocity. When temperature varies, compensation is needed to correct for the temperature differences.

The sensor element (hot film) can be assumed to be a cylinder for purposes of heat transfer study. Various heat transfer relations for a cylinder in cross flow are available. A commonly used relation for air is that by Collis and Williams (1959).

$$N_{u}(T_{f}/T_{e})^{-0.17} = C + DR_{e}^{n}$$
 (A.1)

where:

N₁₁=Nusselt number

R_e=Reynolds number

 $\mathbf{k}_{\mathbf{f}}$ =thermal conductivity of the environment fluid

Yr=kinematic viscosity

of=fluid density

d_=sensor diameter

h =heat transfer coefficient

V =velocity

 $T_f = film temperature = (T_e + T_s)/2$

 T_e =environment temperature

 T_s =sensor surface temperature

The values of C, D and n are dependent on the Reynolds number. Recommended values, for the Reynolds no. range in which present tests were conducted, are C=0.24, D=0.56 and n=0.45.

For measurements with hot-film and hot-wire sensors it is convenient to put equation A.1 in the form:

$$P = [A + BV^{n}] (T_{s} - T_{e})$$
 (A.2)

where:

$$A=k_fLC(T_f/T_e)^{0.17}$$

$$B=k_fLD(T_f/T_e)^{0.17}(d_o/Y_f)^n$$

P=power or heat flux dissipated by sensor L=sensor length

Sample calculations of P for the same velocity but for two different temperatures will provide an indication of the error in the velocity measurement due to neglecting fluid property changes.

Assuming temperatures $T_1=0^{\circ}F$, $T_2=60^{\circ}F$ and $T_s=392^{\circ}F$ the following values for P_1 and P_2 were calculated.

$$P_1 = 2.40 \times 10^{-6} + 1865 \times 10^{-6} \times V_1^{0.45}$$
 (A.3)

$$P_2 = 2.48 \times 10^{-6} + 1497 \times 10^{-6} \times V_2^{0.45}$$
 (A.4)

Assuming V_1 equal to V_2 the ratio of P_1 to P_2 is:

$$P_1/P_2 = 1.245$$

Thus assuming that the anemometer had been calibrated at 60° F and was being used to measure velocity in a medium whose temperature was 0° F, the bridge voltage would be 24.5% too high. However, P_1 can be corrected by multiplying it by the dimensionless temperature ratio $(T_s-T_h)/(T_s-T_c)$ where:

T_s=sensor temperature

 T_h =temperature at which the anemometer was calibrated T_c =temperature at which the measurement was taken

For the assumed temperatures, the dimensionless temperature ratio is .857. Multiplying this times 1.245 we get 1.055. Thus the error would now be 5.5% if the measured air temperature is known and is used in forming a simple correction factor.

A.2 Heat Transfer Through the Ceiling

As a chilled wall jet moves away from the inlet its thermal boundary layer is characterized by a growth in the transverse direction and a decay of the maximum temperature. If heat transfer through the ceiling is neglected, both of these characteristics are due primarily to the entrainment taking place between the wall jet and the still, ambient air. An appreciable amount of heat being transferred through the wall to the chilled wall jet, would have an effect on both the thermal boundary growth and the maximum temperature dif-

ference decay. Consequently calculations were made of the amount of heat transfer through the ceiling for a number of the tests.

Following are the calculations for Test 4.

Knowns: ceiling thickness=.75"

k (for plywood)=.8 BTU-in/hr-ft²-OF

Temperature of incoming air=19OF

Temperature of ambient air=71.3OF

Q_{inlet}=200.5 cfm=16.95 lb air/min ceiling temperatures (next to wall jet)

1	2	3	Stat 4	ion 5	6	7	8
33°F	43°F	50 ° F	55 ⁰ F	59 ° F	62°F	64 ° F	67°F

The temperature on the top side of the ceiling at station 1 was 60°F. Assume the temperature on the top side of the ceiling at stations 2 through 8 to be equal to the room air temperature, 73°F. Thus the average temperature difference across the ceiling for a section four ft wide by 7.5 ft long, would be 16.3°F. Assuming the relative humidity of the incoming air to be 60%, its enthalpy would be 6 BTU/lb air. Assuming the relative humidity of the ambient air to be 30%, its enthalpy would be 22.4 BTU/lb air. Therefore 16.6 BTU must be added to each 1b of air per minute to raise it to the ambient temperature. The total amount of heat which must be added per minute is:

Total amount of heat=16.95 lb air/min x 16.6 BTU/lb air =278 BTU/min

The amount of heat transferred through the ceiling per minute is:

 $Q=(kA/L)(\triangle T)=(.8/.75)(30)(1/60)(16.3)=9.19$ BTU/min Therefore:

heat transferred through the ceiling heat gained by entrainment + heat transfer through ceiling 3.3%

The highest percentage of heat transfer through the ceiling for any of the tests was approximately 6.1%. Thus the heat transfer was assumed negligible.

A.3 Calculating Temperature Using Empirical Expression

The expression for the temperature difference at any location in a chilled wall jet was determined to be:

$$\triangle \bar{T} = \triangle \bar{T}_1 C_5 (x/L)^b/2 y/C_0(x^i)^2$$

As a check on the accuracy of this expression a number of sample calculations were made. As one example the calculated temperatures are compared to the measured temperatures for Test 3.

Test 3
$$C_5 = 4.78$$

 $b = .568$
 $C_0 = .0994$
 $x_0 = 5.12$
 $\triangle \overline{T}_1 = 41.8^{\circ} F$

Station 3 (x=22 inches)

- y=1" $\triangle \overline{T}$ =(41.8)(4.87)(45)/2^{(1/2.695)²}=203.5/9.58=21.3°F This compares to the measured temperature which was 19.8°F. Therefore the error is 4.76%.
- y=3" $\triangle \bar{T}$ =203.5/20.6=9.87°F The measured temperature was 9.8°F. The error 1s.07%.

Station 7 (x=72 inches)

- y=1" $\Delta \bar{T}$ =203.5/17.05=11.8°F The measured temperature was 11.2°F. The error is 5.35%.
- y=5" $\triangle \bar{T}$ =203.5/22.9=8.9°F The measured temperature was 8°F. The error is 11.25%.

These examples are typical of those calculations which were made for other cases. In general the error was largest for those cases where the magnitude of the temperature difference was small (at large transverse distances and large longitudinal distances).

Table A.1 Measured mean velocity data for test no. 1, $\overline{\mathbf{U}}_1$ =1368 ft/min, isothermal case

11	∞		0	0	0	0	Ŋ	Ŋ	m	-	0	0	0	~	m	~	9	Ŋ	σ	9	6	6	9
	tion	Þ	ب	٠,	→	→	≠	†	→	.	†	m	m,	m,	'n	~	~	~	+	i.	ં	o	Ö
	Stat	ħ	2.5	•	0	5	0	•	0	0	0	0	3	00	20.	\$	90	80.	00	25.	50.	•	00
	on 2	Þ	0.4	•	•		•	•					•		•	•	•	•	•	•	•	•	•
	Station	Þ	2.5	•	0	3	0	•	•	•	0	0	。	0	00	20.	\$ 9	90	80.	8	20.	•	75.
	t10n 6	ID	4.5	•	•	•	•	•	•	•	•	•	•	•	•	•	•	•	•	•	•	•	
	Stati	>	2.5	•	0	5	0	•	•	•	•	•	0	0	00	10.	20.	30.	\$	60	80		25.
٠	ition 5	Þ	5.6	•	•	•	•	•	•	•	•	•	•	•	•	•	•	•	•	•	•	•	
	Stat1	> -	2.5	•	0	•	0	5	0	3.	•	0	0	0	0	0	00	10.	20.	•	50.	~	
	7 uo	Þ	7.2	. •	•		. •		•	6. 8	•	•		•	•	•	•	•	•	•			
	Station	٨	2.5	•	•	-	ċ	3.	0	3,	ċ	0	•	•	•	3.	00	15.	•	50.			
	tion 3	Þ		ċ	•	ċ	•	•	•	7.4	•	•		•	•	•	•	•	•				
	Stat	A	2.5	•	•	•	Š	•	5	•	5	0	0	0	0	•	•	0	15.				
	10n 2		12.8	٠,	8	7	2	÷	•	•	•	•	•	•	•	•	•	•	•				
	Station	⊳	2.5		•	•	ċ	3	ċ	25.5	ċ	'n	ó	'n	0	0	0	0	0				
	lon 1		3	。	•	÷	8	•	•	7.4	•	•	•	•									
	Station	₽	•		•	ċ	3.	•	3.	30.5	5.	ċ	ň	0									

Units of y are millimeters

Measured mean velocity data for test no. 2, $\bar{\mathbb{U}}_1$ =1235 ft/min, $\triangle \bar{\mathbb{T}}_1$ =20.7°F Table A.2

10n 8		, e	•	•		•	•	•	•	•	•	•	•	•	•	•	•	•	•	•	•	٥.	ထ္	⊅ .
Station	b	งง งัง	•	•						•			00	20,	•	60	80	00	20.	40.	90	80.	00	50.
10n 2	\Box	20 20	•	•	•	•	•	•	•	•	•	•	•	•	•	•	•	- •	•		ň	9	7.	
Station	>	40 50	•	•	•	•	•	•	•	•	•		00	20.	•	60	80.	00	20.	40.	60	80.	00	-
10n 6	n	~~ **	•	•	•	•	-	•	•	•	•	•	•	•	•	•	•	•	•	ထ္	9.	ů		
Station	⊳	40 50	•	•	•	•	•	•		•	•	•	00	10.	•	30.	40	909	80.	00	40	00		
Station 5	1	4 % 200	•	•	•	•	•	•	•	•				•	•	•	- •	•	•	•	٥.	۰,	ň	ٿ
Sta	>	なみ	•	•	Š	·	×.	-	, ·	-	-	•	-	•	•	00	10.	20.	30.	40,	60	80.	-	40.
Station 4	Þ	6 9	•	•	•	•	•	•	•	•	•	•	~ •	•	•	•	•	•	•	9	٠,	7)	
Sta	⊳	なみ	•	•	3	•	3	0	3	0	'n	0	0	0	•	0	00	10.	20.	30.	0	60.		
Station 3	ıp'	~ ~ ~	8.7	•	•	•		•	•	•	•		1.7	•	.2	⊅•	ň	ن	ٿ	ب				
Sta	>	ン シャ	•	•	3	0	3	•	3	'n	Ś	3	Š	3	•	05.	'n	25.	35.	45.				
Station 2	Þ	10.0	•	1.	•	•	•	•	•	•	•	•	•	•	•	7.	⊅ •	ٿ	~					
Sta	>	24 ひん	•	•	•	3	•	3	o	3	0	'n	•	0	•	0	0	0	# :					
tation 1	ıp (13.6	Š	ě	Ö	•	•	•	•	•	٥.	ထ္	ٿ	⊅•	٣,									
Stat	>	7.4 7.7	•	•	Š	ထံ	ň	ထီ	3	ထံ	ထံ	ထိ	•	ထံ	ω									

Units of y are millimeters Units of $\overline{\mathbf{U}}$ are ft/sec

Station U1=1224 ft/min, \T1=41.8°F Station **>** 444*と*ろかななるのののこれできるののできるとしてのようできられるのでした。 9 10 Station 7 *ᢋᠬᠬᠬᠬᠬᠬᠬᠬᠬᠬᠬ*ᠬᠬᢋ*ᡢᡢᠬ*ᠬᠬ᠐᠐ ᠀᠘ᡮ᠙ᡢᢋ᠙᠒ᠬᠬ᠐ᢁᡢᡈᢁᢋ Station Measured mean velocity data for test no. 3, **>** 4 Station $\begin{array}{c} & 14444 \\ 14494$ **>** νωωωωνναφημα η 10000000νοοναφωνονημα η 1000000νοοναφωνονημα η 1000000 Station Þ 2 |ID Station Þ 4444 600000 600000 600000 600000 6000000 600000 600000 6000000 6000000 6000000 600000 600000 60000000 60000 Table A.3 D Station

Units of y are millimeters

Units of U are ft/sec

A.4 Measured mean velocity data for test no 4, $\vec{\mathbf{U}}_1$ =1230 ft/min, $\triangle \vec{\mathbf{T}}_1$ =52.3°F

ω	10100000000000000000000000000000000000
u D	000000000000000000000000000000000000000
Station y U	$\begin{array}{c} & 1 & 1 & 1 & 1 & 1 & 1 & 1 & 1 & 1 & $
on 2	0
Station y Ū	$\begin{array}{c} & 111111999999999999999999999999999999$
ation 6	\$ \underset \und
Stat1	$\begin{array}{c} 11111199999\\ 11009999999999999999999999$
ition 5	70000000000000000000000000000000000000
Stati	$\begin{array}{c} 114449 \\ 14449 \\ 040404040404040404040 \\ 0404040404040$
n n	とうしょうとう ちょう ちょう しょうしょう しょう しょう しょう しょう しょう しょう しょう しょ
Station y Ū	$\begin{array}{c} 111111\\ 111111\\ 1111111\\ 111111111111$
on 3	@@@@@~~\\\\\\\\\\\\\\\\\\\\\\\\\\\\\\\
Station y Ū	$\begin{array}{c} 149998447200899999999999999999999999999999999999$
on 2	00014 500 10 10 10 10 10 10 10 10 10 10 10 10 1
Station y	$\begin{array}{c} 1 \\ 1 \\ 1 \\ 1 \\ 1 \\ 1 \\ 1 \\ 1 \\ 1 \\ 1 $
on 1	4444 4444 4444 6444
Station y	44000000000000000000000000000000000000

Units of y are millimeters

Table A.5 Measured mean velocity data for test no. 5, $\vec{u}_1=1020$ ft/min, isothermal case

on 8	40000000000000000000000000000000000000
Station y Ū	$\begin{array}{c} 0.00000000000000000000000000000000000$
on 7	00 + 00 0 0 0 0 0 0 0 0 0 0 0 0 0 0 0 0
Station y Ü	$\begin{array}{c} 111119\\ 12822\\ 28222\\ 28222\\ 28222\\ 2822\\$
9 uo.	の4444440011100 9655540011100
Station y Ü	111144 1444 1444 1444 1444 1444 1444 1
on 5 U	4 NNN44 WUU 40 WU W O B N C B O U C
Station y U	4444 4444 4446 4446 4446 4446 4446 444
n d	~~~~~~~~ ~~~~~~~~~~~~~~~~~~~~~~~~~~~~~
Station y Ū	1144476414 00000000000000000000000000000000000
on 3	ろってらられまる のっとるようのようのよ
Station y Ü	$\begin{matrix} & & & & & & & & & & & & & & & & & & &$
on 2 U	αοοααφαμοο ματαφομοταφη
Station y U	$\begin{array}{c} 1 & 1 & 0 & 0 & 0 \\ 0 & 2 & 0 & 0 & 0 & 0 \\ 0 & 2 & 0 & 0 & 0 & 0 & 0 \\ 0 & 2 & 0 & 0 & 0 & 0 & 0 \\ 0 & 2 & 0 & 0 & 0 & 0 & 0 \\ 0 & 2 & 0 & 0 & 0 & 0 & 0 \\ 0 & 2 & 0 & 0 & 0 & 0 & 0 \\ 0 & 2 & 0 & 0 & 0 & 0 & 0 \\ 0 & 2 & 0 & 0 & 0 & 0 & 0 \\ 0 & 2 & 0 & 0 & 0 & 0 & 0 \\ 0 & 2 & 0 & 0 & 0 & 0 & 0 \\ 0 & 2 & 0 & 0 & 0 & 0 & 0 \\ 0 & 2 & 0 & 0 & 0 & 0 & 0 \\ 0 & 2 & 0 & 0 & 0 & 0 & 0 \\ 0 & 2 & 0 & 0 & 0 & 0 & 0 \\ 0 & 0 & 0 & 0 & 0$
on 1	4444 4444 4644 4644 4644 4644 4644 464
Station y Ü	$\begin{matrix} u + u u u u u u u u$

Units of y are millimeters

Units of U are ft/sec

imeters
111m e
y are
its of
Uni

		120
	on 8	
	Stat1 y	$\begin{array}{cccccccccccccccccccccccccccccccccccc$
.3°F	on 2	00000000000000000000000000000000000000
$\Delta \bar{\mathbb{T}}_1 = 21.3$	Station y U	$\begin{array}{c} & & & & & & & & & & & & & & & & & & &$
ft/min,	9 uo	
81	Stat1 y	$\begin{array}{c} & 1 \\ 1 \\ 1 \\ 1 \\ 1 \\ 1 \\ 1 \\ 1 \\ 1 \\ 1$
, U ₁ =9	on 5	44444444400000000000000000000000000000
t no. 6	Station y	$\begin{array}{c} 1111111\\ 8008\\ 8008\\ 8009\\ 80$
r test	7 uo	ようちろうちょれゅうさるる。 られのみるらってららうららまる。 のはのはなるようで
data for	Statio y	$\begin{array}{c} 44444 \\ 440000000000000000000000000000$
1ty	00 J	00000000044000000000000000000000000000
an veloc	Statio	444 4400000000000000000000000000000000
ed mean	on 2	ののののでもろうは ののののできる のののできる のできれる のできる </td
Measured	Stat1	44000000000000000000000000000000000000
A. 6	on 1	00000000000000000000000000000000000000
Table	Stati	44000000000000000000000000000000000000

Table A.7 Measured mean velocity data for test no. 7, \bar{u}_1 =996 ft/min, $\triangle \bar{r}_1$ = $\mu 0^0 {
m F}$

1																												
tation 8	Ð	•	2.5	•	•	•	•	•	•	•	•	•	•	•	•	•	•	•	•	•	•	•	•	•	•	ω	ထ္	Φ
Stat	>	•	•	•	3	0	3	•	7	0	0	0	0	0	0	00	15.	30.	45.	· 09	75.	90	80	20.	40	260.5	80	00
tion 2	ū	•	5. 9	•	•	•	•	•	•	•	•	•	•	•	•	•	•	•	•	•	•	•	•			7.		
Stat	>	•	•	0	3	0	3	0	3	0	•	0	0	0	0	00	20.	9	90	80	00	20.	40.	90	90	320.5		
tion 6	ı	•	3.5	•		•	•	•		•	•	•	•	•	•	•	•	•	•	•	•	•	ထ္	ż	, -	•		
Stat	>	•	6.5	0	Š	0	3	0	3	•	•	0	0	0	0	00	3	30.	45.	909	80	00	25.	50.	75	\ \ -		
tion 5	þ	•	7.4	•	•	•	•	•	•	•	•	•	•	•	•	•	•	•	. •	•	ထ္	⊅.	↑.					
Stat	>	•	9	•	3	ċ	3	0	3	•	0	0	0	0	0	00	3	30.	45.	60	80	99.	19					
h no	Þ	•	5.3	•	•	•	•	•	•		•	•	•	•	•	•	•	ထ္	9.	٠. ال	7.							
Station	Þ		6.5	•	Š	0	5	0	3	•	0	0	0	0	•	00	Š	30.	45.	90	80							
tion 3	ID	•	6,3	•	•	•	•	•	•	•		•	•	•	- •			ů.	↑.	ů.	ب							
Stat	>	•	4.5	•	•	3	0	3	0	•	Ö	3	0	0	0	•	0	10.	'n	30.	50.							
10n 2	þ	•	0 8	•	•	•	- •	•	•	•	•	•	•	ထ္	ż	⊅ •	٣.	<u>.</u>	٣.									
Station	Þ	•	4.5	•	0	3	0	5	0	•	Ô	3	0	0	0	Ō	0	0	20.									
tion 1	ID	9	10.1	ċ	•	•	•	•		•	•	ထ္	9.	↑.	ņ	ٿ	~	7	7.									
Stat	Þ	•	4.5	•	ထံ	ô	3	0	3	•	3	ô	'n	0	5	ċ	0	0	•									

Units of y are millimeters Units of $\overline{\mathrm{U}}$ are ft/sec

Measured mean velocity data for test no. 8, \overline{u}_1 =1015 ft/min, $\triangle \overline{n}_1$ =54.8°F Table A.8

tion 8	Ω	2.0	• •	•	•	•	•	•	•	•	•	•	•	•	•	•	•	.2	9.	ň					
Stat	>	,84 2,7		5.	•	•	0	0	3	0	00	25.	o	75.	00	50.	00	50.	00	50.					
tion 2	n	8.5	• •	•	•	•	•	•	•	•	•	•	•	•	•	•	•	•	•		•	6	<u>~</u> 1	• •	
Stat	.	,0 A	0	3	0	3	0	3	•	0	0	0	'n	00	20.	40	-09	80	00	25.	50.	00	•	90	
tion 6	ū	ω- 2.	• •	•		•	•	•	•	•		•	- •	•	•	•	~ •	-•	•	- •	~ •	•	~	ο-	†
Stat	Δ.	, N		3	•	3	0	• →	0	0	0	0	3	00	20.	30	45.	90	80	00	25.	50.	•	9,0	50.
10n 5	Ū	4 -	• •	•	•	•	•		•	•	•		•		-•	•	~ •	•	6.		٥.	ň			
Statio	>	20,7	•	3	o	•	0	3	0	0	0	0	3	00	20.	40	60	80	00	25	0	00			
tation 4	<u>n</u>	2	• •	•	•	•	•	•	. •	•	-	•	•	•	•	•			9						
Stat	A	2,0		7	0	•	•	3	0	0	0	0	3	00	15.	30.	45.	90	0	00	ı				
tion 3	n	6.7	• •	. •	•	•	•			•	•	•	-	.7		9									
Stat	A	, 44 10, 10		8	0	•	0	3	•	0	•	0	3	00	<i>A</i>	30									
tion 2	n	ω α ~	• •	•	•	•	•	•		•	•	6	6	ω.	ထ္	'n									
Stat	>	2.2	• •	0	3	•	ν,	0	3	0	0	0	0	0	00	0	•								
tation 1	Ū	11.0	•	0	•	•	•	. •	•	•	•			₹,											
Stat	> .	42 ×	• •	•	0	•	•	3	•	3	0	0	0	0											

Units of y are millimeters Units of \overline{U} are ft/sec

Table A.9 Measured mean velocity data for test no. 9, $\vec{\mathbf{U}}_1 = 820$ ft/min, isothermal case

∞	0 N O U N O H A A A A A A A A A A A A A A A A A A
lon	-04040404040
Station y Ū	
Ω.	99999494999949494949494894899888999489994899948999489994899948999948999489994899948948
7	ζιτινονοφοφοτο
ion U	
Station y Ü	44 W 4 A 8 O 4 4 Q 4 Q 4 Q 4 Q 4 Q 4 Q 4 Q 4 Q 4 Q
921	HH H H H H H H H
n 6	
tation y <u>U</u>	u $ u$
Sta	0000 to to 000 to 0000 to 000
M	71078787878 7107878787878
1	« ~ ~ ~ ~ ~ ~ ~ ~ ~ ~ ~ ~ ~ ~ ~ ~ ~ ~ ~
Station y U	α
St	80498000 804980 804980 804980 80498
→	01100th
10n	W4444WWWHH00
Station y Ū	400000000000 <i>u u u u u u u u u u</i>
വ	8042000044000
n G	4 NNNWWW44400 WCCOWOHWHCN
tation y	ηνηνηνηνηνην Τομονικί (ΜΗΗΟΟ
Sta	40476-046 6646-648
211	HHH
n 2	~~~~~~~~~~~~~~~~~~~~~~~~~~~~~~~~~~~~~~
Station y Ü	n n
Sta	000000000000000000000000000000000000000
 	ο ο ω το φια το ο ο ο ο ο ο ο ο ο ο ο ο ο ο ο ο ο ο
non	60000000000000000000000000000000000000
tation y U	n + n + n + n + n + n + n + n + n + n +
\ \(\omega\) \(\frac{1}{3}\)	200707070000 200707070

Units of y are millimeters

Table A.10 Measured mean velocity data for test no. 10, $\overline{\mathrm{U}}_1$ =769 ft/min, $\triangle \overline{\mathrm{T}}_1$ =21.8°F

ω	ı																												
10n	Þ	•	•	•	•	•	•	•	2.4	•	•	•	•	•	•	•	•	•	•	•	•	•	ထ	J.	6	9	9.		
Stat		, •	•	0	5	0	0	0	50.5	•	0	0	•	00	15.	30.	45.	60	75.	90	00	20.	40	90	80	•	60.		
tion 7	Þ	•	•	•	•	•	•	•		•	•	•	•	•	•	•	•	•	•	•	•	•	•	•	•	~	٥.	٠2	٠,
Stat	_{>}	•		•	•	9	.	6	· +	6	• +	6	÷	6	.0	6	6	.0	60	24.	39.	54.	69	844	99.	24.	249.5	74.	46
tion 6	Þ	•	•	•	•	•	•	•	5.9	•	•	•	•	•	•	•	•	•	•	•	•	•	•	6	9	<u>ر</u>	.		
Sta	>	. •	•	0	3	0	γ.	0	35.5	0	0	0	•	0	0	00	10.	20.	40	55.	70.	85.	00	25.	0	75.)		
tion 5	þ	•	•	•	•	•	•	•		•	•	•	•	. •	•	•	•	- •	•	9	ထ္	٠,	6	ر	•				
Sta	l ⊳	, •	•	6	4.	6	†	6	34.5	6	6	6	6	6	6	6	960	15.	39		29.	99.	19.	39.					
tion 4		•		•			•	•	7.4	•	•	•	•	•	•	•	•	•	2.	- •	1.0	7.	⊅ •	↑.	ı				
Stat	 >	, •	•	0	3	0	ν.		35.5	0	0	0	0	0	0	00	10.	20.	30	0	90	80	00	25.	.				
tion 3	Þ			•		•			4.1	•	•	- •	•	•	.7	9	ئ.	2											
Stat	Þ	, •	•	•	• →	6		6	39.5	6	6	6	6	6	6	60	÷	39.											
tion 2	Ь	•	•	•	•	•	•		3.7	•	•	•	. 2	7.	7.	⊅ •													
Sta	 ⊳.	. •	•	•	3	0	ζ.		35.5	0	0	0	•	0	•	0													
tion 1	Þ	•	•	•	•	•	•	•		•	•	2	9	ٿ															
Ø	L	J	Ŋ	Ŋ	Š	N	Y	S	N	5	3	3	3	3															

Units of y are millimeters Units of $\overline{\mathrm{U}}$ are ft/sec

Units of U are ft

its of y are millimeters

11	ω	4000000000000000000000000000000000000
	CI O	O H H H H H H H H H H H H H H H H H H H
	Stati	$\begin{array}{c} 111111111111111111111111111111111111$
1,=41.4°F	on 7	
$\triangle \bar{\mathbb{T}}_1 = 4$	Stat1	$\begin{array}{c} & 1 \\ 0 \\ 0 \\ 0 \\ 0 \\ 0 \\ 0 \\ 0 \\ 0 \\ 0 \\$
ft/min,	on 6 U	
=771 ft	Stat1 y	$\begin{array}{c} 14444444 \\ 1400000 \\ 1400000 \\ 1400000 \\ 1400000 \\ 14000000000000000000000000000000000000$
1, Ü	on 5 U	00000000000000000000000000000000000000
no. 1	Stat1 y	1111111999999999999999999999999999999
r test	7 uo	α ω
data for	Stati	$\frac{1}{4}$
1ty	on 3	~~~~~~~~~~~~~~~~~~~~~~~~~~~~~~~~~~~~~~
n veloc	Stati y	$\begin{array}{c} 111111 \\ 111111 \\ 111111 \\ 111111 \\ 111111$
ed mean	on 2	4 NNNN4 WWWW 4 4 4 0 0 0 0 0 0 0 0 0 0 0 0 0 0
Measured	Stati y	1111 400404440660019 40040400000000000000000000000000000
A.11	on 1	00000000000000000000000000000000000000
Table	Stati y	$\begin{array}{c} 149900000\\ 94000000000000\\ 0000000000000\\ 0000000000$

y detached Station Measured mean velocity data for test no. 12, $\overline{\mathrm{U}}_1$ =760 ft/min, $\triangle \overline{\mathrm{T}}_1$ =55.10F Station 9 4000004 Station α Station 4 Station Station 2 Station Table A.12 Station

Units of y are millimeters

Units of $\overline{\mathrm{U}}$ are ft/sec

Table A.13 Measured mean velocity data for test no. 13, $\vec{U}=604$ ft/min, isothermal case

on 8 U	80ヤマヤテンヤンのくろくらくらくらくりょう
Station y Ū	00000000000000000000000000000000000000
on 2	47000000000000000000000000000000000000
Station y 0	30000000000000000000000000000000000000
on 6 U	00HHHHHNNNN
Station y U	$ \begin{array}{c} 144494940 \\ 19204040000 \\ 00000000000000 \\ 00000000$
on 5 Ū	00000000000000000000000000000000000000
Station y	21122 21142 201112 2027 20112
1 uc	00000000000000000000000000000000000000
Station y Ū	44444 40004400804408 40000000000000000
on 3	~~~~~~~~~~~~~~~~~~~~~~~~~~~~~~~~~~~~~~
Station y Ü	400 82 4 40 4 40 4 40 4 40 4 40 4 40 40 40 40
on 2 U	できませるとまるのできます。
Station y U	40000 4000 4000 4000 4000 400 400 400 4
on 1 U	~~~~~~~~~~~~~~~~~~~~~~~~~~~~~~~~~~~~~~
Station y Ū	44000000000000000000000000000000000000

Units of y are millimeters

A.14 Measured mean velocity data for test no. 14, $\bar{\mathbb{U}}_1$ =570 ft/min, $\triangle \bar{\mathbb{T}}_1$ =21.9 0 F

Station 8	detached flow
on 2	01011011111101111 000400040000000000000
Station y Ū	1114 1114 1104
9 uo	
Station y U	$\begin{array}{c} \begin{array}{c} \begin{array}{c} \begin{array}{c} \begin{array}{c} \begin{array}{c} \begin{array}{c} \begin{array}{c} $
on 5	
Station y U	2000-10-10-10-10-10-10-10-10-10-10-10-10-
17 uo	00000000000000000000000000000000000000
Station y U	$\begin{array}{c} 111111111111111111111111111111111111$
on 3	~~~~~~~~~~~~~~~~~~~~~~~~~~~~~~~~~~~~~~
Station y 0	$\begin{array}{c} 1 & 1 & 1 & 1 & 1 & 1 & 1 & 1 & 1 & 1 $
on 2 U	m4444mmmmm44400000 4450054004000000
Station y Ū	$\begin{array}{c} 444 \\ 444 \\ 400 \\$
on 1 U	3 N N N N N Y W N N N N N N N N N N N N N
Station y U	4444645 40000000000 500000 50000

Units of y are millimeters

Units of $ar{ extsf{U}}$ are ft/sec

Table A.15 Measured mean velocity data for test no. 15, $\bar{\mathbf{U}}_1$ =550 ft/min, $\triangle \bar{\mathbf{T}}_1$ =38.5 F

Station 8	detached flow
Station 7 y Ü	flow
on 6	44444444444444400000000000000000000000
Station y Ū	$\begin{array}{c} 1 \\ 1 \\ 1 \\ 1 \\ 1 \\ 1 \\ 1 \\ 1 \\ 1 \\ 1 $
on 5	
Station y 0	$\begin{array}{c} 1 \\ 1 \\ 1 \\ 1 \\ 1 \\ 1 \\ 1 \\ 1 \\ 1 \\ 1 $
no d	
Station y Ū	$\begin{array}{c} 1 & 1 & 1 & 1 & 1 & 1 & 1 & 1 & 1 & 1 $
on 3	00000 00000000000000000000000000000000
Station y Ü	$\begin{array}{c} 1 & 1 & 1 & 1 & 1 & 1 & 1 & 1 & 1 & 1 $
on 2 U	00000000000000000000000000000000000000
Station y Ü	$\begin{array}{c} 149900044000000000000000000000000000000$
on 1 Ū	4444444444000 ~~~~~~~~~~~~~~~~~~~~~~~~~
Station y Ū	14000000000000000000000000000000000000

Units of y are millimeters

Table A.16 Measured mean velocity data for test no. 16, $\bar{\mathbf{U}}_1$ =620 ft/min, $\Delta \bar{\mathbf{T}}_1$ =50.1°F

Station 8 y Ü	detached flow
Station 7 y 0	detached flow
Station 6 y Ū	22224 22224
Station 5 y 0	22 24 24 24 24 24 24 24 24 24 24 24 24 2
Station 4 y Ū	28 28 28 28 28 28 28 28 28 28 28 28 28 2
$\frac{\text{Station 3}}{\text{y}}$	111111 0000000000000000000000000000000
Station 2 y U	11000000000000000000000000000000000000
	0.00000000000000000000000000000000000

Units of y are millimeters

Table A.17 Measured mean velocity data for test no. 17, \mathbb{U}_1 =450 ft/min, isothermal case

Station 8	detached flow
on 7	
Station y Ü	$\begin{array}{c} 11111111000\\ 1110111111111111111111111$
9 uo U	
Station y U	$\begin{array}{c} 1144444444444444444444444444444444444$
on 5 U	00000000000000000000000000000000000000
Station y Ū	$\begin{array}{c} 1 & 1 & 1 & 1 & 1 & 1 & 1 & 1 & 1 & 1 $
n d	444444400 8 8 4 4 4 4 4 4 6 0 0 0 0 0 0 0 0 0 0 0 0 0
Station y Ū	$\begin{array}{c} 111994\\ 111994$ 111984\\ 111994\\ 111994\\ 111994 111984\\ 111994\\ 111994 111984\\ 111994\\ 111994 111984\\
on 3	00000000000000000000000000000000000000
Station y U	$\begin{array}{c} 111\\ 0\\ 0\\ 0\\ 0\\ 0\\ 0\\ 0\\ 0\\ 0\\ 0\\ 0\\ 0\\ 0\\$
on 2 U	~~~~~~~~~~~~~~~~~~~~~~~~~~~~~~~~~~~~~~
Station y U	11000004400000000000000000000000000000
on 1	24444440000 0mm444000000000
Station y Ū	4400000 44000000000000000 ~~~~~~~~~~~~

Units of y are millimeters

Table A.18 Measured mean velocity data for test no. 18, $\bar{\mathbf{u}}_1$ =410 ft/min, $\Delta \bar{\mathbf{T}}_1$ =18.2 $^{\mathrm{O}}\mathrm{F}$

tion 1	Station y U	on 2 U	Station y Ū	on 3	Station y Ū	7 uo	Station	on 5	Station 6	Station 7 y Ū	Station 8
11 00000000000000000000000000000000000	<i>พ</i> พพพพพพพพพพพพพพพพพพพพพพพพพพพพพพพพพพพ	40040004000040000000000000000000000000	4404004540406880010	- 0 0 0 0 0 0 0 0 0 0 0 0 0 0 0 0 0 0 0	$\begin{array}{c} 1 & 1 & 1 & 1 & 1 & 1 & 1 & 1 & 1 & 1 $	04440004404000000000000000000000000000	44444 44040400000000000000000000000000		detached flow	detached flow	detached flow
120	• •	• •	onono	• • • •		000000 000000 000000	000000	00000			

Units of y are millimeters

Table A.19 Measured mean velocity data for test no. 19, $\vec{\mathbf{U}}_1 = 44$ ft/min, $\Delta \vec{\mathbf{T}}_1 = 40.8^{\circ}$ F

Station 8	detached flow
Station 7	detached flow
Station 6 y Ü	detached flow
Station 5 y Ü	detached flow
	
i i	40000000000000000000000000000000000000
1	
3 Station y U	น้นในน้นในน้นในน้นในน้นในน้นในใน ฯ หลุ หลุ หลุ หลุ หลุ ฯ ฯ ฯ ฯ ฯ ฯ ฯ • • • • • • • • • • • •
3 Station y U	44 44 44 44 44 44 44 44 44 44 44 44 44
2 Station 3 Station y U	40000000000000000000000000000000000000
2 Station 3 Station y U	2200555 24,44,451 26,44,465 26,44,466 26,455 26,465 26,466 27,460 27,4
2 Station 3 Station y U	200.5 20

Units of y are millimeters

ence, for	Station 8	0%		000	00	૾૾૾ૢ	٠٠٠	o →.	°°	0			
ture differ	Station 7	0 27.	16.2°F	,20	<i>⊶∿</i>	,20	٠٠٠	3.6°°	07.	0 0	°6.	•	0 면
tempera	Station 6	000		0 (94.	ی پ	00	1, 4,80	0 8,2°F	000	س≠ ° %	0	0 0 F F
and max1mum	Station 5	007	13 OF 21.80F		97.	7. 4.00	00	00	° °	۰۰۰	2 5.00	00	000
e ceiling	Station 4	009	17 OF 25.20F	, 80 80 80 80 80	96.	5.2°	.20	00	<i>ν</i> ω ο ο ο	3 1.20	၀ တ္ထု	ئى د	06.
ence at th	Station 3	5 0		ω	ω	1. 1.		7	ω. Φ.	ů.	1 8.30F	てら	ω
ture differ ts	Station 2	8 ° ° °	29 OF 37.70F	200	$\infty \sim$	8 9 9	% 89	2°5°	0 %	ν. • 4. • 4.	ر 0 0 1	20 0.40	0 0
O Tempera all tes	Station 1	2 ° 7		64.	6.2° 6.2°	3.2°	ชพู ๑๛	0 0	5 1.10	2.90	0.00	- % - %	7.50
Table A.2	Test no.	2 Arc	3 Are	CNT OFF OFF OFF OFF OFF OFF OFF OFF OFF OF	STIC OIL	7 ATC	8 Are	10 ATC	$\begin{array}{cc} \wedge \mathbf{I} \\ 11 \\ \wedge \mathbf{I} \\ \end{array}$	12 ATC	14 OTC	15 $\triangle T_{\mathbf{L}}^{\mathbf{L}}$	16 ATC

 $\triangle T_{c} \! = \! temperature$ difference at the celling

REFERENCES

Abramovich

	1963	The Theory of Turbulent Jets The M.I.T. Press
Bakke	1957	An experimental investigation of a wall jet J. Fluid Mechanics 2:467-472
Baturin	1, W.W. 1959	Luftungsanlagen fur Industriebauten
Becker	P. 1950	Jets and inlets in ventilation J. Institution of Heating and Ventilating Engrs. 18(5):107-109
Blasius	1913	Das Ahnlichkeitsgesetz bei Reibungsvorgangen in Flussigkeiten VDI Forschungsheft 131, Berlin
Borque	, C. and 1960	Newman, B.G. Reattachment of a two-dimensional incompressible jet to an adjacent flat plate The Aeronautical Quarterly XI:201-230
Boussir	nesq 1877	Theory de l'ecoulement tourbillant Mem. Pre. par. div. Sav. XXIII, Paris
Bradsha	aw, P. a 1960	and Gee, M.T. Turbulent wall jets with and without an external stream A.R.C. 22,008 F.M. 2971
Collis	, D.C. a 1959	and Williams, M.J. Two-dimensional convection from heated wires at low Reynolds numbers J. Fluid Mechanics 6:357
Corrsin	n, S. 1950	Further experiments in the flow and heat transfer in a heated turbulent air jet

NACA Rept. 998

Farquharson, M.C.

1952 The ventilation air jet
J. Institution of Heating and Ventilating
Engrs. 19(1):440-469

Forstall, W. and Shapiro, A.H.

1950 Momentum and mass transfer in coaxial gas jets
ASME J. of Appl. Mech. 72:399-408

Forthmann, E. 1936 N.A.C.A. T.M. 789

Glauert, M.B.

1956 The wall jet
J. Fluid Mechanics 1:625

Goldstein, S.

1939 A note on the boundary layer equations
Proceedings Cambrdige Phil. Soc. 38:388

Hinze, J.O.
1948 Transfer of heat and matter in the turbulent mixing zone of an axially symmetric jet
App. Sci. Res. A-1, 435-461

Hinze, J.O.
1959
Turbulence, An Introduction to its Mechanism
and Theory
McGraw-Hill Book Co., Inc.

Kline, S.J.

1965
Similitude and Approximation Theory
McGraw-Hill Inc.

Koestal, A.

1955 Paths of horizontally projected heated and chilled air jets
Trans. ASHAE 61:213-232

Kruke, V. and Eskinazi, S.

1964 The wall-jet in a moving stream
J. of Fluid Mechanics 20:555-579

Myers, G.E., Schauer, J.J. and Eustis, R.H.
1963a
Plane turbulent wall jet flow development
and friction factor
Trans. ASME, J. of Basic Engr. 47-54

Myers, G.E., Schauer, J.J. and Eustis, R.H.

1963b Heat transfer to plane turbulent wall jets
Trans. ASME, J. of Heat Transfer 209-214

Nottage, H.B., Slaby, J.G. and Gojsza, W.P. 1952 Exploration of a chilled jet Trans. ASHVE 57:357-376

Nottage, H.B.

1951 Ventilation Jets in Room Air Distribution unpublished PhD thesis. Case Inst. of Tech.

Parker, B.F. and White, G.M.

1965 Effectiveness of jets produced by fan-baffle arrangement in mixing and distributing ventilation air

ASAE Paper no. 65-408

Poreth, M. and Cermak, J.E.

1959 Sixth Midwestern Conference of Fluid Mech.
University of Texas, Austin, Texas

Prandtl, L.

1942 Bemerkkungen zur theorie der freien
Turbulenz
ZAMM 22:241-243

Preston, J.H.

1954 The determination of turbulent skin friction by means of pitot tubes
J. of Royal Aeronautical Soc. 58:109

Reichardt, H.

1940 Der Warmeubergang in turbulenten
Grenzschichten
ZAMM 20:297-328

Reichardt, H.

1944 Impuls-und Warmeaustausch in freier
Turbulenz
ZAMM 24:268

Reichardt, H.

1951 Die Grundlagen des turbulenten
Warmeuberganges
Arch. f. Warmetechn. 6/7 129-142

Seban and Back
1961 Velocity and temperature profiles in a wall
jet
International J. Heat and Mass Transfer
3:255-265

Sigalla, A.

1958 Experimental data on turbulent wall jets Aircraft Engineering 30:131-133

Schlichting, H.

Boundary Layer Theory McGraw-Hill Inc.

Schwarz, W.H. and Cosart, W.P.

1961 The two-dimensional turbulent wall jet J. of Fluid Mechanics 10:481-495

Thermo-Systems Inc.

1966 Hot-wire and hot-film measurements and applications
Technical Bulletin no. 4

Tuve, G.L.

1953 Air velocities in ventilating jets Trans. ASHVE 261-282

Zerbe, J. and Selna, J. 1946 N.A.C.A. T.M. 1070

1				
1				
:				
1				
t .				
1				
į				
1				
·				
!				

